Sileshi Tadesse Wodaje

Land Degradation Vulnerability Assessment Using GIS and Remote Sensing in Beshilo River Basin, Ethiopia

Master's Thesis in Natural Resources Management

Trondheim, August 2016

Supervisor: Professor Jan Ketil Rød

Norwegian University of Science and Technology
Faculty of social Sciences and Technology Management
Department of Geography

NTNU – Trondheim
Norwegian University of
Science and Technology

Abstract

Land degradation is a complex environmental problem resulting from various factors. Identification of areas vulnerable to degradation is a first step to develop natural resource management and conservation activities in order to safeguard the environment and the society. This requires a close interaction with the various individual factors, which contributes to degradation. Spatial multicriteria analysis is an important method to deal with such kind of problems. Thus, the objective of this study is to assess land degradation vulnerability in Beshilo basin, Ethiopia, through the integration of GIS, RS and multicriteria analysis. Three groups of land degradation vulnerability indicators, biophysical, chemical, and socioeconomic indicators were identified. More emphasis was given for biophysical and chemical degradation indicators. The biophysical indicators are land use and land cover, soil erosion and vegetation cover. Landsat image for 1986 and 2015 were used to map land use and land cover. The images were classified into five LULC classes such as, agriculture, shrubland, bare land, grassland, and forest using supervised classification. Agricultural land covers a large area followed by shrubland and grassland in both years. Change detection has also been carried out and expansion of agricultural land by 15.3% was the major change observed. Soil adjusted vegetation index (SAVI) has been used to calculate vegetation index and it shows that a large portion of the basin has poor vegetation cover. To model soil erosion, revised universal soil loss equation has been used. The results of RUSLE model reveal that annual soil loss rate is very high in most of the Beshilo basin. The chemical degradation indicators used in the study include organic matter, acidity, salinity, and sodicity. The analysis shows that organic matter is low for 50.4% of the basin. The weights of the indicators were calculated through pairwise comparison and combined using the weighted overlay tool in ArcGIS. The result shows that vulnerability to biophysical land degradation for 61% of the Beshilo basin varies from high to very high. The chemical land degradation vulnerability for 48.76%, 50.87%, and 0.35% of the basin is low, moderate, and high respectively. The combined biophysical, chemical and population density indices show that vulnerability to land degradation is high for 41.4% of Beshilo basin.

Keywords: Land degradation, Vulnerability, GIS, RS, LULC, RUSLE, Multicriteria analysis

Acknowledgments

I would like to express my sincere gratitude for my supervisor professor Jan Ketil Rød for his valuable guidance throughout my thesis work. It is a great honor to work under his supervision.

My beloved families thank you very much for your love and encouragement. I want to express my appreciation to all people who in one way or the other contributed to the accomplishment of my thesis.

I would like thank all organizations who gave me the required data for this study. I want to give special thanks to the National Metrology Agency (NMA), Central Statistics Agency (CSA) of Ethiopia and the Amhara Reginal State Bureau of Finance and Economic Development (BoFED) for giving me their data at no cost.

I would like express my deepest gratitude to the Norwegian Government and Norwegian University of Science and Technology (NTNU) for giving me the chance to study through the Quota Scheme Scholarship program.

Table of Contents

List of Figures

List of Tables

Acronyms and Abbreviations

ABB	Abay Beshilo Basin Livelihood Zone
AHP	Analytic Hierarchy Process
AVHRR	Advanced Very High Resolution Radiometer
BoFED	Bureau of Finance and Economic Development
CSA	Central Statistical Agency
DEM	Digital Elevation Model
DN	Digital Numbers
ECA	Economic Commission for Africa
EPA	Environmental Protection Authority
ESRI	Environmental Systems Research Institute
FAO	Food and Agriculture Organization
GESAVI	Generalized Soil Adjusted Vegetation Index
GIS	Geographic Information System
GLADA	Global Assessment of Land Degradation and Improvement
GLADIS	Global Land Degradation Information System
GLASOD	Global Assessment of Human-induced Soil Degradation
IDW	Inverse Distance Weighted
ISRIC	International Soil Reference and Information Center
km	Kilometer
km^2	Kilometer square
LADA	Land Degradation Assessment in Drylands
LULC	Land Use and Land Cover
MJ mm ha^{-1} h^{-1} y^{-1}	Megajoule /millimeter hectare/hour/year
mm	Millimeter
MoA	Ministry of Agriculture and Natural Resource
MSAVI	Modified Soil Adjusted Vegetation Index
MSS	Multispectral Scanner
NASA	National Aeronautics and Space Administration
NDVI	Normalized Difference Vegetation Index
NMA	National Meteorology Agency

OLI	Operational Land Imager
OSAVI	Optimized Soil Adjusted Vegetation Index
PVI	Perpendicular Vegetation Index
RS	Remote Sensing
RUSLE	Revised Universal Soil Loss Equation
RVI	Ratio Vegetation Index
SAVI	Soil Adjusted Vegetation Index
SRTM	Shuttle Radar Topography mission
t ha h ha^{-1} MJ^{-1} mm^{-1}	metric ton/hectare/hour hectare/ megajoule/ millimeter
TIRS	Thermal Infrared Sensor
TM	Thematic Mapper
TOA	Top of Atmosphere
TSAVI	Transformed Soil Adjusted Vegetation Index
USGS	United States Geological Survey
UNFCCC	United Nations Framework Convention on Climate Change
WMO	World Meteorology Organization

1.Introduction

Land degradation is a slow onset environmental problem, which is the result of natural and human factors, so its effects are cumulative (Eswaran et al. 2001; Bai et al. 2008a; UNFCCC 2012). It is "defined as long-term loss of ecosystem function and productivity caused by disturbances from which land cannot recover unaided" (Bai et al. 2008a, 223). Vulnerability to land degradation is thus the susceptibility of an area to degradation assessed on the basis of the various factors responsible for loss of productivity. Land degradation is one of the most serious environmental challenges and an issue in both developed and developing countries (Bai et al. 2008a). However, the severity and magnitude of its impact are much more pronounced in low income countries at which the livelihood of the majority is dependent on agriculture. Land degradation is a severe problem in Ethiopia (Shiferaw & Holden 1999; Teklu 2014).

In Ethiopia, the problem of land degradation is a result of population density, rugged topography, deforestation, land use change, improper land use and absence of conservation mechanisms (FAO 1986; Amede 2003; Setegn et al. 2009). Deforestation aggravates soil erosion by making the soil more prone to erosion agents (FAO 1986). Soil erosion is one of the most serious physical land degradation process depleting the country's resource for several years (Berry 2003). Soil erosion by water, which is a result of dynamic factors, is a continuous process (Hurni 1988). The damage caused by soil erosion by water is greater than any other degradation processes and it can be taken as the sole indicator for soil degradation (Hurni 1988).

A study by World Food and Agriculture Organization (FAO) shows that in the highlands of Ethiopia, which covers 44% of the country's total area and home for 88% of population, 50% of the land was significantly eroded (FAO 1986). The other 26% was seriously eroded and 3.7% of the land was completely degraded and cannot grow crops anymore (FAO 1986). According to Hurni (1988) and Teklu (2014), Wollo, a zone where large parts of Beshilo basin located in, is highly damaged by water erosion. The soil depth for about 17.6% of Wollo is 35 cm, while the soil in a very large portion (72.2%) of the area has a depth of 10 cm (Hurni 1988). Consequently, the soil is characterized as unsuitable, not only for crop production, but also for grazing and growing trees (Hurni 1988). Analysis of a soil erosion map obtained from GLADIS(Global Land Degradation Information System) database developed by Nachtergaele et al. (2011) shows that annual soil loss varies from high to very high in over three-fourth of the Beshilo basin. Forest or vegetation degradation, both in its spatial extent and loss of species, is also high (Teklu 2014). In the 1950s, the forest cover of the Ethiopia highlands was about

20% and in the year 2000, the figure decreased to 5.6%. The country lost 62,000 ha of its forest resources each year (Berry 2003).

The livelihood of about 85% of the population of Ethiopia is dependent on land resource (Berry 2003). Despite the large portion of the population is dependent on it, the quality and the productivity of land is declining time to time (World Bank 2007; Teklu 2014; Tesfa & Mekuriaw 2014). So, it is not difficult to imagine the economic, social and political consequences or costs of land degradation in Ethiopia. It is threatening the lives of a large portion of the population (Taddese 2001). Soil degradation costs the country in many ways, such as loss of productivity, siltation in the dams, variability in river flow and groundwater resources, and high expense on chemical fertilizers (Shiferaw & Holden 1999; Amede 2003; Berry 2003; World Bank 2007; Tesfa & Mekuriaw 2014). It has also other indirect effects like malnutrition, poverty (Berry 2003) and high internal and extremal migration (Hunnes 2012). The county has experienced food insecurity as a result of severe soil degradation (EPA 2012). It is evident that as the population of the country grows, its pressure on the resource will increase and land degradation is expected to be more serious in the future, unless possible conservation measures are taken (Taddese 2001; World Bank 2007; Tesfa & Mekuriaw 2014).

Most people in Beshilo basin are food insecure and dependent on relief assistance for a long period of time (ABB 2007). Extreme soil erosion affects primarily poor people in rural areas. This is because, much of their effort is towards earning their subsistence from natural resources. Lack of finance and skilled human power or poverty at large is the main factors that forced them to focus on the short-term benefits derived from natural resources instead of long-term resource conservation. As a result, many problems associated with soil degradation, like food insecurity, attacks these people continuously (Dejene et al. 1997). This calls for an urgent land resource conservation and management. However, in low income countries like Ethiopia, resources are usually limited to conduct conservation activities in all the land resources. As a result, identifying the vulnerable areas of land degradation is crucial to utilize the limited resources efficiently. Moreover, emphasizing on the most important land degradation indicators and giving priority to them would be more beneficial. In this regard, the role of geospatial technology such as GIS, remote sensing and multicriteria analysis is an indispensable (van Lynden & Mantel 2001).

There are various land degradation studies conducted at national and reginal levels which are relevant for national planning. To support the efforts in land resource conservation and management, studies at local level would be highly valuable. Such studies would help to focus

on the neediest areas. In the long-run, they may also serve as a basis to investigate the effectiveness of conservation activities and to measure improvements or increments in land degradation vulnerability. Most of the GIS based land degradation assessments are on a basis of a single agent for instance, soil erosion. However, a land degradation assessment that involves a wide range of factors responsible for degradation could be more informative. To the author's knowledge, no such recent GIS based land degradation vulnerability assessments are available for the Beshilo basin. Lack of baseline has been cited as a constraint in many land degradation studies (Nachtergaele et al. 2011; Tully et al. 2015). So, this study would be a contribution to support the efforts towards better natural resource management in the area and also it would have a contribution to land degradation related literatures.

Vulnerability is a dynamic process (Tiani et al. 2015), it changes when the status of one of the components of the system changes. As a result, vulnerability to land degradation needs to be assessed continually to take appropriate resource conservation measurements. Therefore, the aim of this study is to assess land degradation vulnerability in Beshilo basin through the integration of GIS, RS and multicriteria analysis. More specifically, the study is targeted to map the spatial and temporal changes in land use and land cover, to assess soil erosion hazard, and to develop land degradation vulnerability index for Beshilo basin using spatial multicriteria analysis.

2. Previous Work

GIS and remote sensing have been used in land degradation mapping projects at global, national, and local level. The types of degradation and the method used to address them vary accordingly. Global Assessment of Human-induced Soil Degradation (GLASOD) is the first global study to be mentioned. According to van Lynden (2004) GLASOD has been the most significant assessment in its contribution towards policy development concerning land degradation. The study was mainly focused on the assessment of human induced soil degradation (Oldeman 1994). In GLASOD, the soil degradation process is classified into two broad classes, as removal or displacement of materials and on site deterioration of soil. Under the two broad processes, twelve types of degradation were identified. Water and wind erosion are the two soil degradation processes that displaces soil from one area to the other. Oldeman (1994) categorized the soil degradation process that result the in-situ deterioration as chemical and physical degradation process. Under the chemical soil degradation process are loss of nutrients or organic matter, salinization, acidification, and pollution. The physical degradations are compaction, crusting and sealing, waterlogging and subsidence of organic soils. The main causative factors identified are deforestation for the sake cultivation land, inappropriate agriculture practices, clearing vegetation for household use such as for building and fuel, and industrial activities which contributes to pollution (Oldeman 1994).

The GLASOD was aimed to provide information for decision and policy making at the global and national level. However, the study has shortcomings because it is based on expert opinion or judgement involving over 250 scientists and it is also at a very small scale of 1:10,000,000 (Oldeman 1994; Oldeman & van Lynden 1996).

The findings of GLASOD indicate that human induced soil degradation affects about 15% of global land area or 24% of the land area occupied by man. Soil erosion by water is the most important degradation responsible for 56% of the total area affected by human induced soil degradation. The other 28% of degradation is as a result of wind erosion and 12% by chemical degradation (Oldeman 1994).

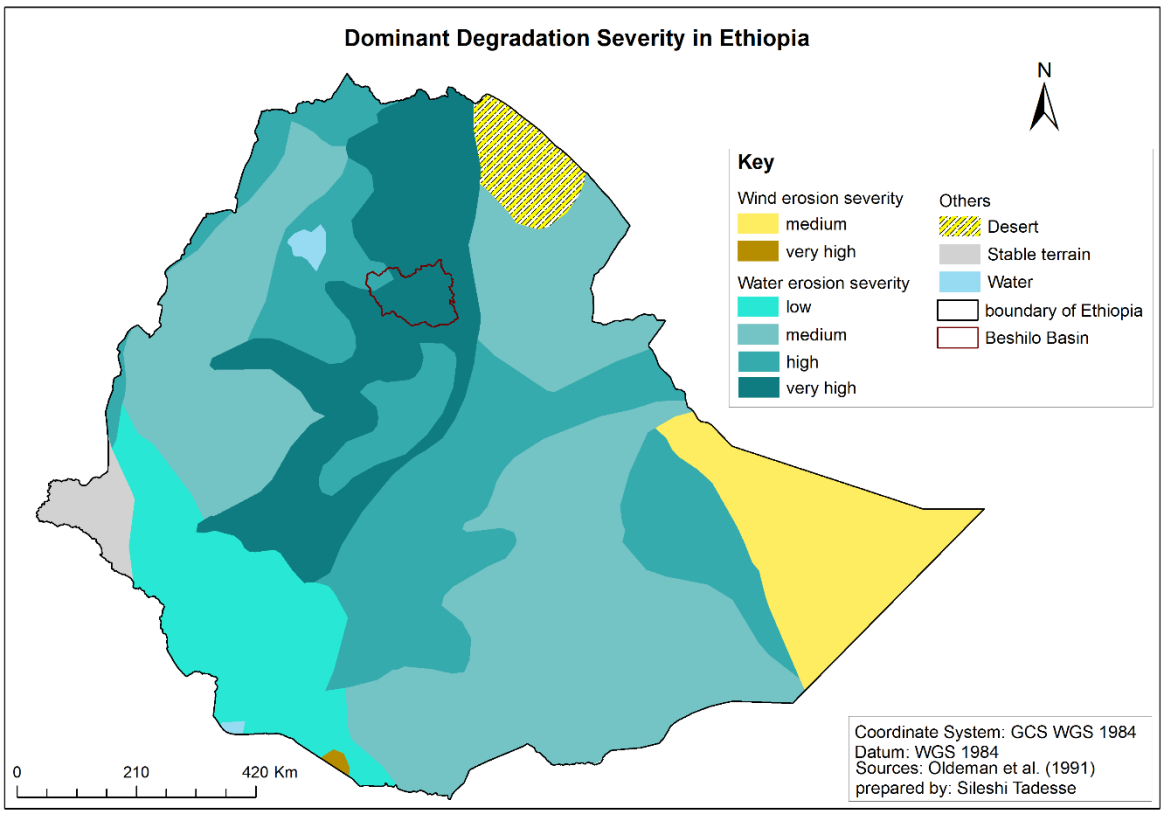

Figure 1.GLASOD dominant degradation severity map of Ethiopia

GLADA is another global land degradation study. It is a remote sensing based study, which uses NDVI as a proxy for assessing land degradation. The NDVI maps are produced from 8km resolution AVHRR satellite images for the years 1981-2003 (Bai et al. 2008b; Nachtergaele et al. 2011). The NDVI and rainfall correlation were analyzed and those areas with negative correlation are taken as an indicator of degradation. According to Nachtergaele et al. (2011), this method is subject to the limitations in that, the result may show the general areas to focus on vegetation cover change rather than the actual areas of land degradation. This is because of the diverse aspects of land degradation other than vegetation.

Global Land Degradation Information System (GLADIS) is one of the comprehensive global GIS and remote sensing based land degradation assessment. "Land degradation has been defined by LADA as the reduction in the capacity of the land to provide ecosystem goods and services over a period of time for its beneficiaries" (Nachtergaele et al. 2011, 9). According to Nachtergaele et al. (2011) the challenges in assessing land degradation as a decline process is usually lack of reference or baseline. In this system, the change in ecosystem good and services is an indicator of its degradation. "Degradation or decline in ecosystem services corresponds with a change in the state of these services due to pressures and resulting in various degradation

processes" (Nachtergaele et al. 2011, 11). In GLADIS, the ecosystem services used to assess degradation are water quantity, soil health, biomass, and biodiversity, economic and social services. Land degradation index is thus the sum of all these indicators.

de Paz et al. (2006) developed a GIS based methodology for assessing soil degradation in Valencia, Spain. They assessed soil degradation through physical, biological, and chemical degradation indices developed through map algebra computation in GIS. However, the variables used in this study are very limited and may not be adequate to reflect the different land degradation processes. They used the soil properties such as percentage of stable aggregates, silt, clay, organic matter, and wilting point for calculating physical land degradation index. For calculating biological land degradation index, only organic matter is considered. Electrical conductivity, exchangeable sodium, and cation exchange capacity were the factors used to calculate chemical soil degradation in GIS (de Paz et al. 2006).

Snakin et al. (1996) have developed a system for assessing soil degradation for Russia. They described soil degradation into three major classes as physical, chemical, and biological degradation. The physical and chemical degradation processes mentioned in their paper are more or less similar with that of the GLASOD approach. They described the biological degradation as a loss of biodiversity in soil and pollution of soil with unwanted materials. The system is based on indicators that are scaled into five classes from zero to four for describing non-degraded to very highly degraded soils respectively. The soil degradation indicators are classified into two classes as factual indicators that describe the soil conditions, for instance, the degree of soil loss, at the time of study. Prognostic indicators are those indicators that explain the temporal conditions, the availability, and level of undesirable properties in the soil (Snakin et al. 1996).

Also Rabia (2012a) used GIS to study land degradation in Tigray, Northern Ethiopia. He developed a model based on the LADA methodology proposed by FAO which group land degradation into four major types. These are degradation of soil, vegetation and water resource, and pollution (soil or water). Under each of these types of land degradation, there are various subdivisions (McDonagh et al. 2009). Rabia (2012a) used different indicators such as, soil physical degradation (soil erosion by water), soil chemical degradation (soil texture and some other nutrients), loss of vegetation, and land use. Rabia used the RUSLE model to prepare soil erosion maps and NDVI for vegetation cover map. All the indicators are classified into five ordinal classes and their weights are derived using pairwise comparison. The indicators are

combined using the weighted overlay technique. Rabia (2012a) concluded that GIS and remote sensing technologies perform well in the assessment of land degradation.

GIS and RS offer numerous advantages in land degradation studies. According to van Lynden & Mantel (2001), GIS and RS play a role, but not limited, to present topographic and other factors, to link spatial and attribute data, helps to overlay different factors and to answer many questions related to land degradation. In addition, GIS and RS help to disseminate spatial information for non-skilled users. van Lynden & Mantel (2001) also stated that GIS and RS play a significant role to investigate land degradation, especially, in areas where field data is limited due to inaccessibility and difficult topography.

3.Methods and Materials

3.1. Study Area

Beshilo Basin is located in Amhara regional state of Ethiopia between 38.2° E to 39.6° E longitudes and 10.8° N to 11.9° N latitudes. As shown in Figure 2, the basin covers parts of South Wollo, North Wollo and South Gonder administrative zones of the region. Beshilo River is one of the largest river that flows to the Blue Nile River. It has many tributary rivers.

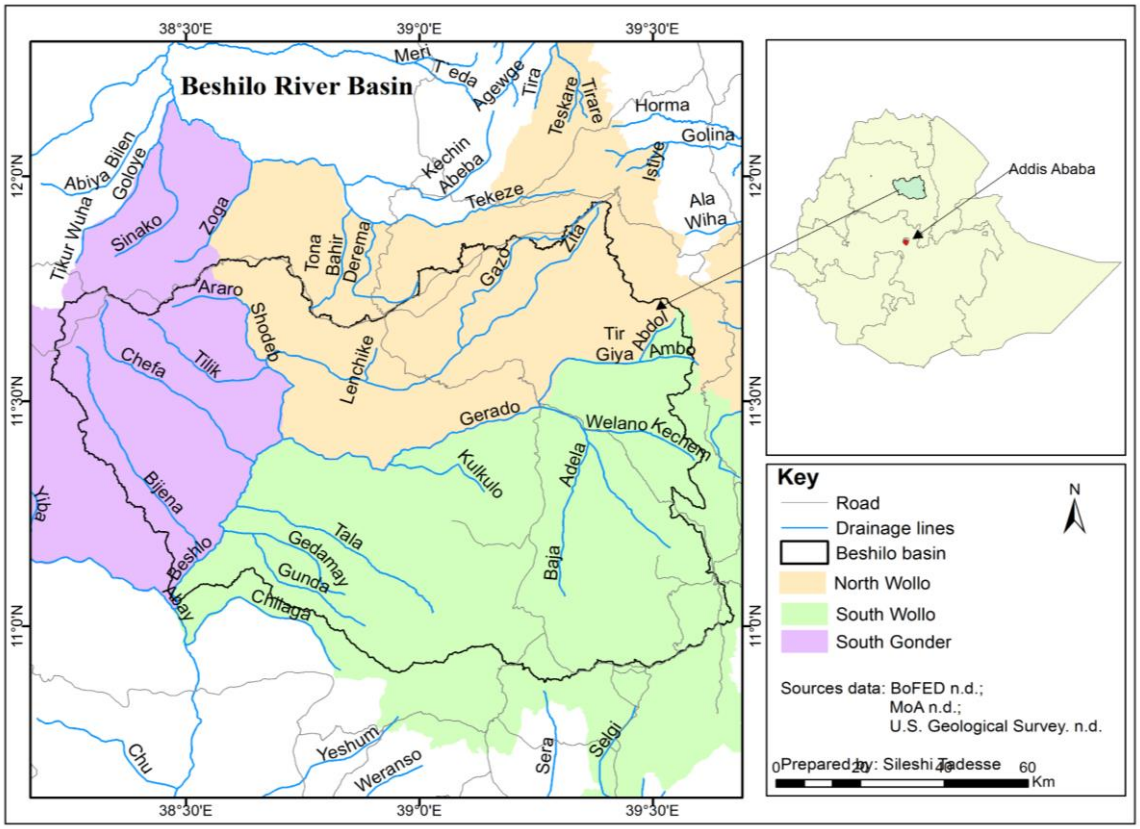

Figure 2. Map of Beshilo river basin

As shown in Figure 3, the altitude of the area ranges from 1202 meters to 4266 meters above mean sea level. The elevation of about 45% of the watershed is in between 2400 meter and 3200 meters. The other 40% of the area has an elevation range of 1500 meter to 2400 meter while the elevation of about 12% of the area is in between 3200 meter and 3700 meter above mean sea level.

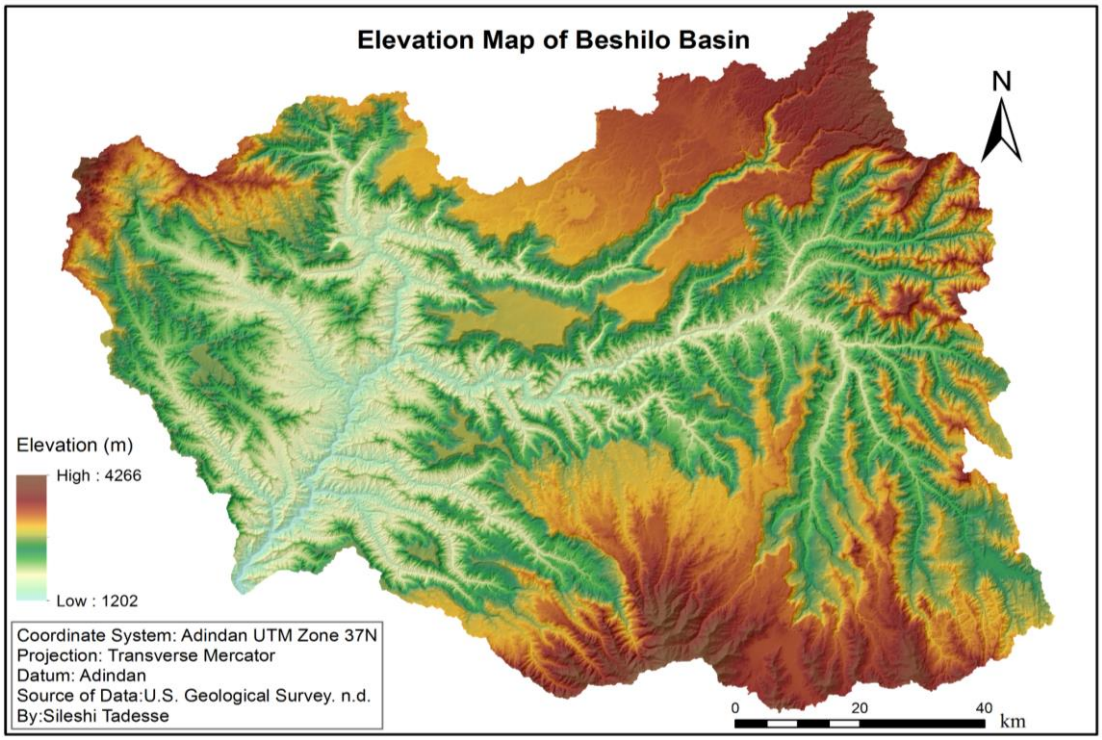

Figure 3. Elevation map of Beshilo basin

The long-term mean annual rainfall of the watershed ranges from 720 mm to 1298 mm. The traditional agroclimatic classification system of Ethiopia is based on elevation and rainfall. Negash (1989) and Hurni (1998) discussed the agroclimatic zones of Ethiopia and their classification system. The classification method given by Hurni (1998) has been used to identify the agroclimatic zones through the intersection of altitude and mean annual rainfall using geoprocessing tools in ArcGIS. The result shows that the watershed has seven agroclimatic zones. The four most dominant agroclimatic zones are moist dega (cool & humid), moist weyna dega (semi-humid), dry weyna dega (semi-humid) and moist wurch (cold & humid), covers about 45%, 26%, 14% and 12% of the basin respectively. The rest 3% of the area has moist kolla (warm semi-humid), high wurch (extreme cold & wet) and dry kolla (semi-arid) agroclimatic zones.

3.2. Nature and Sources of Data

This research is based on both primary and secondary data sources. The primary data source in this research is Landsat imageries. Landsat images were used to analyze spatial and temporal changes in land use and land cover (LULC) and to calculate a vegetation index. Acquisition years of the images are 1986, 2014 and 2015. Images of 1986 and 2015 are acquired during dry season, whereas the 2014 images are from the wet season. Landsat images in the dry season

are important to discriminate the different land use and cover types in the study area based on their reflectance (Fonji & Taff 2014). Landsat 2014 images are used to consider vegetation in the wet season. Regarding the selection of years for land use and land cover change detection, in most cases it depends on the conditions of land use and land cover change in a particular area of interest. The conditions and years, for instance, may mark a change in land use policy. In this case, the years before and after the change may be used to compare the influence policy change have on land use. If the changes are rapid, selecting images with shorter time interval could be more preferable to be able to determine the trend or rate of change more accurately. For instance, El-Kawy et al. (2011) used four different years 1984, 1999, 2005 and 2009 for LULC change detection in a semi-urban setting in the western Nile Delta. Selection of years of study may also depend on the quality and availability and of satellite images, experts and the time allocated for the work. Therefore, 1986 and 2015 are selected for mapping the types and the changes in land use and land cover by taking into consideration the aforementioned factors.

Landsat imageries and shuttle radar for topography mission (SRTM) digital elevation model (DEM) with 30 meter resolution have been obtained from United States Geological Survey (U.S. Geological Survey. n.d.). Administrative boundaries for districts and kebeles.[1] or wards were collected from Amhara regional state Bureau of Finance and Economic Development (BoFED n.d.) and surface water resource data were obtained from Ministry of Agriculture (MoA n.d.). Rainfall data from 12 stations were acquired from the National Meteorology Agency (NMA n.d.) (Figure 7; Appendix A). The 2007 population data for kebeles were used from the Central Statistical Agency (CSA 2010) and the population projection for 2015 and 2030 were also obtained from BoFED (n.d). Soil properties with 250 meter resolution (Hengl et al. 2015) were downloaded from the International Soil Reference and Information Center (ISRIC) website.[2]

3.3. Spatial Multicriteria Evaluation

Multicriteria analysis involves various steps from problem definition, setting objectives, developing criteria to the final analysis of the results. As it is stated in the previous section, the objective of this study is to assess land degradation vulnerability. To attain the objective various

[1] Kebele is the smallest administration unit in Ethiopia.

[2]The soil data were downloaded from http://www.isric.org/content/african-soilgrids-250m-geotiffs (accessed October 2015) and cited as Hengl et al. (2015) in this text as recommended in the website.

criteria or indicators have been identified. These indicators of land degradation are categorized into three groups as biophysical degradation indicators, chemical degradation indicators, and socio-economic indicators. The biophysical degradation indicators used include land use and land cover, vegetation index and soil erosion (Nachtergaele et al. 2011). Chemical degradation indicators considered in this study includes organic matter, acidity, salinity and sodicity (Abrol et al. 1988; Oldeman 1994; Osman 2013). Socio-economic indicators are related with the underlying cause of land degradation. They are the drivers of biophysical and chemical land degradations. For instance, population, income level, education, infrastructure etc. have a contribution to the vulnerability of a place for degradation. Socio-economic indicators in land degradation vulnerability can be utilized in different ways. It can be used to investigate the impact of social and economic factors on land degradation. For instance, people with low income may exert significant pressure on the land resource to earn their daily subsistence, so that its vulnerability to degradation increases. On the other hand, socio-economic indicators can also be used to analyze the impacts of land degradation on the society because of their status such as low level of income, low level of education and etc. Most of the analysis in this study is based on the biophysical and chemical degradation indicators. Due to the absence of spatial data, only population density was used as a proxy for the socio-economic pressure on land degradation. Figure 4, shows the analytical structure of the land degradation vulnerability in multicriteria analysis. The description of the indicators and the procedures applied to prepare them is provided in the next sections.

According to Malczewski & Rinner (2015) the three basic concepts in multicriteria analysis are value scaling, criteria weighting and combination. Multicriteria analysis needs the criteria's to be adjusted in similar units and to a common scale, so as to make the comparison meaningful. Value scaling, also termed as standardization is a process of converting criteria to a common unit. Reclassifying and assigning a value range is one of the commonly used methods to standardize the values of criteria maps in spatial multicriteria evaluation (Eastman 2012; Malczewski & Rinner 2015). In this study, the raster maps are scaled to a value range from 1 to 5 indicating very low and very high vulnerability respectively.

Another important concept in multicriteria analysis is criterion weighting. A weight is a value given for an indicator or criterion showing its relevance or significance in relation to other indicators or criteria. The three most widely used weighting methods in spatial multicriteria decision analysis are ranking, rating, and pairwise comparison (Malczewski 2006). Using ranking method, the weights are determined by ranking the criteria based on investigators

preference. In rating method, the weights are specified based on predetermined scale and a value is assigned to criteria based on their importance. However, the weights determined using ranking and rating methods may not be correct (Malczewski & Rinner 2015). As a result pairwise comparison method, which, according to Malczewski (2006), is a widely used method in spatial multicriteria analysis studies, have been employed to determine the weights in this thesis.

Pairwise comparison is a method used to compare two criteria at one time based on the scale given in Saaty (2008). The criteria are weighted through a comparative judgement. In this method, when two criteria are compared, the less important criteria will get a reciprocal value of the most important criteria. Some sorts of inconsistency may occur during the assignment of preference values. As a result, the consistency of pairwise comparison needs to be checked. This can done using a scripted extension of ArcGIS, known as Analytic Hierarchy Process (AHP). The reference consistency ratio determined by Saaty, who invent the AHP in 1980, is 0.10 or 10%. If the value of consistency ratio is less than 0.10, it is considered as consistent comparison but if, the value is higher than 0.10 it is considered as less accurate or inconsistent and it needs to be revisited (Malczewski & Rinner 2015).

The next stage after fixing the criteria weights is an evaluation. Evaluation is a stage at which the criteria maps are combined to get the final composite index (Eastman 2012; Malczewski & Rinner 2015). Weighted overlay technique have been used to combine the criteria maps. Each standardized criterion was multiplied by its weight in the overlay process (Eastman 2012).

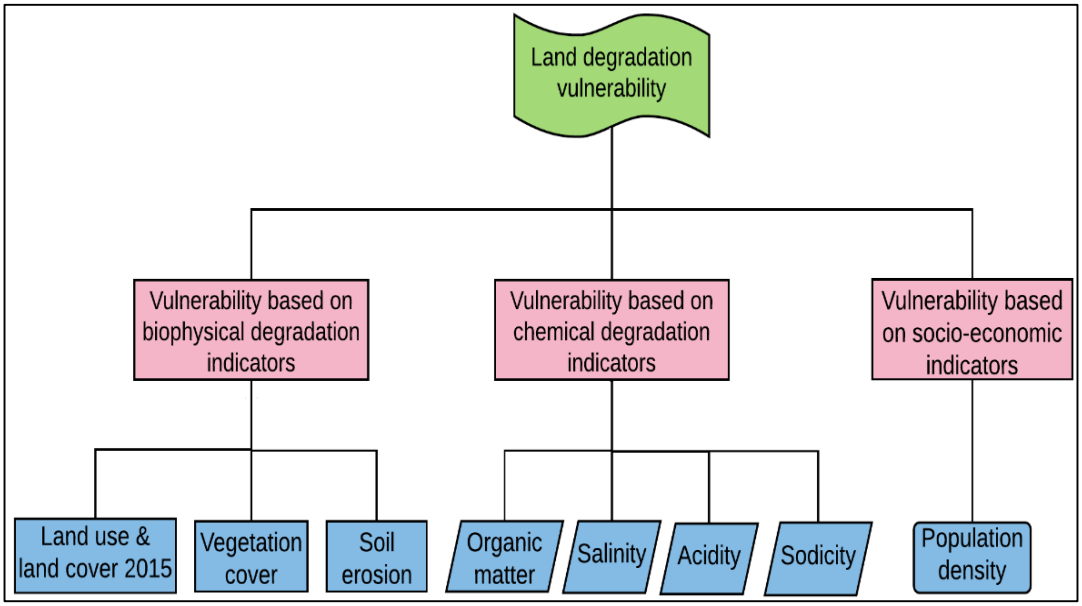

Figure 4. Hierarchical structure of land degradation vulnerability model in multicriteria analysis

3.3.1. Developing Biophysical Indicators

i. Land Use and Land Cover

"Land cover has been defined by the attributes of the Earth's land surface and immediate subsurface, including biota, soil, topography, surface and groundwater, and human structures" (Lambin et al. 2006, 4). Land cover change is a shift or modification of the physical and biotic conditions of the earth's surface, for instance conversion of wetland to cropland (Lambin et al. 2006; FAO 2007). Land use implies the purpose or utilization of a particular land by man (Lillesand et al. 2015). Land use change may lead to change in management of land. Human activities such as overgrazing, deforestation for fuelwood or cultivating land have a direct consequence on land degradation (Lambin et al. 2006; FAO 2007). Though the term land use and land cover are different, with the availability of remotely sensed images and development of classification systems, presenting both in a single map is possible and it is also a very efficient way of mapping (Lillesand et al. 2015).

According to (Nachtergaele et al. 2011), land use and land cover has a relationship with richness in biodiversity. For instance, forested areas are areas of high biodiversity while areas used for agriculture are characterized by low biodiversity (Nachtergaele et al. 2011). So that, areas that are rich in biodiversity could be indicator of low level of degradation, but those areas with poor biodiversity can indicate less conservation and degraded environment. Taking this into consideration, land use and land cover of 2015 has been used as one indicator of biophysical degradation. The different land use and land cover types have been reclassfied and values have been assigned based their impact on biodiversity and sucepitablity to degradation. In this section, the image processing, classfication, accuracy assessment and change detection methods are presented.

Image Processing: to facilitate visual interpretation and to be able to extract information through classification, applying image processing techniques is important. As a result, the image rectification (to line up the 2014 image with the other images) and restoration and image enhancement techniques have been used.

Image rectification and restoration also referred to as image preprocessing are techniques applied to raw image data to restore the geometric distortion, radiometric distortion (such as the influence of atmospheric condition, scene illumination etc.) and noise (unwanted disturbance like striping in image data (Lillesand et al. 2015).

For land use and land cover mapping, Landsat 5 Thematic Mapper (TM) and Landsat 8 Operational Land Imager (OLI) level 1T (L1T) (geometrically and radiometrically corrected orthorectified) images were used. Landsat 5 satellite launched in 1984 with Multispectral Scanner (MSS) and Thematic Mapper (TM) sensors and it was in use until 2013. Landsat 5 was used to collect images in seven bands in the visible and in the near, shortwave and thermal infrared regions of the electromagnetic spectrum. Landsat 8 was launched in 2013 with an advanced Operational Land Imager (OLI) and Thermal Infrared Sensor (TIRS). Landsat 8 collects data which match with Landsat 5 and another four additional bands (U.S. Geological Survey 2015a).

Though Landsat 5 TM and Landsat 8 OIL images come with the same map projection and datum, there is a little bit geometrical distortion. For instance, Landsat 2014 image does not perfectly fit with other images and datasets. Therefore, automatic image to image registration was applied to correct the shift in location. Landsat "images are processed in units of absolute radiance using 32-bit floating point calculations" (U.S. Geological Survey 2015b, 61). However, images are scaled to 8 bit for Landsat TM (Chander & Markham 2003) and 16 bit for Landsat OIL images (U.S. Geological Survey 2015b) before dissimination. The images downloaded from EarthExplorer website are in this format. Therefore, it is necessary to perform radiometric calibration to restore the images back to their spectral radiance before subsequent processing. Radiometric calibration comprises radiance and planetary or Top of Atmosphere (TOA) reflectance. This is very important to reduce the variability between scenes and increases the comparability of data acquired at different time and by different sensors (Chander et al. 2009). According to Chander & Markham (2003), it is more advantageous to use reflectance image than the radiance. This is because it corrects variation between different scene images mainly resulted from differences in the earth-sun distance and solar illumination angles at times of data acquisition (Chander & Markham 2003).

Six bands have been used for land use and land cover classification from both images. As shown in Table 1, the bands selected from Landsat 5 and Landsat 8 are comparable in wavelength. The resolution of both images is 30 meter. As a result, it is rational to compare land use and land cover maps extracted from them.

Table 1. Comparison of bands used and their wavelength for Landsat 5 and Landsat 8

Landsat 5		Landsat 8	
Band	Wavelength	Band	Wavelength
Band 1 - Blue	0.45 - 0.52	Band 2 - Blue	0.45 - 0.51
Band 2 - Green	0.52 - 0.60	Band 3 - Green	0.53 - 0.59
Band 3 - Red	0.63 - 0.69	Band 4 - Red	0.64 - 0.67
Band 4 - Near Infrared	0.76 - 0.90	Band 5 - Near Infrared (NIR)	0.85 - 0.88
Band 5 - Short-wave Infrared	1.55 - 1.75	Band 6 - Short-wave Infrared (SWIR) 1	1.57 - 1.65
Band 7 - Short-wave Infrared	2.08 - 2.35	Band7 - Short-wave Infrared (SWIR) 2	2.11 - 2.29

Source: U.S. Geological Survey (2016)

Top of Atmosphere (TOA) reflectance has been calculated following the procedures and equations given in U.S. Geological Survey (2015b) and Chander et al. (2009). For TM sensor, the Digital Numbers (DNs) values should be converted to spectral radiance first and then used as an input to the subsequent calculation of Top of Atmosphere (TOA) reflectance. Spectral radiance of Landsat TM image was calculated using Equation 1 given in Chander et al. (2009).

$$L\lambda = \left(\frac{LMAX\lambda - LMIN\lambda}{Qcalmax - Qcalmin}\right)(Qcal - Qcalmin) + LMIN\lambda\,, \quad (1)$$

Where

Lλ= Spectral radiance at the sensor's aperture [W/(m2 sr μm)]

Qcal= Quantized calibrated pixel value [DN]

Qcalmin= Minimum quantized calibrated pixel value corresponding to LMINλ [DN]

Qcalmax= Maximum quantized calibrated pixel value corresponding to LMAXλ [DN]

LMINλ= Spectral at-sensor radiance that is scaled to Qcalmin [W/(m2 sr μm]

LMAXλ= Spectral at-sensor radiance that is scaled to Qcalmax [W/(m2 sr μm]

Raw pixel values or digital numbers in a satellite image represents the intensity of the spectral energy recorded by the sensor. These raw digital numbers are usually scaled or calibrated to binary numbers before dissemination for the users (Chander & Markham 2003). For instance, the Landsat 5 TM images used in this study comes in 8 bit format, values range from 1 to 255. So for a particular band, the minimum quantized calibrated pixel (Qcalmin) in this case 1 corresponds to the minimum spectral radiance recorded by the sensor (LMINλ) in that particular band. Also Qcalmax (255) and LMAXλ do the same (Chander et al. 2009). While the Qcalmin

and Qcalmax values for all TM bands used in this study are the same, LMINλ and LMAXλ values corresponding to each band are provided in Table 2.

The top of atmosphere reflectance for Landsat 5 TM scene was determined using Equation 2 (Chander et al. 2009).

$$P\lambda = \left(\frac{\pi * L\lambda * d^2}{ESUN\lambda - \cos\theta s} \right), \quad (2)$$

Where

Pλ = Planetary TOA reflectance [unitless]

π = Mathematical constant approximated to 3.14159

Lλ = Spectral radiance at the sensor's aperture [W/(m2 sr μm)]

d = Earth–Sun distance [astronomical units] ESUNλ= Mean exoatmospheric solar irradiance [W/(m2 μm)]

θs = Solar zenith angle [degrees]

The parameter values used for radiometric calibration of Landsat TM images are available in Chander et al. (2009) and in the metadata of the images as text file, downloaded from EarthExplorer together with GeoTIFF images.

Table 2. Input values for atmospheric calibration of Landsat 5 TM imageries

Band	LMAXλ	LMINλ	ESUNλ [W/(m2 μm)]
1	169	-1.52	1983
2	333	-2.84	1796
3	264	-1.17	1536
4	221	-1.51	1031
5	30.2	-0.37	220
7	16.5	-0.15	83.44

Sources: Chander et al. (2009)

For calculation of reflectance of Landsat 5 TM images sun elevation angle and earth-sun distance are important variables. The sun elevation angle refers to the sun illumination angle over a specific area at the time of capturing the imagery (NASA 2011). The seasonal variation in the suns elevation angle results in different illumination over specific place. This results

differences in objects reflectance that is manifested in the images captured at different periods (NASA 2011). Sun elevation angle for path 168 and row 52 images is 40.87132155°, and for path 169 and row 52 image is 40.49322117° (provided in metadata of the Landsat TM images). The values indicate that the area was illuminated by the sun at these specified angles, so that the values are used in calculating the reflectance. Similar to the sun elevation angle, the distance between the earth and sun is variable throughout the year (Chander et al. 2009). This variation also affects the incoming solar radiation and thereby the reflectance. As a result, the calculation of the TOA reflectance for landsat image takes into account the earth-sun distance of the acquisition date of the images. Chander et al. (2009) tabulated the earth-sun distance values for the whole days (Julian day, which is counted starting from January 1) of the year. The acquisition date for path 168 and row 52 is 1986-12-23, which means the image is acquired on the 357th day of 1986 and the value of earth-sun distance obtained is 0.98363 astronomical units (Chander et al. 2009). The acquisition date for Landsat 5 TM path 169 and row 52 image is 1986-12-30, which is on the 364th day of 1986 and its earth-sun distance value is 0.98335 astronomical units (Chander et al. 2009). Therefore, all the aforementioned variables are used to calculate top of atmosphere reflectance for Landsat TM images using Equation 2.

For Landsat 8 OIL, the digital numbers (DN) of the images were converted to the Top of Atmosphere reflectance using the formula given in U.S. Geological Survey (2015b) and the parameters in Table 3.

$$\rho\lambda = \frac{M_p * Qcal + A_p}{\sin(\theta)}, \quad (3)$$

$\rho\lambda$ = Top of Atmosphere Planetary Reflectance.

M_p = Reflectance multiplicative scaling factor for the band.

A_p = Reflectance additive scaling factor for the band.

Qcal = Level 1 pixel value in DN

θ = Solar Elevation Angle

Table 3. Parameters for Landsat 8 images radiometric calibration obtained from images metadata

Date	Path and Row	M_p	A_p	Sun Elevation angle (θ)
2/6/2015	168, 052	0.00002	-0.1	50.65169913
1/28/2015	169, 052	0.00002	-0.1	49.10585537
10/17/2014	168, 052	0.00002	-0.1	60.19496735
10/24/2014	169, 052	0.00002	-0.1	58.61730454

Coming into the software environment, there are different available options for radiometric calibrations in many commercial and open source GIS and image analysis software. For this study, all the calibrations of the 1986, 2014, and 2015 images (six scenes multiplied by six bands, a total of 36 images for the three years) have been done using ArcGIS map algebra function in batch processing mode.

Image enhancement is a method applied to the image to add a value in visual interpretation. Enhancing the image lets the interpreter extract or distinguish features easily. There are various types of image enhancement techniques such as contrast enhancement, linear stretching, histogram equalization, etc. The selection of enhancement techniques may depend on the purpose and the nature of the image data. Histogram equalization has been used to enhance the images and improve its display for land use feature extractions through image classification. It is commonly used technique because of its abilities to improve image detail (Campbell & Wynne 2011).

Image classification is the next task after the preprocessing and image enhancement. In remote sensing, there are two major types of image classification methods: supervised and unsupervised classification (Liu 2005). Supervised classification, an important tool to drive quantitative data from satellite, has been used for preparing land use and land cover maps. Among the algorithms in supervised classification, maximum likelihood classification (MLC) is the most widely used algorithms (Liu 2005) and the one employed for this thesis.

Training samples have been collected by digitizing polygon around the pixels, which have been identified as representative for a particular land use and land cover type. According to Lillesand et al. (2015), in theory, if n numbers of bands are used, the number of pixels in a signature for one land use class should be n+1. In practice, the number of pixels used are minimum ten to hundred times the number of bands (Lillesand et al. 2015). According to Jensen (1986), pixels more than ten times the number of bands per class is a general rule for collecting signature. This

is to have sufficient spectral statistics and to improve the classification. The number of bands used in this study are six for each scene (Table 1). As a result, minimum 60 pixels (10 times 6 bands) have been used in a signature for a class.

The mean spectral signature was used to analyze the separability between the signatures. As seen from Figure 5, there is a bit overlap in the mean spectral reflectance of the signatures between LULC classes, for instance, in band 3 and band 5 of Landsat TM (Figure 5). Small overlap in the mean spectral reflectance of LULC signatures is also observed in Landsat 8 OLI (Figure 5). Such overlaps in spectral reflectance of objects or features may happen for different reasons. One reason can be the similarity of reflectance between deferent objects; in this case,

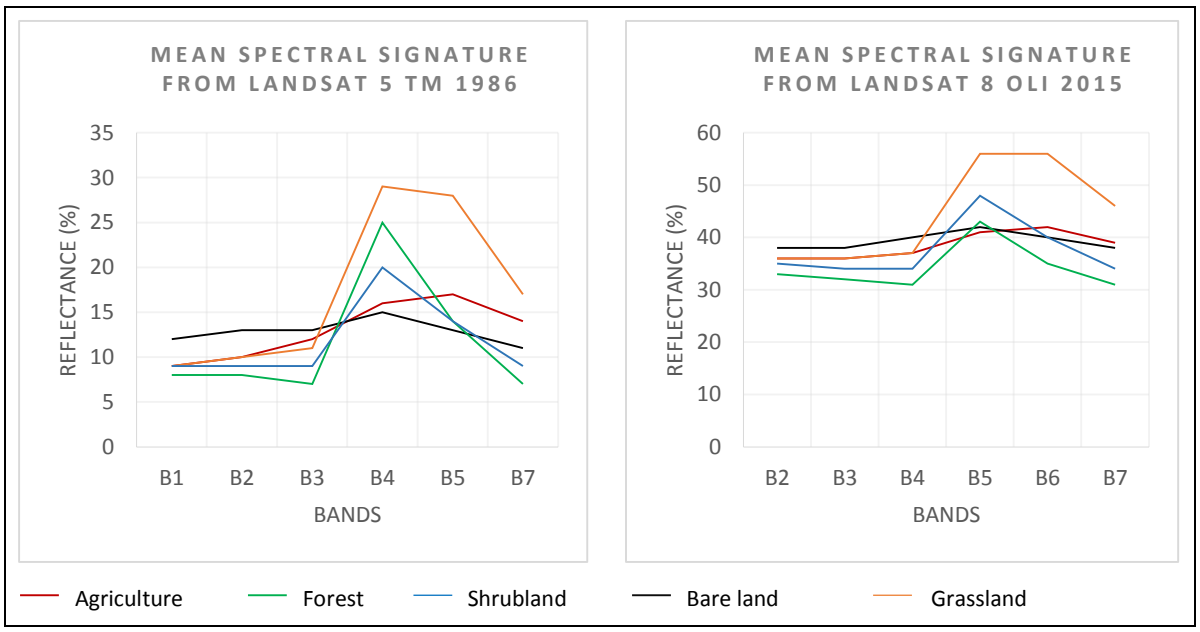

Figure 5. Mean spectral signature for land use/land cover classes for 1986 and 2015

it will be difficult to find a distinct spectral reflectance. For example, crops and grasses may have overlapping reflectance. The other important reason is that the LULC classes in this study are general. For instance, under agriculture land, there are different types of crops, crops at the middle of their growth, crops that are dry and ready for harvest and already harvested land reflect differently. Such variations results in spectral similarity and overlap in the signature with other land use and land cover features. Nevertheless, the mean spectral signatures are separated in most of the bands.

In addition to the analysis of the mean spectral reflectance of signatures, statistical analysis known as transformed divergence distance measure, was used to examine the separability of signatures in order to improve the outcomes of classification. According to Jensen (1996), the

scale value of transformed divergence ranges from 0 to 2000. Jensen (1996) suggests that classes can be separable if the value is higher than 1900, fairly good separation if it is between 1700 and 1900 and not good if it is below 1700. As it is seen from Table 4, the maximum values for signatures collected from both 1986 and 2015 images are 2000 indicating that most land use and land cover signatures are highly separable. The average separability for signatures collected from 1986 and 2015 images are 1985.5 and 1974.7 respectively. In addition to the suggestions by Jensen (1996), these values have been used to examine how far the separability of a class is from the average separability. Separability between shrubland and forest is relative low in both 1986 and 2015 signatures.

This is due to the fact that both classes represent vegetation. Healthy vegetation reflects in green and infrared and it absorbs blue and red. The reflectance in blue and red increases if there is a reduction in chlorophyll content (Lillesand et al. 2015). As a result of spectral similarity, there will not be clear separability between these classes. The same is true for the separability of bare land and agriculture signatures for 2015 image. However, separability between these signatures is fairly good because the value falls between 1700 and 1900.

Table 4.Separability evaluation of signatures

Year	Signature name	Agriculture	Bare land	Forest	Grassland	Shrubland
1986	Agriculture	0	1999.91	2000	2000	2000
	Bare land	1999.91	0	2000	2000	2000
	Forest	2000	2000	0	2000	1858.34
	Grassland	2000	2000	1996.64	0	1999.93
	Shrubland	2000	2000	1858.34	1999.93	0
2015	Agriculture	0	1893.07	2000	2000	1999.92
	Bare land	1893.07	0	2000	2000	2000
	Forest	2000	2000	0	2000	1854.37
	Grassland	2000	2000	2000	0	1999.99
	Shrubland	1999.92	2000	1854.37	1999.99	0

After evaluating and editing, the signatures are used to classify images using the maximum likelihood classifier. Post-classification smoothing, specifically 3 by 3 majority filter were applied to minimize the salt-and-pepper appearance from land use and land cover maps (Lillesand et al. 2015). As it can be seen, the small pixels in Figure 6a, for instance, those

represent bare land that are scattered within the agricultural land, are removed after applying the 3 by 3 majority filter (Figure 6b).

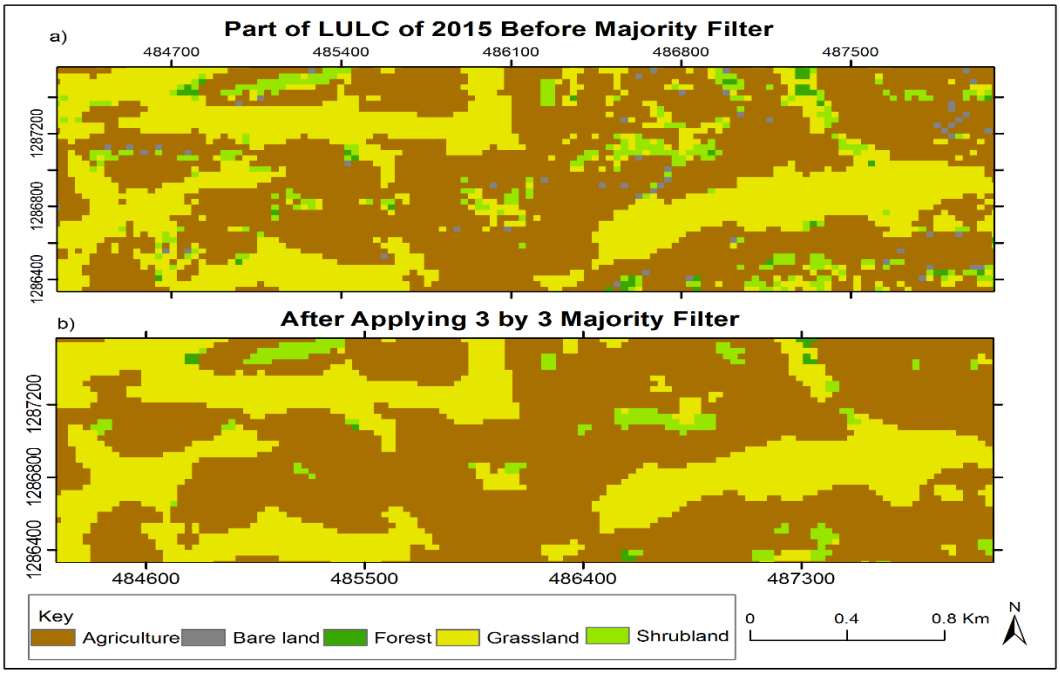

Figure 6. Post-classification processing using 3 by 3 majority filter, an example from 2015 LULC

Accuracy Assessment: Classification error matrix, also called as a confusion matrix, has been developed in order to assess the accuracy of the results of image classification. This error matrix is the comparison of the collected reference data and the results of the classification (Lillesand et al. 2015). The reference data can be collected from the field or existed data. Collecting reference data from the field is very time consuming and costly. However, some reliable higher resolution satellite images, aerial photograph, topographic maps and old sketch maps can be used as reference data to minimize such costs (El-Kawy et al. 2011). The method of using high resolution images for accuracy assessment is discussed in detail by Kloditz and others (Kloditz et al. 1998). Regarding the number of reference points, the general guideline is that minimum 50 points for each land use and land cover types or classes are identified in the image data (Lillesand et al. 2015). One challenge in assessing accuracy is lack of high resolution images or any other reliable maps which can be used to collect reference points for the old image from 1986. For this reason, about 259 points have been collected from areas that are unchanged in both 1986 and 2015 Landsat images, as identified through visual interpretation. Then, to be sure in which land use and land cover features a particular point fall, Bing aerial image has been used. The image is a very high resolution aerial image, used in the Microsoft owned Bing web mapping service, provided by companies such as DigitalGlobe (Microsoft Corporation and its

Table 5. Land use and land cover classification accuracy assessment report

		Reference Data								
Year	Classified Data	Agriculture	Bare land	Forest	Grassland	Shrubland	Row Total	Producers Accuracy (%)	Users Accuracy (%)	Kappa Statistics
	Agriculture	47	6	6	3	1	63	94%	75%	0.69
	Bare land	1	40	0	0	0	41	78%	98%	0.97
1986	Forest	0	1	36	0	2	39	69%	92%	0.90
	Grassland	2	2	1	50	2	57	93%	88%	0.84
	Shrubland	0	2	9	1	47	59	90%	80%	0.75
	Column Total	50	51	52	54	52	259	Overall Accuracy =	84.94%	Overall Kappa = 0.81
	Agriculture	49	10	0	6	1	66	98%	74%	0.68
	Bare land	0	39	0	0	0	39	76%	100%	1.00
2015	Forest	0	0	34	0	2	36	65%	94%	0.93
	Grassland	1	0	1	47	1	50	87%	94%	0.92
	Shrubland	0	2	17	1	48	68	92%	71%	0.63
	Column Total	50	51	52	54	52	259	Overall Accuracy =	83.78%	Overall Kappa = 0.79

data suppliers 2016). It is available for use as a basemap in ArcGIS 10.3 by requesting Bing Maps Key from Microsoft.[3] As presented in Table 5, 1986 and 2015 images are classified with overall accuracy of 84.9% and 83.7% respectively. The overall Kappa statistics is 0.81 and 0.79 for 1986 and 2015 respectively. According to Viera & Garrett (2005) guideline for Kappa statistics interpretation, 0.81 shows almost perfect agreement and 0.79 indicates substantial agreement between the classification results and reference data.

Change Detection: investigating the changes in land use / land cover is very essential to take appropriate management action. Change detection, in remote sensing, is a technique used to analyze the difference in an object's status by using multi-temporal spatial data sets. The idea behind using satellite imageries for change detection is that a change in land use and land cover manifest itself through differences in spectral radiance (Singh 1989).

In remote sensing, there are three main methods of change detection which are image subtraction, image ratio method and the method of change detection after classification (Xu et al. 2009). Image subtraction is used when performing change detection on the basis of gray values of pixels. While image ratio method, as its name indicates, is used in order to calculate the ratios of pixels in each band of the image (Xu et al. 2009). Post classification change detection, on the other hand, is the most obvious method and conducted after independent processing and classification of images for different periods (Singh 1989). So, the first and second method of change detection is not relevant to show land use changes in this study. Here, change detection was conducted after preparing land use and land cover map using supervised classification.

Cultivated sloping land: the percentage of cultivated land on a steep slope is an important indicator of pressures that leads to land degradation. Cultivating sloping land aggravates soil erosion particularly in areas with less management or protection and results in the gradual degradation of resources (FAO 2007). The slope gradient map has been derived from digital elevation model and reclassified according to FAO slope gradient class presented in Table 14 (FAO 2006). The reclassified slope gradient and land use map has been converted to polygon and intersect overlay was used to categorize land use by slope class and the results are presented in graph (Figure 14).

[3] https://www.arcgis.com/home/item.html?id=ae8ed793f2fb4ab0be1b7638082e95b5 (accessed March 2016)

ii. Vegetation Cover

Land degradation can manifest itself in terms of reduction in biological activity (Burch et al 1987). This can be reflected in various vegetation properties like green leaf biomass and green leaf area, density and growth conditions. All of these vegetation properties can be inferred from vegetation indices derived from satellite imageries (Waswa et al. 2012). This makes vegetation indices preferable to be used as a proxy for assessment of land degradation. In the past, different methods were developed to derive vegetation indices from remote sensing data. Some of the vegetation indices are listed in Table 6 (Gilabert et al. 2002).

Table 6. Vegetation indices

1	RVI	Ratio Vegetation Index
2	NDVI	Normalized Difference Vegetation Index
3	PVI	Perpendicular Vegetation Index
4	SAVI	Soil Adjusted Vegetation Index
5	TSAVI	Transformed Soil Adjusted Vegetation Index
6	OSAVI	Optimized Soil Adjusted Vegetation Index
7	MSAVI	Modified Soil Adjusted Vegetation Index
8	GESAVI	Generalized Soil Adjusted Vegetation Index

These first three earliest vegetation indices are highly sensitive to soil background of vegetation area (Gilabert et al. 2002). To improve this problem different scholars proposed indices which minimize the influence of a soil surface in estimating vegetation cover. These indices are sometimes referred as SAVI family (Qi et al. 1994; Gilabert et al. 2002). According to the experiment by Gilabert et al. (2002), SAVI and GESAVI have better efficiency to calculate vegetation index by reducing the influence of soil background of vegetation. Some coefficients, such as GESAVI, are not parameterized, which makes it impossible to calculate from satellite images. Therefore, SAVI will be used to drive better vegetation index in this study. The equation is given by (Huete 1988):

$$\mathrm{SAVI} = \frac{(\mathrm{NIR} - \mathrm{Red})}{(\mathrm{NIR} + \mathrm{Red} + \mathrm{L})}(1 + \mathrm{L}), \tag{4}$$

Where

NIR = spectral reflectance measurements in the near-infrared regions

Red = spectral reflectance measurements in the visible (red)

L = constant or correction factor, ranges from 0 to 1.

The value of L will be zero when the vegetation density is high, in which case SAVI and NDVI values will be identical. For areas with no green vegetation cover, the value of L is one. According to Huete (1988), 0.5 is an intermediate value and it works well when the vegetation cover is unknown. It is widely used value in literatures and also by U.S. Geological Survey. Three vegetation indices have been calculated based on the constants, such as 0.25, 0.5, and 0.75, proposed by Huete (1988) and the one determined by using 0.5 deemed as better representation than the others, when compared with the original image through visual interpretation. As a result, it has been selected for the subsequent analysis.

iii. Soil Erosion

Soil erosion is the main indicator of land degradation vulnerability. The agent of erosion may be water or wind. Since the climate condition of large parts of Beshilo watershed is humid, water erosion is a predominant form of erosion. In order to assess the soil erosion hazard and calculate soil loss, Revised Universal Soil Loss Equation (RUSLE) has been used within the GIS environment. RUSLE is a model used to estimate "longtime average annual soil loss" from sheet and rill erosion (Renard et al. 1997b,15). According to Renard et al. (1997b), it is a widely used model globally which demonstrates the importance and validity of RUSLE to estimate soil loss. The formula for RUSLE is given as follows (Renard et al. 1997b; Renard et al. 2011):

$$A = R*K*LS*C*P, \quad (5)$$

Where

A = annual soil loss
R = rainfall erosivity factor
K = soil erodibility factor
LS = slope length and steepness factor
C = cover and management factor
P = support practice factor

Rainfall erosivity factor (R) in RUSLE indicates the power or the potential of a given storm event to detach or erode soil particles. According to Renard et al. (1997a), rainfall erosivity index (R) has a direct relationship with the average annual total rainfall values. Since rainfall

is variable both in time and space, it is essential to use an average value of annual long-term precipitation record (Wischmeier & Smith 1978; Renard et al. 1997a). Average annual rainfall from 1992 to 2014 has been used to estimate the erosivity (R) values. Rainfall erosivity (R) has been calculated using the model proposed by Nigussie et al. (2014) as follows:

$$\mathrm{Ra} = 0.0032\,(\mathrm{Pa})^2 - 2.0474(\mathrm{Pa}) + 1348, \quad (6)$$

Ra = annual erosivity values in mega joule per millimeter hectare per hour per year (MJ-mm/ha-h-y); Pa = average annual rainfall amounts (mm) and the numbers in the equation are the coefficients in the regression model derived by Nigussie et al. (2014)

The rainfall data from 1992 to 2014 for about twelve stations in study site and neighboring areas are acquired from Meteorology Agency of Ethiopia (Figure 7 & Appendix A). In order to produce the average annual rainfall raster map of Beshilo watershed Inverse Distance Weighted (IDW) interpolation method has been used. In IDW interpolation, sample points that are closer to the points of unknown values will have more weight or influence than those at far distance (Li & Heap 2008). Therefore, it has been used because it gives the advantage of creating rainfall surface with the more influence of meteorology stations within Beshilo basin or at closer distance than those located far (Figure 7).

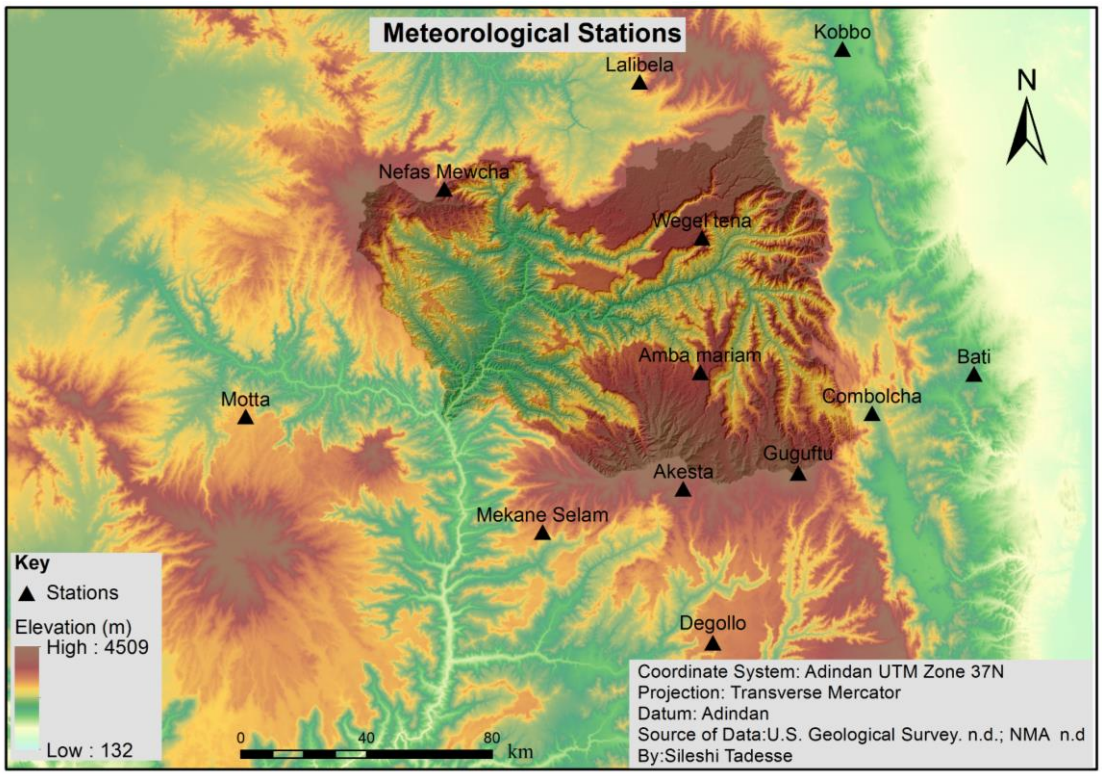

Figure 7. Location of meteorological stations

Soil-erodibility factor (K) reflects the influence of soil properties on soil loss (Römkens et al. 1997). Having the same slope, land cover, and rainfall condition, some soils wear down more easily than others do. This is a result of the intrinsic characteristics of the soil which is referred to as erodibility (Wischmeier & Smith 1978). Silt, sand, and clay particles influence the erodibility of the soil. According to Wischmeier & Smith (1978), the proportion of silt particles highly influence the soil erodibility. Usually, soils with low silt proportion are less erodible. In addition to the soil particles, organic matter is another soil property that affects the soil erodibility (Wischmeier & Smith 1978). Römkens et al. (1997) outlined different formulas developed by scholars to determine soil erodibility. Most of these formulas used to estimate erodibility only in specific geographical area (Römkens et al. 1997). Equation 7 and 8 outlined below are formulas used to calculate erodibility for different environments. These equations utilize different soil properties to calculate the soil erodibility factor. Thus, the type of data available in the study area governs the choice of the formulas. Wischmeier & Smith (1978) defined soil erodibility factor (K) as follows**:**

$$K = [2.1\ M^{1.14}(\ 10^{-4})(12 - a) + 3.25\ (b - 2) + 2.5(c - 3)/100], \qquad (7)$$

Where

M = [(silt fraction % - very fine sand fraction %) /100] - clay fraction %

a = percent organic matter,

b = the soil-structure code used in soil classification,

c = the profile-permeability class

Due to lack of soil structure and profile permeability class data required to employ the above formula, the soil erodibility factor (K) has been determined using an alternative equation given by (Williams et at. 1990). This equation was also used in Song et al (2011), to assess soil erosion Danjiangkou reservoir, China.

$$K = \{0.2 + 0.3exp\left[0.0256SAN\left(1.0 - \frac{SIL}{100}\right)\right]\}\left(\frac{SIL}{CLA + SIL}\right)^{0.3}\left[1.0 - \frac{0.25C}{C + \exp(3.72 - 2.95C)}\right]\left[1.0 - \frac{0.7(1 - \mathrm{SNA}/100)}{(1 - \mathrm{SNA}/100) + \exp(-5.51 + 22.9(1 - \mathrm{SNA}/100))}\right], \quad (8)$$

Where

SAN= sand in %
SIL= silt in %
CLA= clay in % and
C = organic carbon in %

Slope length and steepness factors (LS) reflect the influence of topography on soil erosion. There is strong relationship between slope length and soil loss. Soil loss increases on longer slopes (Wischmeier & Smith 1978; McCool et al. 1997).

> Slope length is the distance from the point of origin of overland flow to either of the following, whichever is limiting for the major portion of the area under consideration: (1) the point where the slope decreases to the extent that deposition begins, or (2) the point where runoff water enters a well-defined channel.
>
> Smith & Wischmeier 1957, 892

The slope steepness factor (S) takes into account the effects of gradient of the slope on water erosion. On steeper slope, water wear down soil more speedily than it did on the gentle slopes (Wischmeier & Smith 1978). Different formulas have been developed in the past to calculate

LS factor. The aim of most of these formulas is to make the GIS based calculation of slope length and slope steepness factors easy. Desmet & Govers (1996) developed a procedure for GIS based automated calculation of slope length (L) factor given in Equation 9. This formula is based on flow accumulation (contributing area) and topographic correction factors (X) which is the sum of sine and cosine of aspect. Slope length (L) has been calculated by implementing Equation 9 as map algebra. However, the result obtained was not satisfactory. An alternative add-in for ArcGIS, which is named as GISus-M, developed by Oliveira et al. (2015) was therefore used instead. The add-in has LS-tool, calculates LS factor using digital elevation model as an input. The algorithm used to calculate slope length in LS-tool is the same as Equation 9. It returns the slope length and steepness factor as American Standard Code for Information Interchange (ASCII) file and combined LS factor in Tagged Image File Format (TIFF). The ASCII file was converted to raster format using ArcGIS conversion tool and projected to Adindan UTM zone 37, which is a common projection used to all the layers used in this study. The steepness factor was calculated using map algebra based on Equation12. One advantage of GISus-M is that it has the options for single flow direction and multiple flow direction algorithms. Both algorithms deals with the downslope flow. However, they differ in that multiple flow direction takes into account distributed flow for many downslope cells (Figure 8).

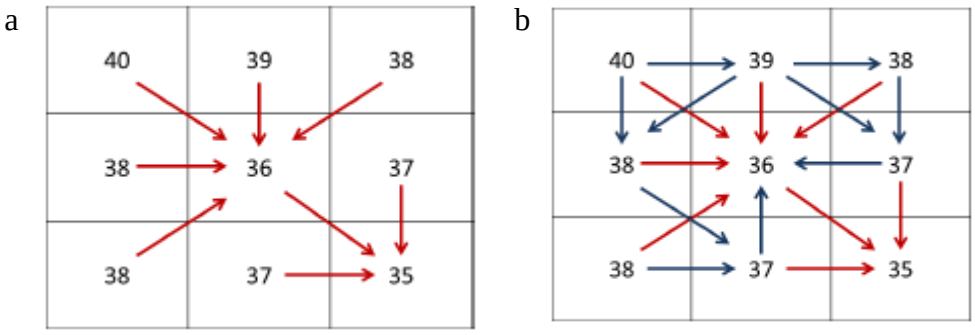

Figure 8. Single flow direction (a) and multiple flow direction (b) (Cooper 2013)

In reality, runoff may not necessary flow only in downslope direction, in some cases, it may distribute to parallel slope for instance in flat areas (Cooper 2013). For this reason, the multiple flow direction algorithm has been used in Equation 9 for the calculating slope length.

$$L_{i,j} = \frac{\left(A_{i,j-in} + D^2\right)^{m+1} - A_{i,j-in}^{m+1}}{D^{m+2} X_{i,j-in}^{m} (22.13)^{m}}, \quad (9)$$

Where *Li,j* is the *L* factor for grid cell (*i,j*); *Ai,j–in* (inlet) is the contributing area at the inlet of a grid cell with coordinates (*i,j*) (unit square meters); *D* is the grid cell size (unit *meters*); *Xi,j* is the (sin$\alpha i,j$ + cos$\alpha i,j$); $\alpha i,j$ is the aspect direction for the grid cell with coordinates (*i,j*) in radians; and *m* is a variable slope length exponent (Winchell et al. 2008).

The slope length exponent (m) is explained by the ratio of rill to interrill erosion. "Erosion occurring in rills is defined as rill erosion, and erosion occurring on the interrill areas is defined as interrill erosion" (Khanbilvardi et al. 1984, 64). In interrill erosion, the agent for detaching and transporting the soil is rainfall. Rills are small channels where runoff detaches soil from the surface and transport together with sediments come from interrill areas to larger rivers or areas of deposition (Khanbilvardi et al. 1984). Interrill area is an area that is found between rills. Figure 9 depicts slope length and rill erosions. Slope length exponent (m) has been determined by the following formula (Foster et al. 1977):

$$m = \beta/(1 + \beta), \tag{10}$$

Where β is the ratio of rill to interrill erosion and its value is calculated as follows (McCool et al. 1989).

$$\beta = (\sin\theta/0.0896)/[3.0(\sin\theta)^{0.8} + 0.56], \tag{11}$$

Where sin θ = slope angle.

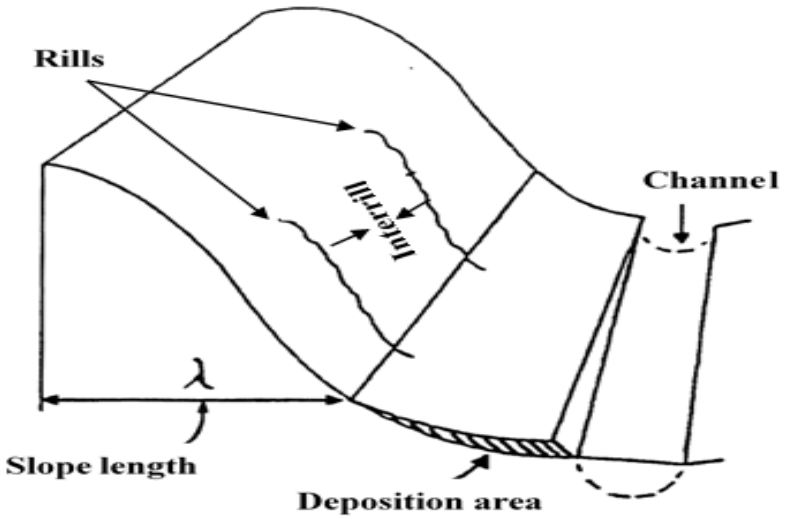

Figure 9. Slope length, interrill, and rill erosion Renard et al. (1997b)

Slope steepness(S) factor has been calculated using formula developed by Nearing (1997):

$$S = -1.5 + 17/[Exp(2.3 - 6.1 \sin\theta)], \quad (12)$$

Shuttle Radar Topography Mission (SRTM) digital elevation model (DEM) with 30 meter resolution has been processed and slope angle was calculated using spatial analyst tool in ArcGIS. Slope length and steepness factor maps have been combined using map algebra to get topographic (LS) factor raster.

Cover management factor (C) is one of the important factors in RUSLE and describes the effects of land cover management on the soil loss. It is the ratio of an actual soil loss from a particular land surface to the losses under continuous fallow condition (Yoder et al. 1997). In RUSLE, the value of C is a multiplied effect of five sub-parameters such as canopy cover, prior land use, surface cover, roughness and soil moisture (Yoder et al. 1997). The value of C vary between 0 for the non-erodible state of soil and 1 for highly susceptible soil conditions, for instance, extensive cultivation of land makes the surface smoother which increases runoff and erosion (Renard et al. 2011). Vegetation cover has an influence on the amount of soils eroded (van der Knijff et al. 2000; Lin et al. 2002). In many studies, linear regression analysis has been used to estimate C factor value from NDVI (van der Knijff et al. 1999; Lin et al. 2002; Karaburun 2010; Durigon et al. 2014). Durigon et al. (2014) used Equation 13 to calculate the C factor.

$$\mathrm{C} = \frac{-\mathrm{NDVI} + 1}{2}, \quad (13)$$

Where

C= cover management (C) factor

NDVI= normalized difference vegetation index (ranging from -1 to +1)

The C values have been calculated using Equation 13. This equation was developed to rescale the NDVI to values ranging from 0 (forested) to 1 (bare land areas). The NDVI values calculated for Beshilo basin varies from - 0.35 to 0.66. As a result, C factor values calculated from NDVI tends to be a bit exaggerated for some land use and land covers types, for instance, forest areas,

as compared to the values available in the literature. This exaggerated value causes high estimated soil loss values on forest areas. Due to this reason, the C factor values presented in Table 7 have been used.

Table 7. Cover management (C) factor values

Land use and land cover type	C factor value	Sources
Agriculture	0.15	Tiruneh & Ayalew (2016)
Bare land	0.60	BCEOM (1998) cited in Bewket &Teferi 2009)
Forest	0.01	Hurni (1985) cited in Bewket & Teferi 2009)
Grassland	0.05	Tiruneh & Ayalew (2016)
Shrubland	0.20	Tiruneh & Ayalew (2016)

Support practice factor (P) "is the ratio of soil loss with a specific support practice to the corresponding loss with upslope and downslope tillage" (Foster et al. 1997, 186). Contouring, strip-cropping and terracing are the main support practices (Wischmeier & Smith 1978). The P factor implies the effects of these supporting activities in runoff characteristics (Wischmeier & Smith 1978). The support practices play a vital role in the reduction of soil loss by diverting the direction and reducing the erosivity power of runoff (Rabia 2012b). Many researchers used different techniques to determine the P values. For instance, Prasuhn et al. (2013) calculated P values as a function of slope gradient. Bizuwerk et al. (2003), Bewket & Teferi (2009), Ayalew (2015), and Tiruneh & Ayalew (2016) used slope and land use to determine P values for assessing soil loss in different parts of Ethiopia. Shi et al. (2002) also used similar method to assess soil erosion risk in Hanjiang River, China. According to Shi et al. (2002), it is a method used in a soil conservation manual for Changjiang basin in China. It takes into account the influence of land use and slope in modifying the runoff characteristics, such as its flow path and power. In this method, the slope gradient is classified into six classes and land use and land cover types are also categorized as agriculture and non-agriculture. The non-agricultural land uses across all slope classes have assigned P value of 1 and the agriculture land across the different slope classes assigned P values as given in Table 8.

Table 8. Support practice factor (P)

Land Use Type	Slope (%)	P factor
Agriculture Land	0-5	0.10
	5-10	0.12
	10-20	0.14
	20-30	0.19
	30-50	0.25
	50-100	0.33
Other land uses	All	1.00

(Wischmeier & Smith 1978; Bizuwerk et al. 2003; Bewket & Teferi 2009)

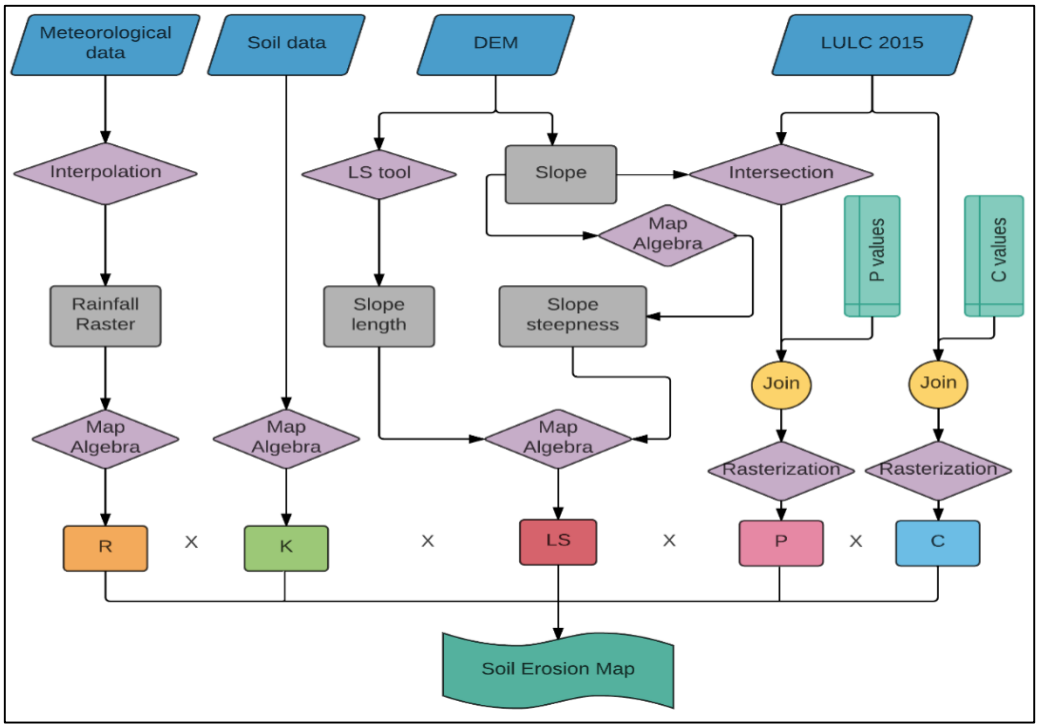

Figure 10. General workflow of soil erosion model[4]

3.3.2. Developing Chemical Degradation Indicators

"Chemical degradation of a soil refers to the undesirable changes in soil chemical behavior so that the quality of soil declines due to human interventions"(Osman 2013, 125). The most important indicators of chemical degradation vulnerability are losses of organic matter, acidity,

[4] The flow charts are prepared using Lucidchart at www.lucidchart.com

salinity and sodicity (Abrol et al. 1988; Oldeman 1994; Osman 2013). In this section, these indicators and their representation are outlined.

Organic matter in the soil comprises living and dead organic materials. Organic matter is a vital constitute of soil which has an impact on its functioning (Osman 2012). Loss of organic matter may happen as a result of the continuous cultivation of areas with low or medium fertile soils without the addition of fertilizers. It may also happen due to deforestation (Oldeman 1994). The soil organic matter content map has been derived from soil organic carbon obtained from Hengl et al. (2015). It is assumed that soil organic matter contains 58% organic carbon, so that it can be calculated using map algebra following Equation 14 (Combs & Nathan 1998).

$$\text{Percentage of organic matter} = \text{Percentage of total organic carbon} \times 1.72, \quad (14)$$

The organic matter is classified according to FAO classes used to characterize soils in Ethiopian into four categories. The classes are 0-1, 1-3, 3-10 and greater than 10, corresponds for very low, low, moderate and high soil organic matter respectively (FAO l984).

Soil salinity characterize soils based on its soluble salt content (Abrol et al. 1988). Salinity may occur in different climatic conditions. In arid areas, salinity is mainly a result of water shortage and high evapotranspiration. In humid areas, it may occur as a result of increasing groundwater table due to excessive discharge from mismanaged irrigation activities. It may also happen due to poor drainage condition of an area (Oldeman 1994; Osman 2013).

Table 9. Standard classes of soil salinity based on EC values

Electrical conductivity (dS/m)	Soil Salinity Class
0-2	Non-saline
2-4	Slightly saline
4-8	Moderately saline
8-16	Strongly saline
> 16	Very strongly saline

Source: (Nachtergaele et al. 2008)

Soil salinity highly affects the growth and yields of plants (Osman 2013). Salinity can be determined from electrical conductivity (EC) measurements in soil saturated in water (Abrol et al. 1988). It is expressed as deciSiemens per meter (dS/m). The soil electrical conductivity map

obtained from Hengl et al. (2015) in raster format was reclassified based on the value ranges given in Table 9.

Soil acidity is another important indicator of chemical soil degradation. Acidity may be caused by natural factors like weathering process or manmade factors such as the application of chemical fertilizers. It may also happen as a result of erosion (Osman 2013). The extreme acid in soil results in deficiency or unavailability of important nutrients such as magnesium, phosphorous, calcium, etc. Soil acidity may cause a reduction in crop productivity and increases dependency on chemical fertilizers (Osman 2013).

Table 10. Classes of soil acidity levels

Soil PH	Description
< 5.5	Acid soils
5.5 - 6.7	Slightly acid soils
6.7 -7.3	Neutral soils
7.3 - 8.0	Slightly alkaline soils
> 8.0	Very alkaline soils

Source: FAO (1984)

pH is the measurement of acidity from solution soil in water (Nachtergaele et al. 2008). In order to identify the status of acidity in the Beshilo basin, the soil pH raster data developed by Hengl et al. (2015) has been used. The acidity map has been classified based on the class ranges of FAO (1984) used to classify soil acidity in Ethiopia (Table 10). The descriptions for the soil pH classes in Table 10 are based on Nachtergaele et al. (2008) and Jensen (2010).

Sodicty occurs as a result of high amount of exchangeable sodium. It has a significant influence on the soils physical as well as nutritional properties. Its effect includes a reduction in permeability of water and air which may cause the total hindrance of plant growth (Abrol et al. 1988). The exchangeable sodium percentage can be used to determine the level of sodicity in soil (Nachtergaele et al. 2008). Exchangeable sodium percentage (ESP) has been calculated following the formula given in Nachtergaele et al. (2008) and (Robbins 1984) using map algebra and reclassified based on Table 11.

$$ESP = Na \times 100 / CEC, \quad (15)$$

Where Na is the exchangeable sodium and CEC is the cation exchange capacity. The unit of expression for both CEC and Na is milliequivalents per 100 grams (meq/100g).

Table 11. Classes of soil sodicity based on ESP values

ESP	Percentage
Low	< 6
Moderate	6-15
High	15-25
Very High	> 25

Source: (Nachtergaele et al. 2008)

3.3.3. Population Density

Population density is one of socio-economic indicators or factors that aggravate the pressure on the land resource. As a result, it is important to consider the population density in land degradation vulnerability analysis. Population numbers were obtained with the name of the kebeles (wards) as a text file. It was imported to ArcMap and joined with the shapefiles representing kebeles. Population density for each kebele has been calculated and rasterized using the polygon to raster conversion tool in ArcGIS by setting the cell assignment type to maximum area. Then, its values were reclassified to a scale of 1 to 5 indicating very low and very high population density. In areas of high population density, the pressure on land resource is high, especially areas where livelihood is predominantly dependent on traditional agriculture like Beshilo basin. Thus, vulnerability to land degradation will also be high.

4.Results

4.1. Biophysical Indicators of Land Degradation

In this section of the study, the biophysical indicators of land degradation such as land use and land cover, vegetation cover and soil erosion were presented, and interpretation was made based on the statistics of each map.

4.1.1. Land Use and Land Cover

Land use and land cover types of Beshilo basin has been categorized into five classes for the purpose of this study. These include agricultural land, shrubland, bare land, grassland and forest areas. The classification of land use and land cover types from satellite image may depend on the purpose, nature of the study area and resolution of the satellite imagery. For instance, settlements have been classified as agricultural land for two reasons. One is that, in 1986 most houses were tukuls with the roof made up of grass and they were surrounded by cultivated land. So, they closely appear similar to cultivated land in the images. As a result, distinguishing between settlement and agriculture land from Landsat images is difficult. In addition, the area is rural and houses are dispersed and small in size, which makes it difficult to detect them from 30 meter resolution image. On the other hand, some urban areas can be identified in the 2015 image, but it may be misleading to compare with land use and land cover images classified from 1986 images. The other reason is that settlements and agricultural land, more or less, have similar impacts on land degradation in Beshilo basin and other rural areas of Ethiopia. Due to this reason, settlements have been classified as agricultural land. Similarly, rock surface and sand deposits along rivers, including watercourses are classified as bare land. Shrubland comprises of areas covered by bushes, and dispersed trees. Grassland includes grazing areas, grass and wetlands, and forest refers to areas covered by dense trees.

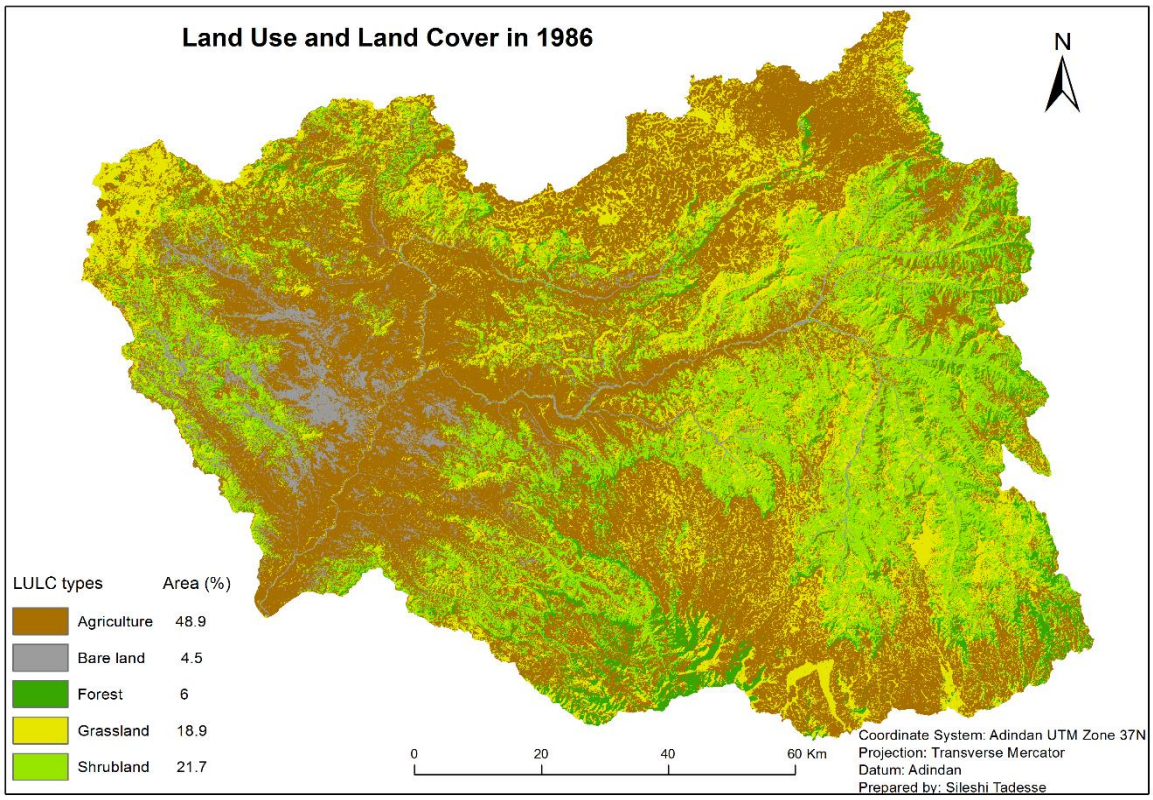

Figure 11. Land use and land cover map Beshilo basin in 1986

As seen from Table 12 and Figure 11, in 1986 agriculture was the main land use and land cover type covering 48.9% of Beshilo basin followed by shrubland and grassland, which accounts 21.7% and 18.9% respectively. As it is noted from the statistics of land use and land cover map of 2015 and Figure 12, agriculture covers more than half or 64.2% of the basin. In the same year, the area coverage of shrubland and grassland was 20.3% and 9.5% respectively.

Table 12. Area coverage of land use and land cover classes in 1986 and 2015

	1986		2015		
LULC types	Area (km^2)	Area (%)	Area (km^2)	Area (%)	Change
Agriculture	5939	48.9	7800	64.2	15.3
Bare land	549	4.5	369	3	-1.5
Forest	732	6	369.8	3	-3
Grassland	2295	18.9	1151.6	9.5	-9.4
Shrubland	2642	21.7	2466.5	20.3	-1.4
Total	12157	100	12157	100	

From this, it is clear that agriculture showed a significant increment in its spatial extent by 15.3%. Another major change that has been observed was a reduction of grassland coverage by

9.4%. All the remaining land use and land covers types also showed a decrement in their area coverage.

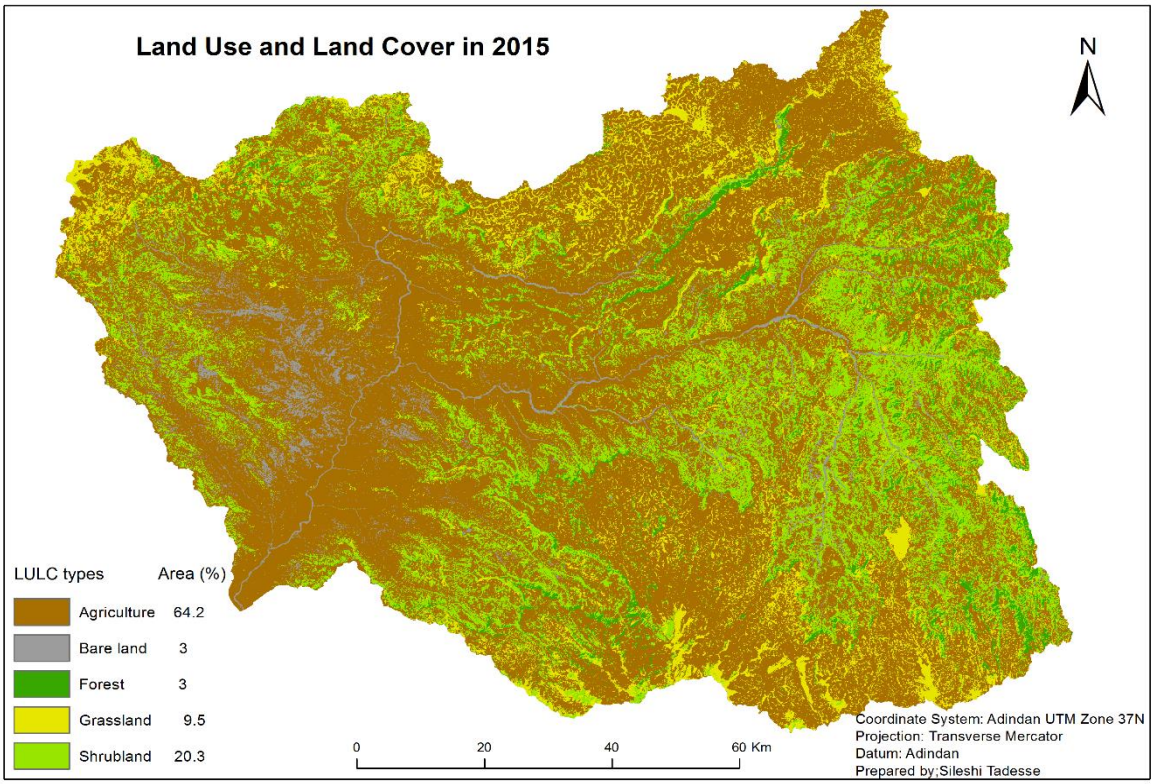

Figure 12. Land use and land cover map Beshilo basin in 2015

As seen from the change matrix in Table 13, almost 42.7% of agricultural land remained unchanged in the year 2015. Much of the gains for agricultural land are from grassland and shrubland, which accounts for about 9% and 8.6% respectively.

Table 13. Land use and land cover change matrix from 1986 to 2015

		2015 (%)					
	LULC types	Agriculture	Bare land	Forest	Grassland	Shrubland	Total
1986 (%)	Agriculture	**42.7**	0.7	1.2	1.4	2.9	48.9
	Bare land	2.4	**2**	0	0	0.1	4.5
	Forest	1.4	0	**1.5**	0.4	2.6	5.9
	Grassland	9	0.1	0.1	**7.3**	2.4	18.9
	Shrubland	8.6	0.3	0.2	0.4	**12.2**	21.7
	Total	64.1	3.1	3	9.5	20.2	100

On the other hand, about 2.9% of agricultural land was converted to shrubland. In addition, 2.4% of grassland and 2.6% of forested areas were converted to shrubland. The spatial patterns of the changes in land use and land cover can be seen in Figure 13.

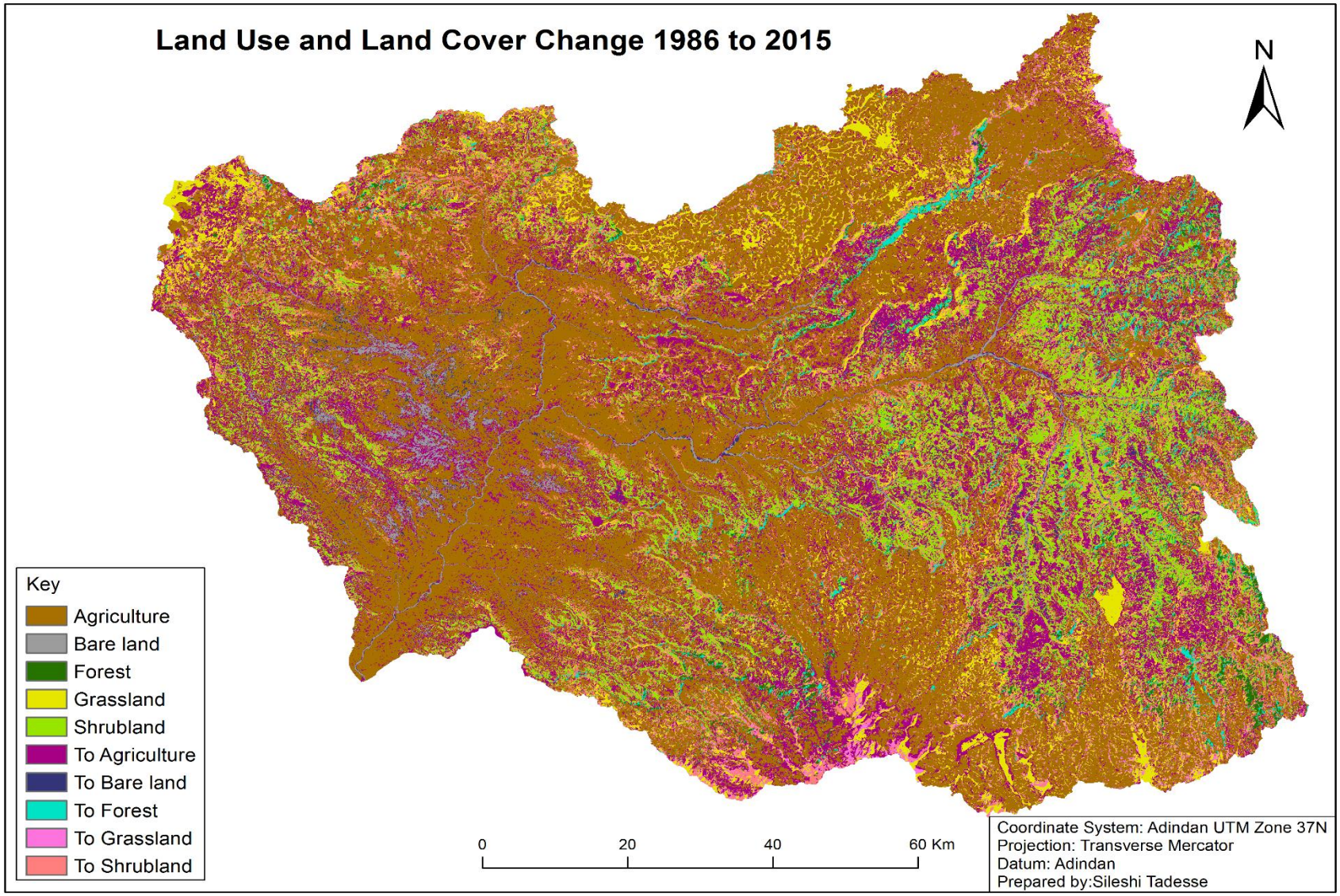

Figure 13. Land use and land cover change between 1986 and 2015

Some of the observed changes in land use and land cover would have an implication on the vulnerability of Beshilo basin to land degradation. One of the most important changes, which may have a significant impact on land degradation, is the expansion of cultivated land. This will leave the soil less covered and the increasing pressure would make it more vulnerable to degradation. The slope gradient for half of the Beshilo basin is steep and very steep, according to FAO slope classes. As it can be seen in Figure 14, the comparison of cultivated land in 1986 and 2015 across the slope gradient classes shows a substantial increment of cultivated land on steep slopes. Such expansion of cultivated land on the steep slopes would aggravate soil erosion and other forms of degradation. Cultivation on steeper slopes, particularly above 30% is not recommended because it increases the vulnerability to land degradation. Though its total coverage is small relative to other LULC types in Beshilo basin, the reduction in forest cover would also have an impact on land degradation. Forest reduces the erosivity power of rainfall and protects the surface from sheet erosion. In addition, the presence of vegetation means that the soil would have better organic matter, and becomes less erodible by water erosion.

*Table 14.*Percentage area of Beshilo basin classified into different slope gradient classes

Slope classes	Description	Area(km^2)	Area (%)
< 5	Flat to gently sloping	750	6
5 - 10	Sloping	1156	10
10 - 15	Strongly sloping	1109	9
15 - 30	Moderately steep	3075	25
30 - 60	Steep	4364	36
> 60	Very steep	1703	14
		12157	100

The slope gradient classes Table 14 are based FAO classification (FAO 2006), with slight modification by merging five narrow slope gradient classes between zero and five percent into a single class of slope < 5%.

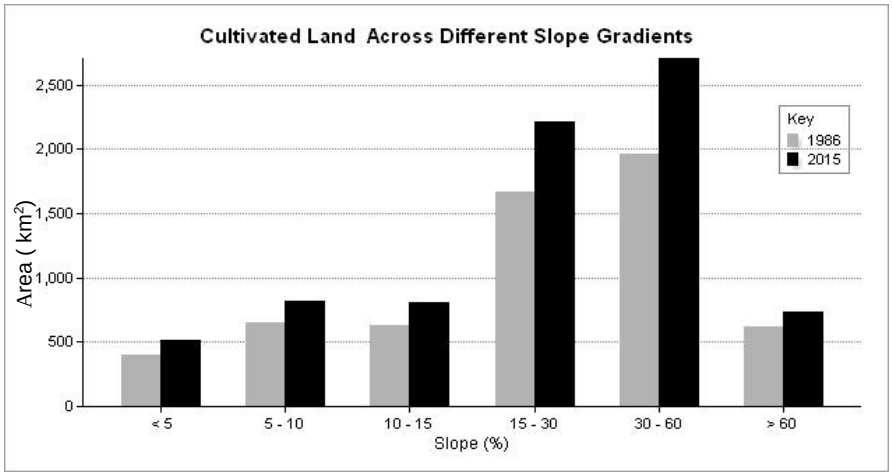

*Figure 14.*Distribution of cultivated land in 1986 and 2015 across slope gradients

4.1.2. Vegetation Cover

The soil adjusted vegetation indices were calculated from two images representing the vegetation condition in the wet (2014) and dry (2015) seasons using SAVI formula (Equation 4). The SAVI equation has been defined in the Add Function utility of the ArcGIS image analysis extension. The values of the calculated vegetation indices are dependent on the greenness or chlorophyll content, which varies in wet and dry seasons. During the rainy season, chlorophyll content is high and results high value in vegetation index, so that the area looks highly vegetated. The reverse is true in the dry season. This variation can be clearly reflected in Figure 15a & 15b. In addition to this, in the rainy season the presence of temporary grass and crops that has less protection importance from degradation, would also contribute to the high value of the vegetation index. So, taking vegetation index which is calculated only from one season will mislead or may not be appropriate in the subsequent land degradation modeling. As a result, the mean of the dry and wet season vegtation indices was calculated to create a vegetation cover map of Beshilo basin, which would be used as one indicator of land degradation in this study. The vegetation cover map was reclassified into five classes and values from 1 to 5 which correspond to very good to very poor vegetation conditions (Table 15).

Table 15. Statistics of mean soil adjusted vegetation index (SAVI)

SAVI classes	Area (km²)	Area (%)	Vegetation cover	Assigned values	Vulnerability
< 0.1	1070	8.8	Very Poor	5	Very High
01-0.2	6820	56.1	Poor	4	High
0.2-0.3	3881	31.9	Moderate	3	Medium
0.3-0.4	376	3.1	Good	2	Low
> 0.4	10	0.1	Very Good	1	Very Low
Total	12157	100			

As seen from Table 15, 8.8% and 56.1% of the basin has very poor and poor vegetation cover respectively. As it is discussed in the previous sections, areas with low vegetation cover are vulnerable for land degradation. So, based on the statistics presented in Table 15, almost 65% of the basin is susceptible to degradation vary from high to very high. A very small proportion (3.2%) of the basin has a good vegetation cover. Figure 15 shows the spatial patterns of vegetation indices in the Beshilo basin.

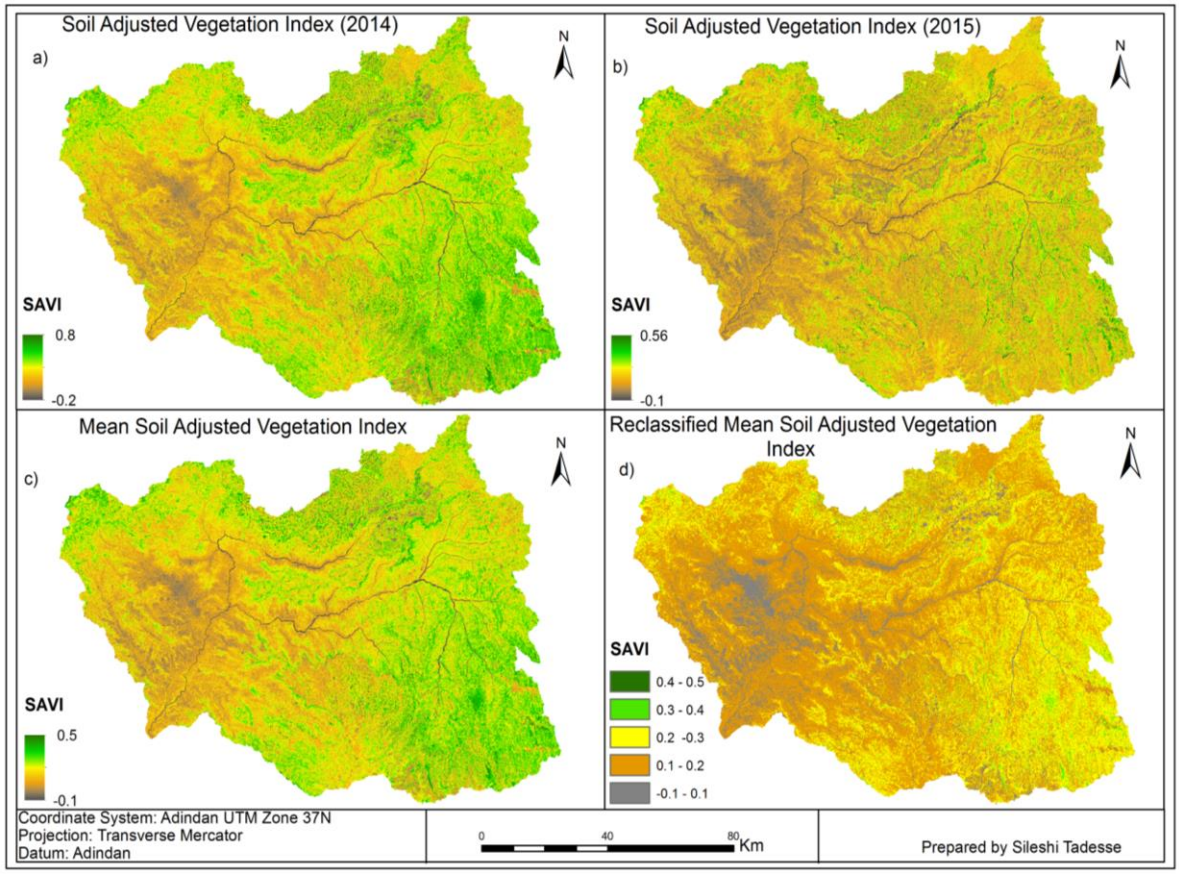

*Figure 15.*Soil Adjusted Vegetation Index maps

4.1.3. Soil Erosion

Soil erosion has been analyzed using the RUSLE model. All the factors used to estimate the annual soil loss are presented in this section.

Rainfall erosivity factor (R) was derived from a rainfall map. To develop the rainfall map of the Beshilo basin, long-term mean annual rainfall from 1992 to 2014 for twelve meteorological stations were used. The rainfall data has XY coordinate location of the stations and it was transformed to a point feature in ArcGIS (Figure 7). Then, the points were projected to Adindan UTM zone 37 coordinate system and interpolated to create a raster map of mean annual rainfall using Inverse distance weighted (IDW) technique. The result of the interpolation in Figure 16 shows that rainfall is higher in the west, northwest and southeast parts of the basin. The interpolated mean annual rainfall was used in Equation 6 to calculate the rainfall erosivity map, which is one of the input factors of RUSLE model.

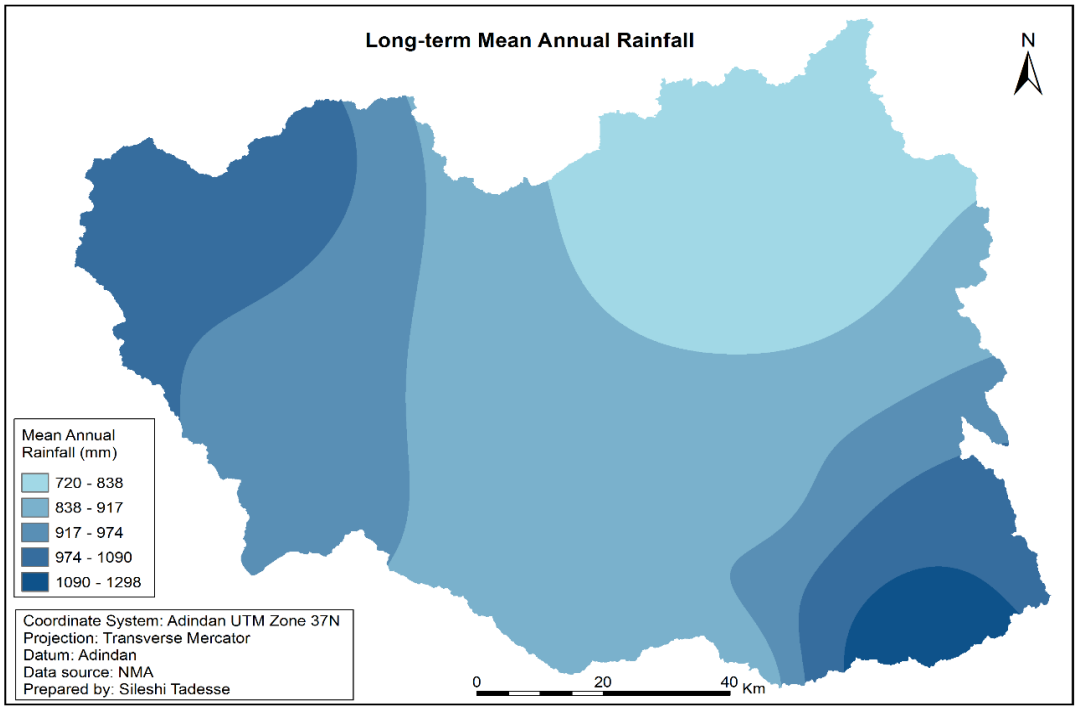

Figure 16. Mean annual rainfall map

As shown in Figure 17, the rainfall erosivity values for Beshilo basin varies between 1533 to 4083 $MJ\ mm\ ha^{-1}\ h^{-1}\ y^{-1}$. The higher the erosivity value, the more powerful the rainfall to erode the soil from the surface.

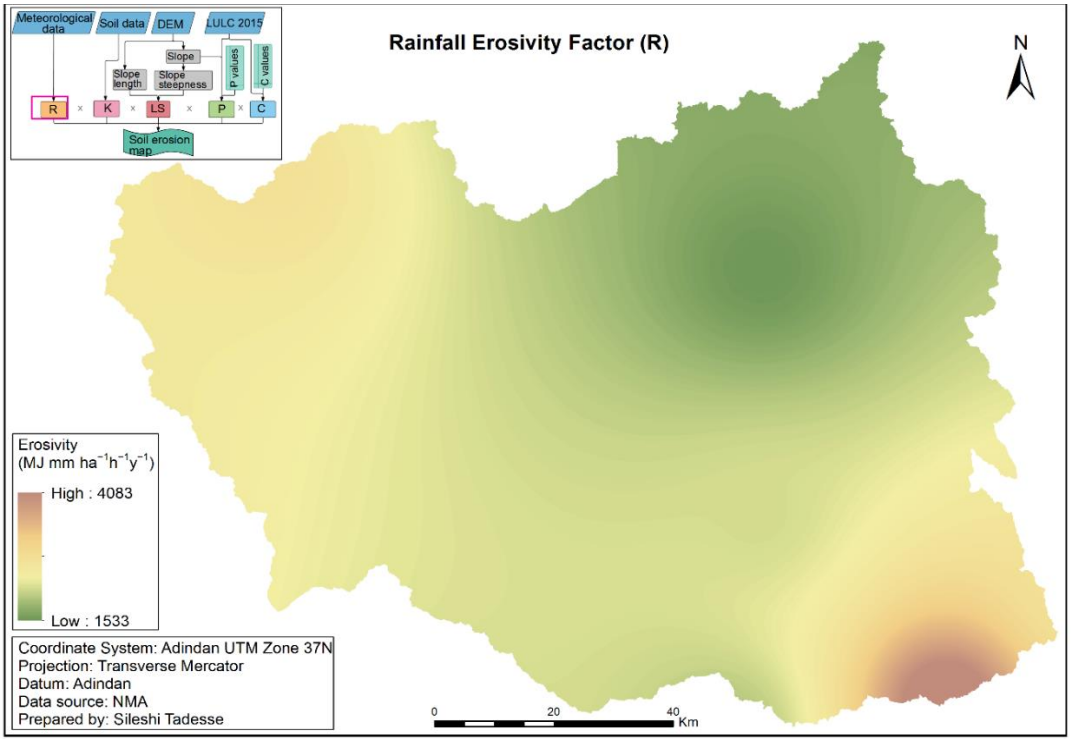

Figure 17. Rainfall erosivity factor

Soil erodibility factor (K) was developed using the Equation 8. The input datasets used to calculate the soil erodibility factor map shown in Figure 18 includes the percentage clay, silt, sand and organic carbon in the soil.

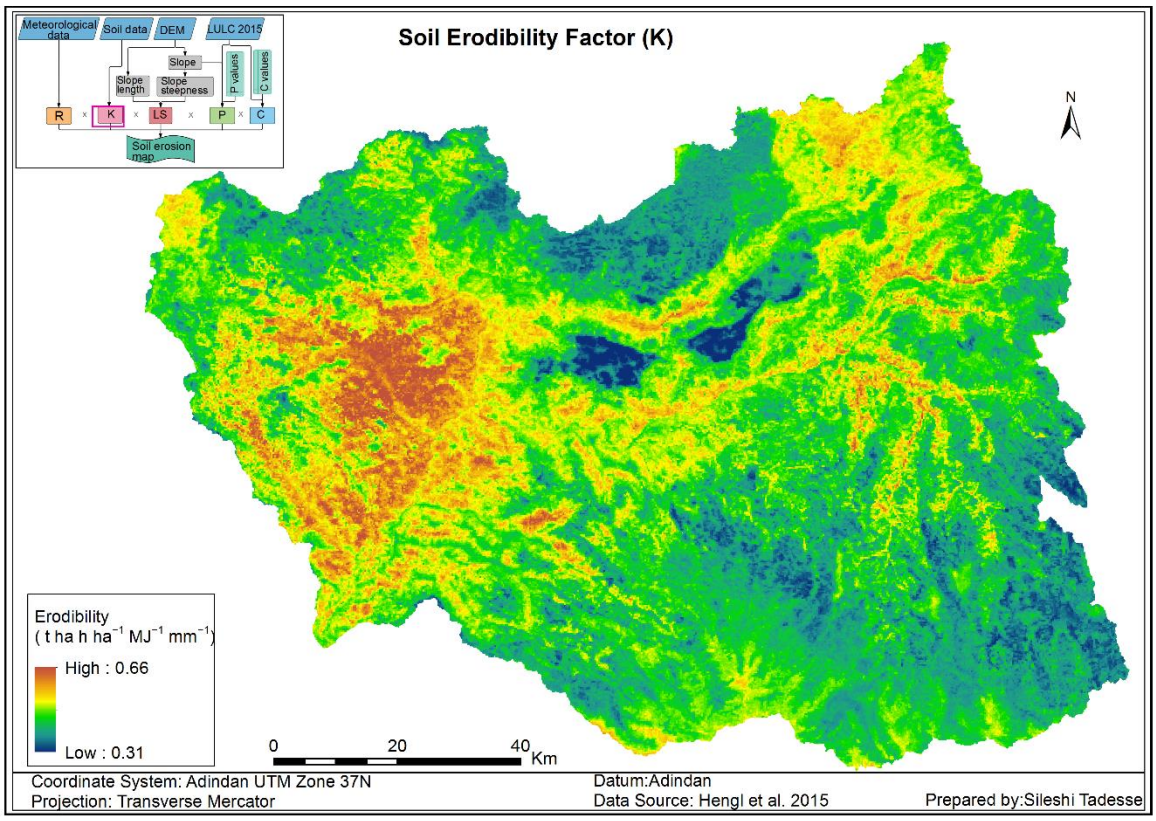

Figure 18. Soil erodibility factor map

Areas with high soil erodibility are characterized by relatively high percentage of sand and low organic carbon content in the soil. The soil properties that are used to calculate the soil erodibility can be seen in appendices B, C, D, and E.

Slope length and steepness factors (LS) are the two important features of topography used in modeling soil erosion. The slope map of the Beshilo basin used as an input to calculate slope length exponent and slope steepness is presented in Appendix F. The value of the slope length exponent (m) ranges from zero to 0.7 (Appendix G). To examine the relationship between slope gradient, slope length and slope steepness (LS) factor and slope length exponent (m), 50 sample points were generated using create random points tool and values of the aforementioned variables were extracted to the points using extract values to point in ArcGIS (Appendix J). The examination of the values presented in Appendix J shows relative increment of slope length

exponent (which is related to rill to interrill ratio) as the slope gradient increases. This means that depending on the support practice, surface cover and runoff, low slopes are predominantly susceptible to interrill erosion and rill erosion is more prevalent at higher slopes.

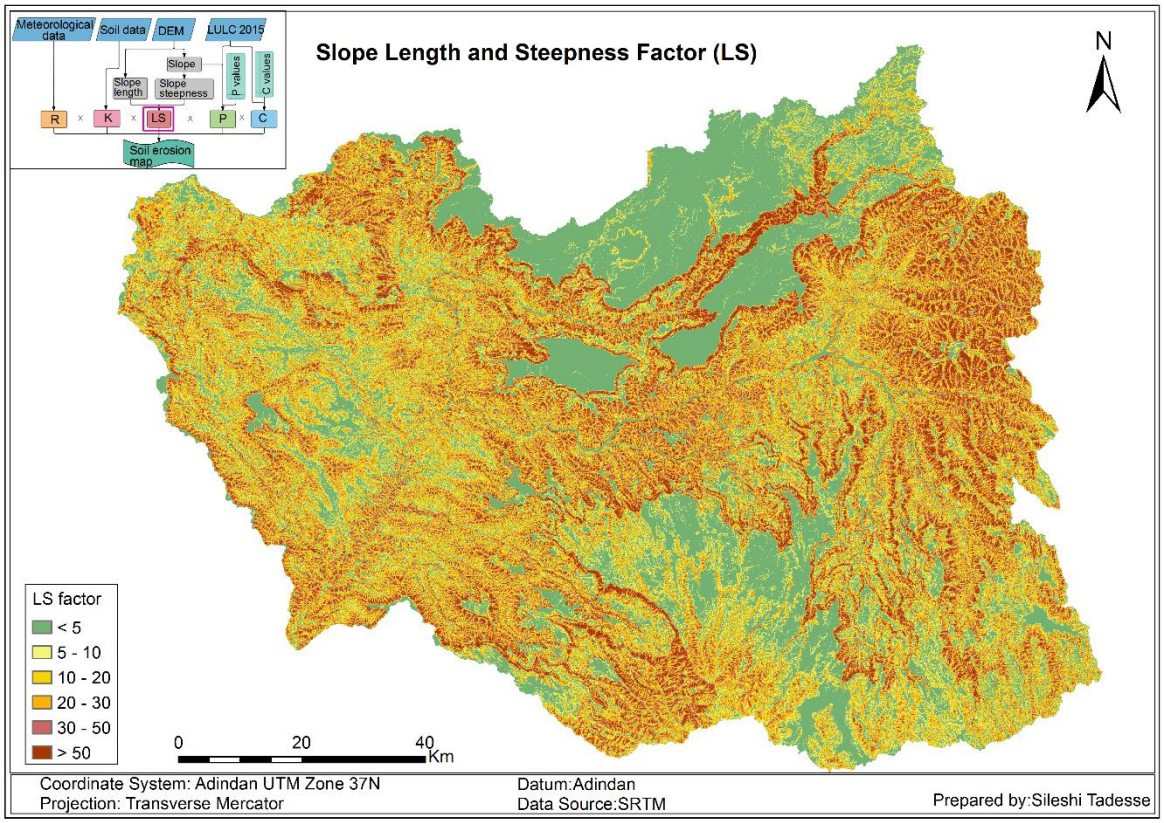

Figure 19. Slope length and steepness factor

The slope length (L) values of Beshilo basin range from 1 meter to 79 meter (Appendix H). The larger the slope length, the higher is the susceptibility to soil erosion. The steepness(S) factor value calculated based on Equation 12, varies from 0.04 to 15.6 (Appendix I). Similarly as slope length, soil erosion increases with increasing slope steepness. Slope length and steepness maps are multiplied to produce a single topographic (LS) factor of the RUSLE model (Figure 19). The higher the value of LS factor, the higher would be the susceptibility of the area to soil erosion by water.

Cover management factor (C) values for Beshilo basin ranges from 0.01 to 0.6. The small value of C factor, in this case 0.01, indicates that the area is covered by vegetation and less susceptible to soil erosion. Large values of C factor, on the other hand, indicate that the area is less covered by vegetation so that it is highly vulnerable to soil erosion. The C factor map of the basin is presented in Figure 20.

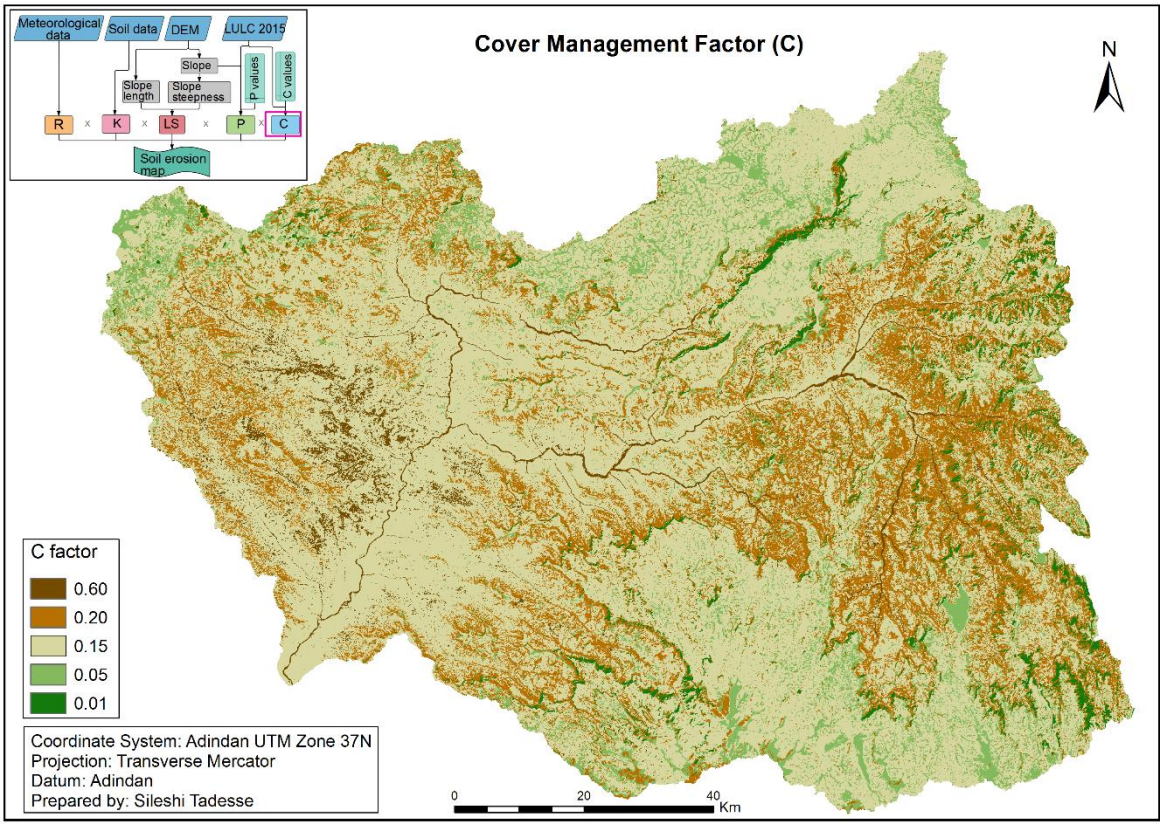

Figure 20. Cover management factor

Support practice factor (P) value varies from 0.1 to one (Figure 21). A P factor value of 0.1 is for cultivated land on flat and gentle slopes. Smaller values indicate less vulnerability to soil erosion. These areas are found at low slope gradients. As slope values increase, the P values for cultivated land increase as well. Conservation practices on cultivated land are rare. It is also not common in the other land use and land cover types, so that the P factor value set to one. The GLADIS database also confirms that land management is poor in the Beshilo basin (Nachtergaele et al. 2011).

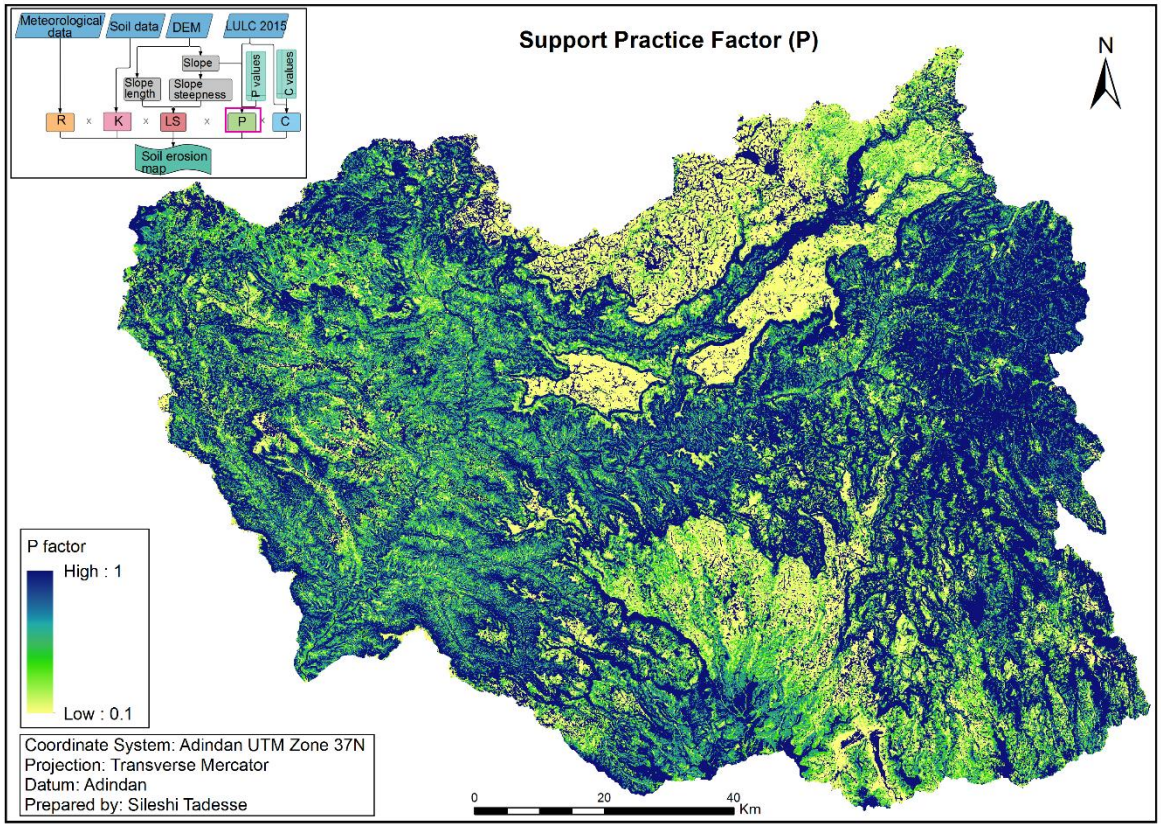

Figure 21. Support practice factor map

Annual Soil Loss has been estimated based on the five factors of RUSLE model. The results in Table 16 show that the estimated annual soil loss for about 6% of the basin is less than 10 ton/ha/yr, which is characterized as very slight soil erosion risk. The annual soil loss for about 33% of Beshilo basin varies from 10 to 150 ton/ha/yr., this is regarded as slight to moderate soil erosion risk.

Table 16. Annual soil loss class and the risk levels

Soil Loss(ton/ha/yr)	Area (km^2)	Percentage	Severity	Assigned value	Vulnerability
Less than 10	679	6	Very Slight	1	Very Low
10 – 50	1883	15	Slight	2	Low
50 – 150	2214	18	Moderate	3	Medium
150 – 300	1710	14	High	4	High
300 – 500	1597	13	Very High	5	Very High
Above 500	4075	34	Catastrophic	5	Very High

Based on the statistics in Table 16, 27% of the basin is under high to very high soil erosion risk with estimated annual soil loss of 150 to 500 ton/ ha/yr. The soil erosion risk for about 34% of Beshilo basin is catastrophic with annual soil loss of more than 500 ton/ha/yr.

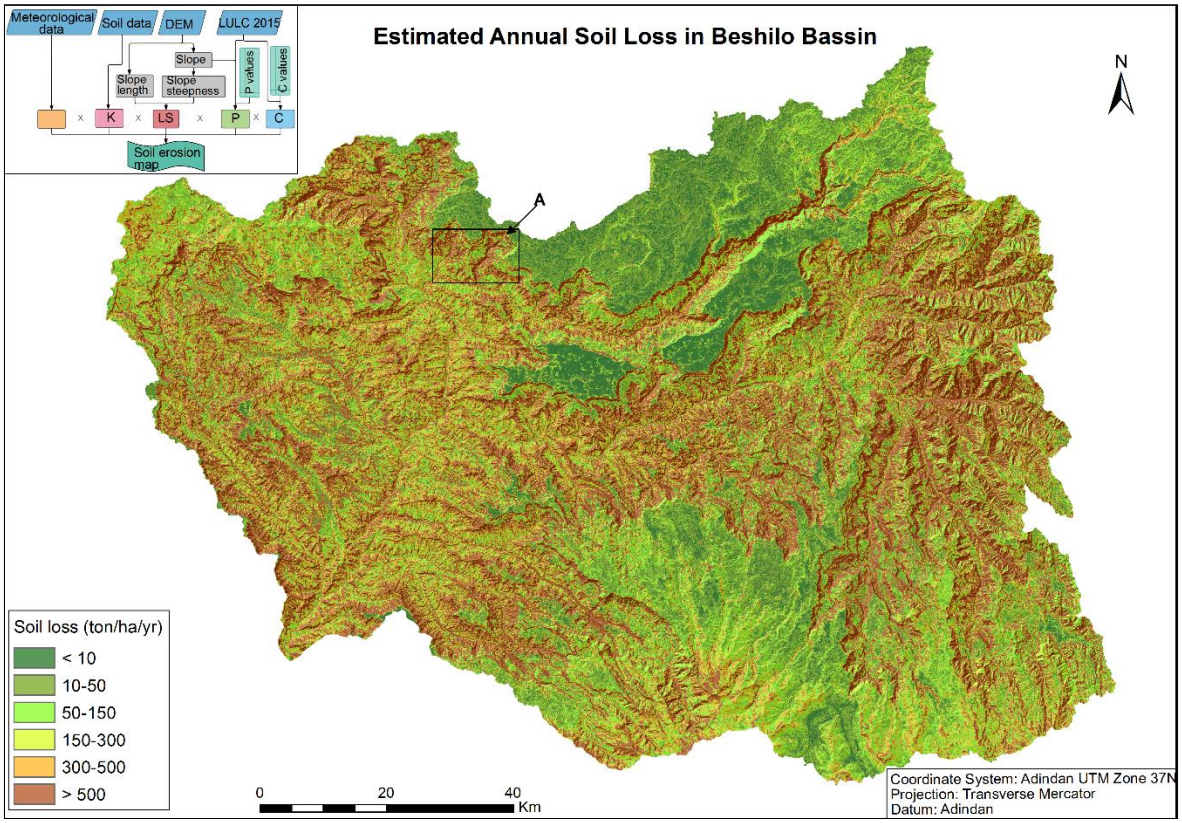

Figure 22. Estimated annual soil loss for Beshilo basin

The maps presented in this thesis are at very small scale. However, they can be printed to a better map scale. The scale of the map can be determined based on the raster cell resolution (Nagi 2010). Nagi (2010) provided the following formula for calculating map scale.

$$\text{Map Scale} = \text{Raster resolution (in meters)} * 2 * 1000, \quad (16)$$

With 30 meter resolution, the map can be presented on a medium scale map of up to 1:60,000. The area designated by letter A in Figure 22 is presented in Figure 23 to the details of the soil erosion map on a scale of 1:60,000 when printed on A4 size paper. As seen from Figure 22 and Figure 23, most areas of extreme soil erosion have steep and rugged terrain.

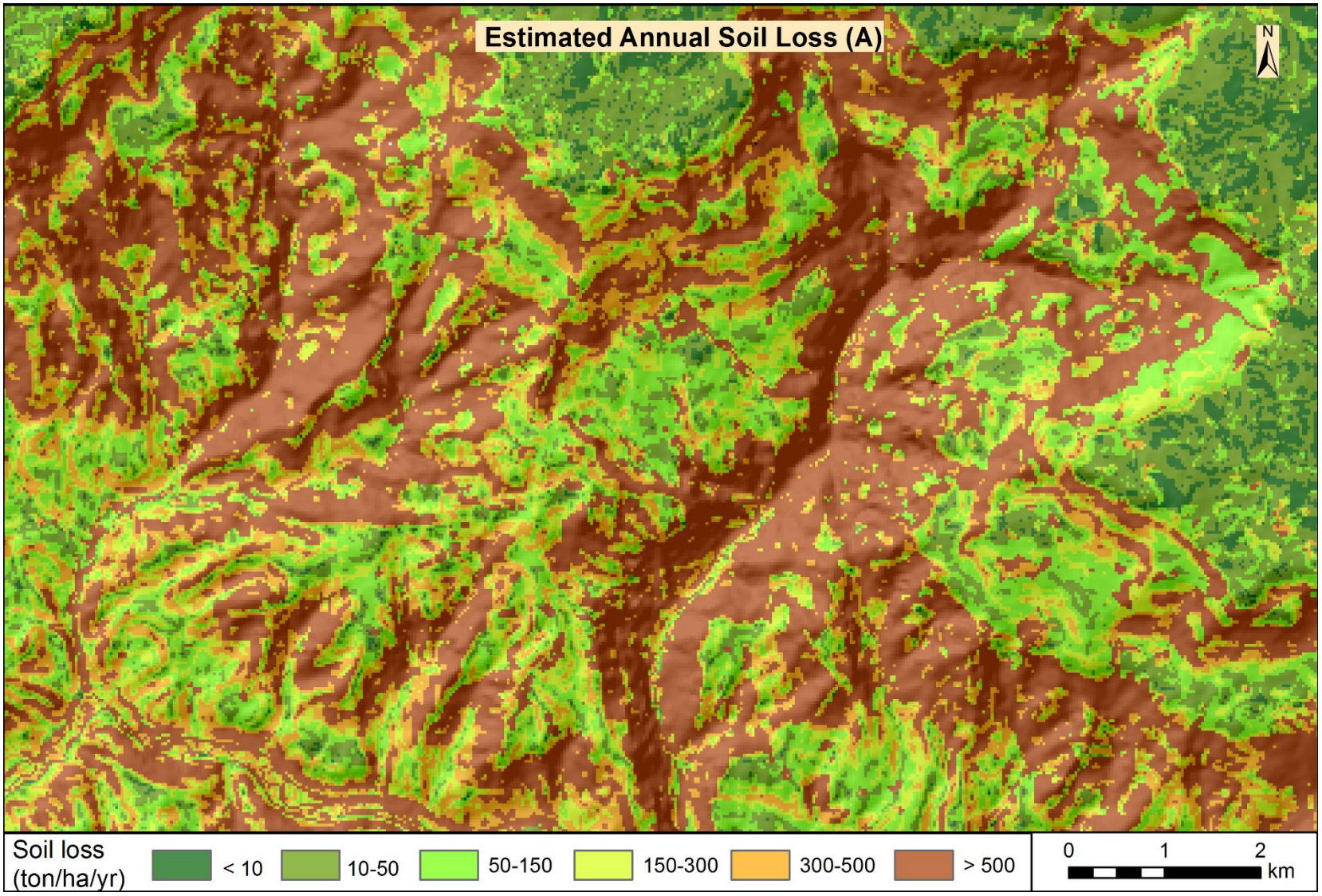

Figure 23. Subset map of annual soil loss for the area labeled by letter A in Figure 22

4.2. Chemical Soil Degradation Indicators

The soil organic matter of Beshilo basin ranges from 1% to 18% (Table 17). Table 17 shows that the soil organic matter for 50.76% of the basin is between 1% and 3%, which is low. The organic matter for 46.31% of the basin is between 3% and 10% and this was considered as the moderate soil organic matter for the study area. The rest of the basin has high soil organic matter content. Low soil organic matter indicates that the area is highly vulnerable whereas soil with high organic matter is less vulnerable. In other words, low organic matter in the soil can be the result of severe degradation while good level of organic matter can reflect better soil management and thus low level of degradation. Based on the calculated exchangeable sodium percentage, 98.8% of the basin has very low soil salinity. Soil acidity for 37% of the basin ranges from 5.5 to 6.7, which is classified as slightly acidic.

Table 17. Statistics for chemical degradation indicators

Factors	Classes	Area (km²)	Percentage (%)	Assigned value	Vulnerability
Organic matter (%)	1-3	6170	50.76	4	High
	3-10	5630	46.31	3	Medium
	10-18	357	2.94	2	Low
Salinity (electrical conductivity(dS/m))	0-2	12011	98.8	1	Very Low
	2-4	69	0.57	2	Low
	4-8	7	0.06	3	Medium
	8-16	14	0.11	4	High
	16-29	56	0.46	5	Very High
Acidity (pH)	5.5-6.7	4498	37	2	Low
	6.7-7.3	7090	58.32	1	Very Low
	7.3-7.8	568	4.67	3	Medium
Sodicity (ESP)	0-6	11517	94.74	2	Low
	6-15	525	4.32	3	Medium
	15-25	70	0.57	4	High
	25-66	44	0.36	5	Very High

As seen from Table 17 and Figure 24, the soil acidity level for about 58.32% of the basin ranges from 6.7 to 7.3, this is a class considered as neutral soil. The pH for the remaining 4.67% of the basin ranges from 7.3 to 7.8, characterized as alkaline soil. In addition, the sodicity of the soil has been determined using the electrical conductivity of the soil. As presented in Table 17, approximately 95% of the basin soil sodicity is low. The sodicity of soil for 4.32% of Beshilo basin is moderate. All the classifications of soil properties are based on the classes discussed under Section 3.3.2.

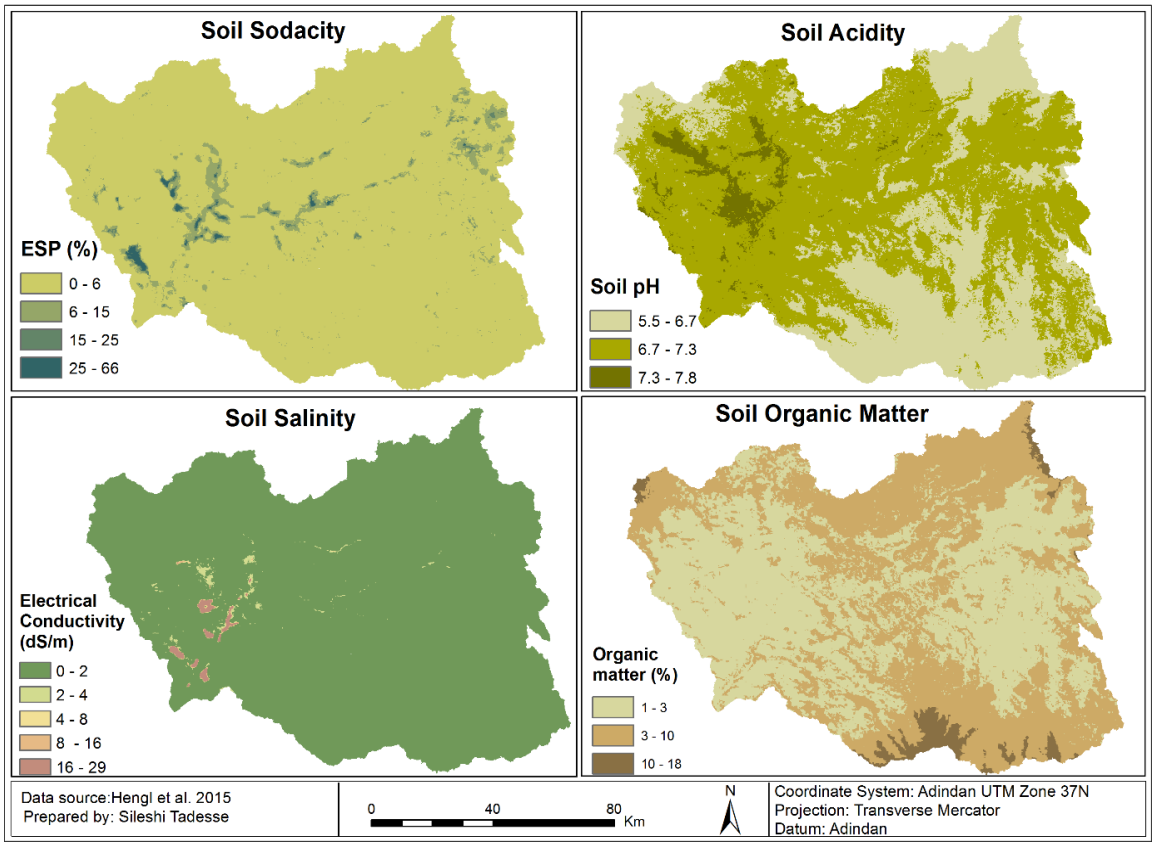

Figure 24. Chemical soil degradation indicators

4.3. Population Density

Based on the analysis of the data from CSA (2010), in the year 2007 the population of Beshilo basin and its surrounding kebeles (Figure 25) was about 1.9 million. The analysis of the population projection data obtained from the Amhara Regional State Bureau of Finance and Economic Development (BoFED n.d.), shows that the population was increased to 2.3 million in 2015 and estimated to increase to 2.8 million by 2030. The proportion of the population lived in a rural area was about 90 and 87 percent in 2007 and 2015 respectively. The livelihood of the rural population is dependent on agriculture. The mean population density of Beshilo basin and its surrounding kebeles was 207 and 264 people per square kilometer in 2007 and 2015 respectively. Based on the projected population for 2030, the population density will increase to 394 people per square kilometer. The population density map of the year 2015, calculated based on the available population projection[5] for kebeles in the Beshilo basin and its surrounding, is presented in Figure 25.

[5] Since the latest available population census was from 2007, the population density was calculated based on the 2015 population projection obtained from BoFED (n.d.)

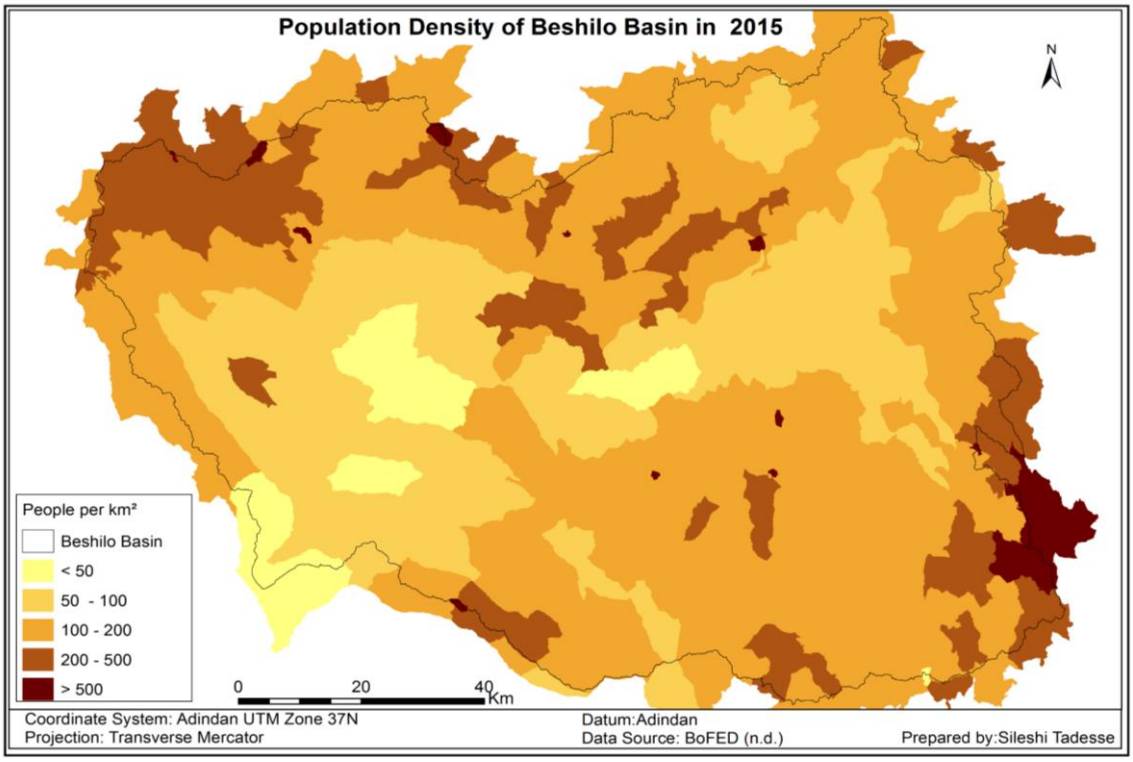

Figure 25. Population density in Beshilo basin

Table 18. Population density per square kilometer

People per km²	Area (km²)	Area (%)	Assigned value	Vulnerability
< 50	592.2	5	1	Very low
50 - 100	3528.2	29	2	Low
100 - 200	6317.4	52	3	Medium
200 - 500	1614.9	13	4	High
> 500	104.2	1	5	Very High
	12157	100		

As seen from Table 18, the population density for more than half of the study area is between 100 and 200 people per square kilometer. Twenty nine percent of the area has a low population density. Thirteen percent of the Basin has a high population density that varies between 200 and 500 people per square kilometer. High population density exerts high pressure on land resource and this increases susceptibility for degradation.

4.4. Modeling Land Degradation Vulnerability

4.4.1. Biophysical Land Degradation Vulnerability

The weights of the three indicators which contribute to the biophysical land degradation namely, soil erosion, vegetation, and land use and land cover were derived through pairwise comparison as presented in Table 19. As presented in the previous sections, the soil erosion map used as an indicator of biophysical degradation vulnerability was the output of the RUSLE model. Amede (2003) pointed that soil erosion is the main degradation agent in the Amhara region. Similarly, the analysis of this study shows that it is the most important of all indicators of biophysical degradation vulnerability in Beshilo basin. So, the weights calculated from the pairwise comparison reflect this reality. For land use and land cover, the map that was produced from the supervised classification of the 2015 Landsat 8 image was used. For vegetation cover, the mean of the wet and dry season vegetation indices were used. This is done to consider the effects of the seasonal variation of vegetation cover in the biophysical land degradation vulnerability.

Table 19. Pairwise comparison matrix for biophysical land degradation indicators

Criteria	Soil erosion	Vegetation	LULC	Criteria weights
Soil erosion	1	3	2	55
Vegetation	0.33	1	2	26
LULC	0.5	0.5	1	19

The results of the overlay analysis presented in Figure 26, shows that the biophysical degradation vulnerability for 61% of the Beshilo basin vary between high and very high. 31.8% of the basin is also moderately vulnerable. The vulnerability for the rest 7.2% of the basin is low.

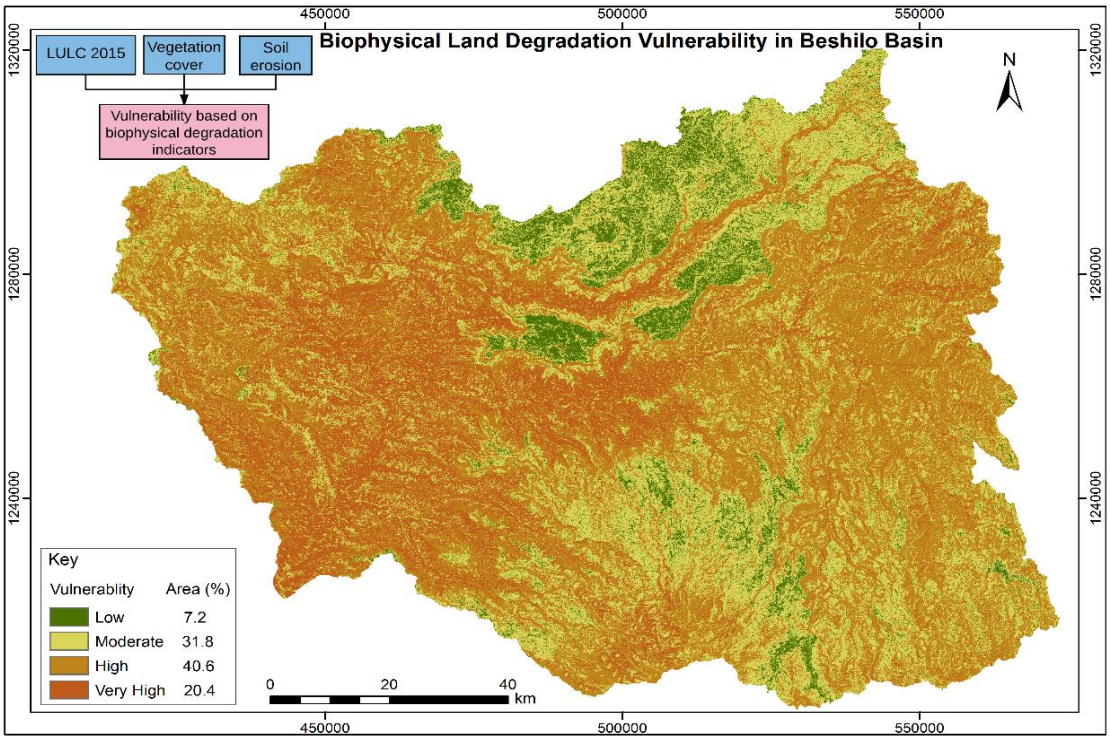

Figure 26. Biophysical land degradation vulnerability of Beshilo basin

4.4.2. Chemical Degradation Vulnerability

Similar to the biophysical degradation indicators, the weights for chemical degradation indicators were calculated using the pairwise comparison method. Based on the weights calculated through pairwise comparison matrix presented in Table 20, organic matter, salinity, acidity and sodicity are from the most to least important indicators respectively. The consistency ratio is 0.0487, which is less than one. In other words, it means that the error in the pairwise comparison matrix is less than 10%, so that it is consistent comparison.

Table 20. Pairwise comparison matrix of chemical degradation indicators

Criteria	Organic matter	Sodicty	Acidity	Salinity	Criteria weights
Organic matter	1	5	3	5	56
Sodicity	0.2	1	0.33	0.33	8
Acidity	0.33	3	1	2	22
Salinity	0.2	3	0.5	1	14

As the overlay result of chemical degradation indicators presented in Figure 27, shows that the vulnerability status for 48.76% of the Beshilo basin is low. The chemical degradation vulnerability for 50.87% of the basin is moderate. Very small portion (0.35%) in the western part the basin falls under the high chemical degradation vulnerability class.

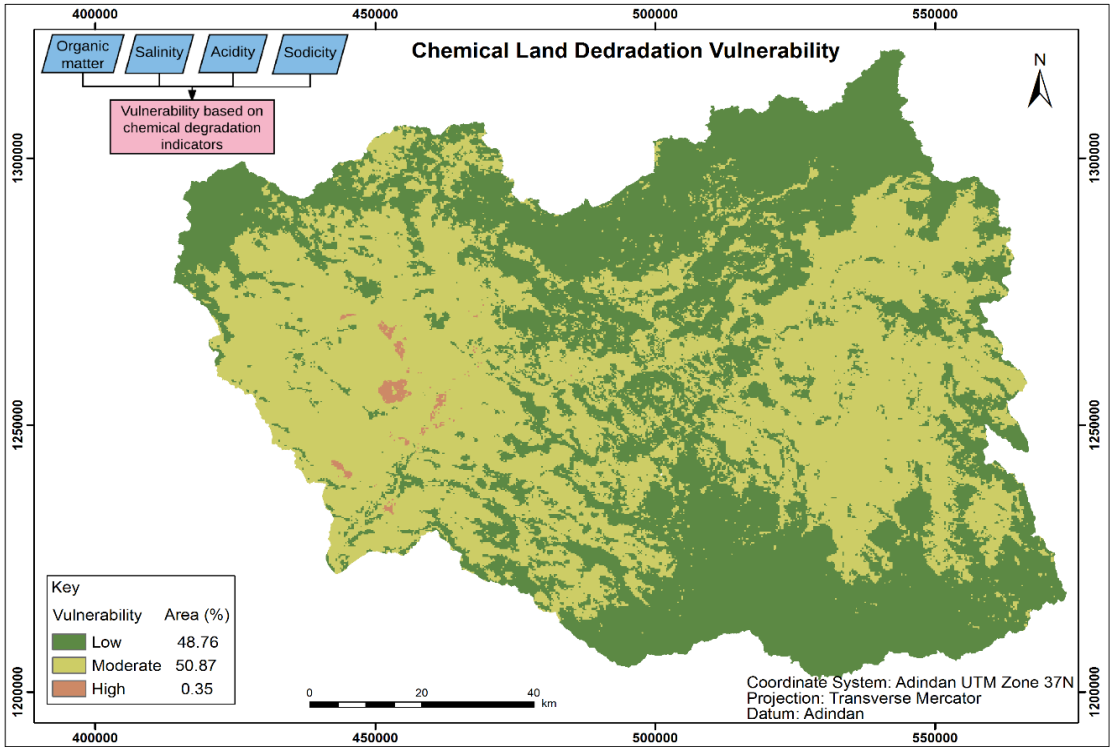

Figure 27. Chemical land degradation vulnerability of Beshilo basin

4.4.3. Land Degradation Vulnerability Index

The final land degradation vulnerability index map was developed through the integration of biophysical degradation vulnerability index, chemical degradation vulnerability index and reclassified population density map. As seen from the pairwise comparison matrix shown in Table 21, the biophysical degradation vulnerability is the most important index with a weight of 63%. Following the biophysical degradation vulnerability index is the chemical degradation index and reclassified population density with 28% and 9% weight, respectively. The weights were calculated with a consistency ratio of 0.0824, which is less than 1. As described in the previous section for the pairwise comparison matrix of the chemical degradation indicators, it is considered as a consistent comparison because the errors are less than 10% (Malczewski & Rinner 2015).

Table 21. Pairwise comparison matrix for land degradation vulnerability indicators

Criteria	Biophysical degradation	Chemical degradation	Population density	Criteria weights
Biophysical degradation	1	3	5	63
Chemical degradation	0.33	1	4	28
Population density	0.2	0.25	1	9

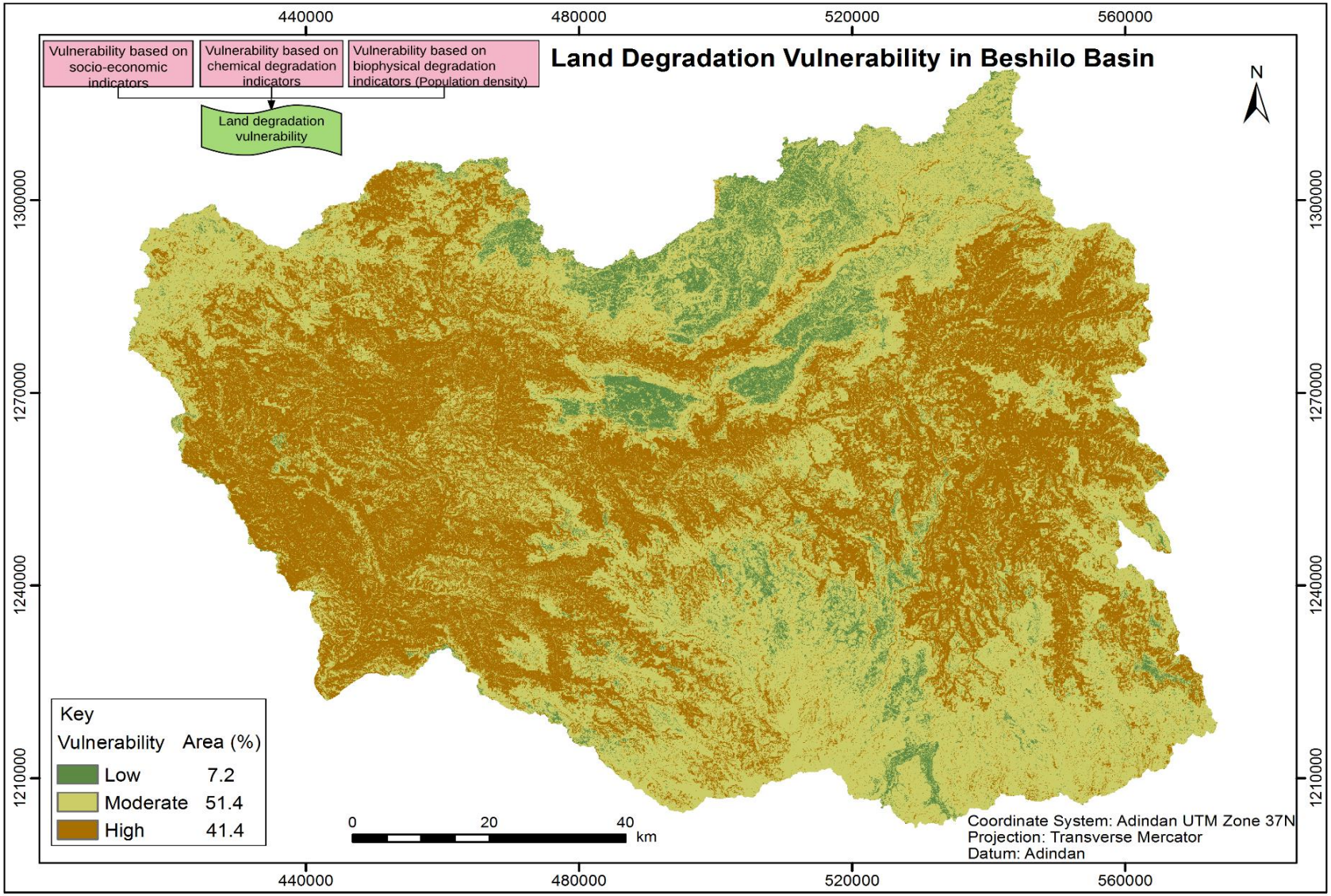

Figure 28. Land degradation vulnerability map of Beshilo basin

The weighted overlay result of biophysical vulnerability, chemical vulnerability, and population density presented in Figure 28, show that 41.4% of Beshilo basin is highly vulnerable for land degradation. In addition, 51.4% of the basin falls under the moderate land degradation vulnerability class. The vulnerability of the rest 7.2% of the Beshilo basin is low.

5.Discussion

5.1. Land Use and Land Cover

Landsat 5 TM and Landsat 8 OLI images were used to prepare land use and land cover maps of the Beshilo basin at two time spots specifically 1986 and 2015. Landsat images are useful in mapping long-term changes in land use and land cover for different reasons. These include similarity in the spatial and spectral resolution of the scenes acquired by Landsat sensors at different time spots, availability at no cost and for a long period.

Visual interpretation of Landsat images and high resolution Bing aerial image has been used as a reference to digitize an area of interests (AOI) for creating signature files. The same method has been applied to collect reference points used for the accuracy assessment of land use and land cover classification results. The overall accuracy has been evaluated using ERDAS IMAGINE 2014. The results show good level of accuracy of the LULC classification. In addition to the overall accuracy, kappa statistics which is a measure of agreement (Viera & Garrett 2005), between the classified and the reference data, has been calculated. Kappa statistics is important to check the "classification is meaningful and significantly better than a random classification" (Congalton & Green 2009, 107). The results of the Kappa statistics for both the 1986 and 2015 LULC classification are good (Table 5). As discussed in Kloditz et al. (1998), the present study also demonstrates that high resolution satellite image is a good alternative to assess the accuracy of land use and land cover maps in circumstances where field data is unavailable due to accessibility, time and financial constraints.

The results of land use and land cover classification shows that agriculture is the dominant land use type in the Beshilo basin in both 1986 and 2015. The major change observed between the study periods is also the expansion of agricultural land. Its spatial extent was increased in 2015 and covers more than half of the basin. According to Nachtergaele et al. (2011) land used for agriculture has low biodiversity than other land uses for instance, forest and shrubland. So, expansion of agriculture implies that reduction in biodiversity and this could be considered as an indicator of vulnerability for degradation. Moreover, as the analysis of agricultural land across the different slope gradient shows, there is more land utilized for agriculture on steep slopes in 2015 than 1986. This could be further evidence for the negative implications that the expansion of agricultural land would have on the vulnerability of Beshilo basin to land degradation.

5.2. Soil Erosion Model

Modeling soil erosion using RUSLE utilizes the basic factors that govern the erosion process such as, climate, topographic, soil, land cover, and land management. The outcome of the model is the interplay of these factors, so that its accuracy is dependent on the quality of the input datasets, such as resolution and other properties. In this study, attempts have been made to utilize datasets with moderate resolution such as SRTM DEM to develop topography parameters, and Landsat to represent land cover and the support practice factors. In addition, the ISRIC soil database which is the best available soil data set for the study site, has been used to develop the soil erodibility map of the Beshilo basin. Though there are different internet sources of long-term climate datasets (rainfall) for instance, Climatic Research Unit (CRU) of the University of East Anglia, the resolution is very low for such kind of studies focused on the local level of land degradation vulnerability assessment. As a result, data from meteorological stations that are found within and surrounding areas of the Beshilo basin were used to develop a better representation of rainfall through inverse distance weighted interpolation.

Table 22. Comparison of the soil erosion results to GLADIS database[6]

	Area (%)		
Soil loss (ton/ha/yr)	Based on this thesis	Based on GLADIS	Severity
Less than 10	6	0	Very Slight
10 – 50	15	1	Slight
50 – 150	18	14	Moderate
150 – 300	14	39	High
300 – 500	13	45	Very High
Above 500	34	1	Catastrophic

The RUSLE model output shows that more than 61% of the Beshilo basin is vulnerable to soil erosion with severity level varying between high and catastrophic. As seen from Table 22, the classification of soil loss shows that the values are distributed across all the six classes. However, the area under the catastrophic soil loss class is relatively higher than the area under the other soil loss classes. According to the GLADIS database by Nachtergaele et al. (2011), 98% of the Beshilo basin fall under the moderate, high and very high soil erosion classes (Table 22). Because the soil erosion in GLADIS is at the global level, the comparison here is not to evaluate its accuracy. However, it is used to show how much the soil erosion is severe, even on

[6] The statistics is from the map presented in Figure 29,which is extracted from GLADIS database developed by Nachtergaele et al. (2011)

a very coarse resolution global level study. The difference in the soil erosion map from GLADIS database and from this study is mainly due to the differences in the input factors used to calculate soil loss. For instance, in the GLADIS, the cover management factor (P) is constant (0.75) for the whole of Beshilo basin, while the P factor used in this study vary from 0.1 to 1 (Figure 21). The level of detail in any GIS analysis, more or less, is dependent on scale. Studies covering the whole globe are relatively very small in map scale, they involve high level of generalization than studies at a national level. Similarly, the same level of detail cannot be expected from soil erosion assessments conducted at global and local level. So, the variations between these two maps could be seen from such perspectives. Despite the differences in the percentage of the areas categorized under each severity classes, the visual comparison show that, the spatial pattern of soil erosion in the two maps is related to some extent.

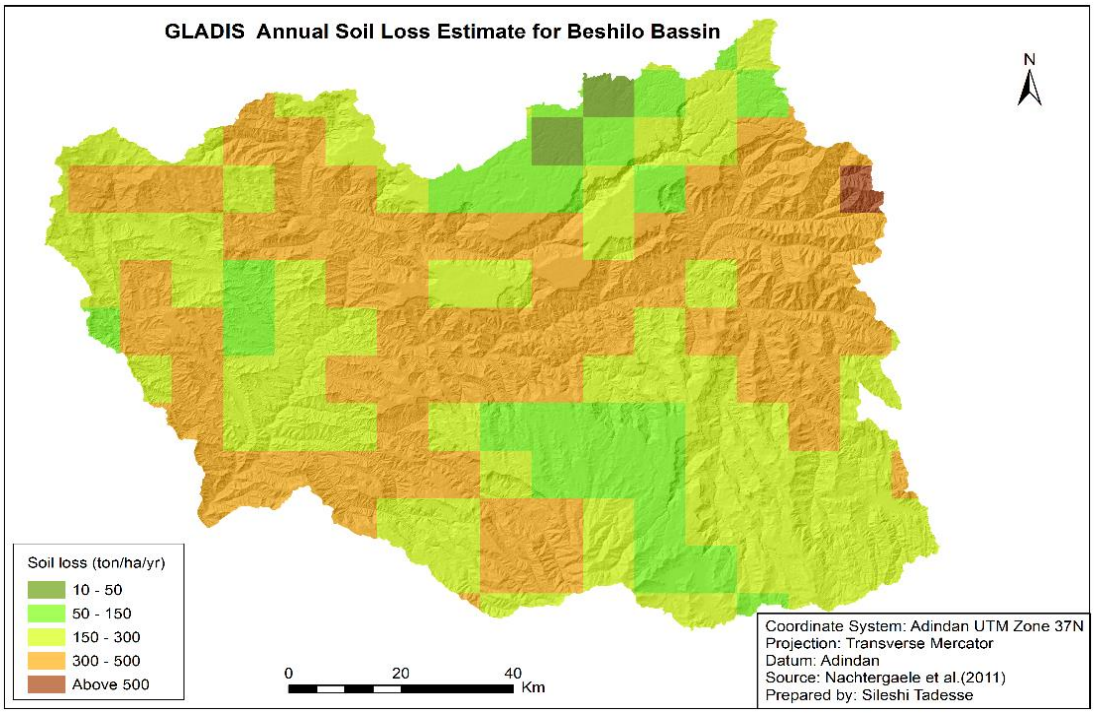

Figure 29. Annual soil loss by water erosion in Beshilo basin from GLADIS database

5.3. Land Degradation Vulnerability Model

Land degradation vulnerability is often the result of a wide range of factors. In GIS, these factors usually are represented at different measurement scales. One of the challenges in modeling land degradation vulnerability is the integration of these factors into a single index. GIS based multicriteria analysis is an important method to deal with such problem. Not all the factors contribute equally to land degradation in every place. Their contribution differs from one place

to the other depending on, for instance, economic activities (industry vs agriculture), climate condition and etc. Due to this reason, calculating weights or relative importance of each factor in Beshilo basin trough pairwise comparison method is necessary to develop land degradation vulnerability index. To make the comparison of indicators easy and to minimize problems in weighting, breaking down them into groups or parts is essential. This is also one of the main principles of AHP (analytical hierarchy process) in multicriteria analysis. The whole procedures in this study can be classified into three levels or hierarchies. The first in the hierarchy was the preparation of indicator maps and analysis of degradation based on each indicator. The Reclassify tool in ArcGIS plays a great role at this stage to reclass the indicators on a scale varying between 1 and 5, where 1 corresponds to very low and 5 to very high vulnerability. The important thing is that, there should be a reference to base the reclassification, such as standards developed by organizations or scientists. Most of the indicators are classified in this way. Reclassification plays two roles, it helps to analyze the vulnerabilities based on individual indicators by classifying their attributes into different classes, and it facilitates the integration of these indicators to produce biophysical and chemical degradation indices. The latter is important in the next stages. Second stage is categorizing indicators into biophysical, chemical and socio-economic (population density) indicators and performing pairwise comparison to calculate weights and prepare an index map for each category. The results of this stage are the biophysical degradation vulnerability index, chemical degradation vulnerability index and vulnerability based on socio-economic (population density) indicators. Population density is the only indicator in the third category due to the absence of other socio-economic datasets. Separating these land degradation vulnerabilities into categories is very helpful, for instance, in conservation as it narrows the focus or scope. Land manager can easily identify the most important land degradation vulnerability type in a specific area within the basin. So that priorities in land conservation can be given accordingly. The final stage in the analytic hierarchy process is combining the indices developed in the second stage to produce a single land degradation vulnerability map. The weights of the three indices from the second stage were calculated through pairwise comparison. So, the final land degradation vulnerability map was produced through weighted overlay. The biophysical degradation vulnerability for 61% of Beshilo basin falls under high and very high classes. About 50.87% of the basin is also moderately vulnerability for chemical degradation. The overall land degradation vulnerability result indicates that 41.4% of the Beshilo basin is highly susceptible.

6. Conclusion

Several tasks have been carried out in this study to assess land degradation vulnerability in Beshilo basin. The major tasks were land use and land cover classification and change detection, calculating vegetation indices, modeling soil erosion, developing chemical degradation indicator maps and calculating population density and multicriteria analysis. The findings of land use and land cover classification show that agriculture is the dominant land use type in Beshilo basin. The main change observed between the 1986 and 2015 was also an expansion of agricultural land at the expense of 15.3% of other land use and land cover classes. The slope analysis show that half of the basin falls under steep and very steep gradient classes. A large proportion of agricultural land is on moderately steep and steep slope gradients. Cultivation on steep slopes will aggravate land degradation processes.

The soil erosion assessment using revised universal soil loss equation (RUSLE) shows that erosion is a serious problem that affects many part of Beshilo basin. The RUSLE model takes into account the basic factors of soil erosion like topography rainfall, land cover, and land management. A good representation of these input factors is essential to employ RUSLE model effectively. In this regard, spatial data with moderate resolution, such as SRTM digital elevation model and Landsat satellite imageries obtained from USGS plays a greater role.

The spatial multicriteria analysis reveals that vulnerability to biophysical degradation varies from high to very high for 61% of the basin. Vulnerability to chemical degradation for a little bit more than half of Beshilo basin is moderate. The findings also indicate that soil erosion and organic matter are the two most important biophysical and chemical degradation indicators respectively. The result of the land degradation vulnerability model shows that the susceptibility of 41.4% of Beshilo basin is high.

Generally, the integration of GIS, RS, and multicriteria analysis provides a great utility to investigate land degradation vulnerability. The overall result of land degradation vulnerability assessment obtained from this study suggest the need for land conservation and management, especially in the vulnerable parts of the basin and detailed studies on the various aspects of land degradation are very essential. This requires the collaboration of all the stakeholders such as the government, non-governmental organizations, researchers and the farmers who are the first victims of the problem of land degradation.

References

ABB. 2007. Livelihood profile, Amhara Region, Ethiopia. http://www.heawebsite.org/download/file/fid/197 (accessed October 2015).

Abrol, I. P., Yadav, J. S. P., & Massoud, F. I. 1988. *Salt-affected Soils and Their Management.* FAO Soils Buletin No. 39. Rome: Food & Agriculture Organization.

Amede, T. 2003. Opportunities and challenges in reversing land degradation: The regional experience. Amede, T. (*ed*.) *Natural Resource Degradation and Environmental Concerns in the Amhara National Regional State*: *Impact on Food Security* 173 -183. Addis Ababa: Ethiopian Soils Science Society.

Ayalew, G. 2015. A Geographic Information System based soil loss and sediment estimation in Zingin watershed for conservation planning, highlands of Ethiopia. *World Applied Sciences Journal* 33(1), 69-79. doi: 10.5829/idosi.wasj.2015.33.01.14568

Bai, Z. G., Dent, D. L., Olsson, L., & Schaepman, M. E. 2008a. Proxy global assessment of land degradation. *Soil Use and Management 24(3),* 223-234. doi:10.1111/j.1475-2743.2008.00169.x

Bai, Z.G., Dent, D.L., Olsson, L., & Schaepman, M.E. 2008b. *Global Assessment of Land Degradation and Improvement 1: Identification by Remote Sensing*. Report 2008/01. Wageningen: ISRIC-World Soil Information.

Berry, L. 2003. Land degradation in Ethiopia: Its extent and impact. ftp://ftp.fao.org/agl/agll/ladadocs/ETHIOPIA_LD_CASE_STUDIES.doc (accessed December 2015).

Bewket, W. & Teferi, E. 2009. Assessment of soil erosion hazard and prioritization for treatment at the watershed level: case study in the Chemoga watershed, Blue Nile basin, Ethiopia. *Land Degradation & Development* 20(6)**,** 609-622.

Bizuwerk, A., Taddese G. & Getahun,Y. 2003. Application of GIS for modeling soil loss rate in Awash river basin, Ethiopia. Addis Ababa: International Livestock Research Institute (ILRI).

BoFED. n.d. *Population Projection and Administrative Boundary Shapefiles.* http://www.amharabofed.gov.et (accessed Augest 2015).

Burch, G., Graetz, D. & Noble, I. 1987. Biological and physical phenomena in land degradation. Chisholm, A. and Dumsday, R. (eds.) *Land Degradation: Problems and Policies,* 27-48. New York: Cambridge University Press.

Campbell, J. B. & Wynne, R. H. 2011. *Introduction to Remote Sensing* 5th ed. New York: Guilford Press.

CSA. 2010. *The 2007 Population and Housing Census of Ethiopia: Statistical Report for Amhara Region; Part I: Population Size and Characteristics*. Addis Ababa: Central Statistical Agency.

Chander, G. & Markham, B. 2003. Revised Landsat-5 TM radiometric calibration procedures and postcalibration dynamic ranges. *IEEE Transactions on Geoscience and Remote Sensing* 41(11)**,** 2674-2677.

Chander, G., Markham, B. L. & Helder, D. L. 2009. Summary of current radiometric calibration coefficients for Landsat MSS, TM, ETM+, and EO-1 ALI sensors. *Remote Sensing of Environment* 113(5)**,** 893-903.

Combs, S.M. & Nathan, M.V. 1998. Soil organic matter. Brown, J.R., (ed.) *Recommended Chemical Soil Test Procedures for the North Central Region*, 53-58. NCR Publication No. 221. Missouri Agricultural Experiment Station.

Congalton, R. G., & Green, K. 2009. *Assessing the Accuracy of Remotely Sensed Data: Principles and Practices* 2nd ed. Boca Raton: CRC Press.

Cooper, W. 2013. Multi-flow direction algorithms in GIS. University of Pennsylvania.

de Paz, J.M., Sánchez J. & Visconti, F. 2006. Combined use of GIS and environmental indicators for assessment of chemical, physical and biological soil degradation in a Spanish Mediterranean region. *Journal of Environmental Management* 79(2)**,** 150-162.

Dejene, A., Shishira, E. K., Yanda, P.Z., & Johnson, F.H. 1997. *Land Degradation in Tanzania: Perception from the Village*. World Bank Technical Paper No. 370. Washington: World Bank.

Desmet, P., & Govers, G. (1996). A GIS procedure for automatically calculating the USLE LS factor on topographically complex landscape units. *Journal of Soil and Water Conservation 51*(5), 427-433.

Durigon, V., Carvalho, D., Antunes, M., Oliveira, P. & Fernandes, M. 2014. NDVI time series for monitoring RUSLE cover management factor in a tropical watershed. *International Journal of Remote Sensing* 35(2)**,** 441-453.

Eastman, J.R. 2012. *IDRISI Selva Manual.* Manual Version 17, Clark University

El-Kawy, O. A., Rød, J., Ismail, H. & Suliman, A. 2011. Land use and land cover change detection in the western Nile delta of Egypt using remote sensing data. *Applied Geography* 31(2)**,** 483-494.

EPA. 2012. National Report of Ethiopia. *The United Nations Conference on Sustainable Development (Rio+20)*. Rio de Janeiro, 20-22 June 2012. Federal Democratic Republic of Ethiopia, Addis Ababa.

Eswaran, H., Lal, R. & Reich, P.F. 2001. Land degradation: an overview. Bridges, E.M., Hannam, I.D., Oldeman, L.R., Pening de Vries ,F.W.T., Scherr, S.J., & Sompatpanit,S. (eds). *Responses to Land Degradation. Proceedings of the Second International Conference on Land Degradation and Desertification* (Khon Kaen, 25-29 January 1999), 30-35. New Delhi:Oxford Press.

FAO. l984. *Assistance to Land Use Planning. Ethiopia. Land Evaluation. Part Three: Crop Environmental Requirements.*Edwards, S.B., Niemeyer, J.K.W., & Ridgway, R.B. Technical Report 5. AGOA ETH/78/003. Rome: Food and Agriculture Organization of the United Nations.

FAO. 1986. *Ethiopian Highlands Reclamation Study Ethiopia.* Final Report Vol.1. Rome: Food and Agriculture Organization of the United Nations.

FAO. 2006. *Guidelines for Soil Description* 4th ed. Rome: Food and Agriculture Organization of the United Nations.

FAO. 2007. *Land Degradation Assessment in Drylands (LADA): Biophysical Indicator Toolbox (Pressure/State)*.Technical Report 2. Food and Agriculture Organization of the United Nations.

Fonji, S. F. & Taff, G. N. 2014. Using satellite data to monitor land-use land-cover change in North-eastern Latvia. *SpringerPlus* 3(61), 1-15.

Foster, G. R., Meyer, L. D., & Onstad, C. A. 1977. A runoff erosivity factor and variable slope length exponents for soil loss estimates. *Transactions of the ASAE* 20 (4), 683-687.

Foster, G. R., Weesies, G. A., Renard, K. G.,Yoder, D.C., McCool, D.K., & Porter, J.P. 1997. Support practice factor (P). Renard, K. G., Foster, G. R., Weesies, G. A., McCool, D.K & Yoder, D.C. (eds.) *Predicting Soil Erosion by Water: A Guide to Conservation Planning with the Revised Universal Soil Loss Equation (RUSLE)*, 183-252. Washington DC: U.S. Government Printing Office.

Gilabert, M., González-Piqueras,J., Garcıa-Haro, F. & Meliá, J. 2002. A generalized soil-adjusted vegetation index. *Remote Sensing of Environment* 82(2-3)**,** 303-310

Hengl, T., Heuvelink, G.B.M., Kempen, B., Leenaars, J.G.B., Walsh, M.G., Shepherd, K.D., Sila, A., MacMillan, R., de Jesus, J.M., Tamene, L. & Tondoh, J.E. 2015. Mapping soil properties of Africa at 250 m resolution: Random forests significantly improve current predictions. *PloS ONE 10(6)*, doi: http://dx.doi.org/10.1371/journal.pone.0125814

Huete, A. R. 1988. A soil-adjusted vegetation index (SAVI). *Remote Sensing of Environment* 25(3)**,** 295-309.

Hunnes, D. 2012. Understanding rural to urban migration in Ethopia: Driving factors, analytical framework and recommendations. *J. Global. Health Perspect 2*(1), 12-31.

Hurni, H. 1988. Degradation and conservation of the resources in the Ethiopian highlands. *Mountain Research and Development* 8 (2/3), 123-130.

Hurni, H. 1998. *Agroecological Belts of Ethiopia: Explanatory Notes on Three Maps at Scale of 1:1, 000,000.* Centre for Development and Environment University of Bern: University of Bern in association with the Ministry of Agriculture, Ethiopia.

Jensen, J. R. 1996. *Introductory Digital Image Processing*: A Remote Sensing Perspective 2nd ed. Upper Saddle River: Prentice Hall.

Jensen, T. L. 2010. Soil pH and the Availability of Plant Nutrients. No.2. International Plant Nutrition Institute. http://www.ipni.net/ipniweb/pnt.nsf/0/97c1b6659f3405a28525777b0046bcb9/$FILE/Plant%20Nutrition%20Today%20Fall%202010%202.pdf (accessed February 2016).

Karaburun, A. 2010. Estimation of C factor for soil erosion modeling using NDVI in Buyukcekmece watershed. *Ozean journal of Applied Sciences* 3(1)**,** 77-85.

Khanbilvardi, R. M., Rogowski, A. S. & Miller, A. C.1984. *Rill-interrill Erosion and Deposition Model of Stripmine Hydrology*. Washington DC: U.S. Environmental Protection Agencey.

Kloditz, C., Boxtel, A. V., Carfagna, E. & Deursen, W. V. 1998. Estimating the accuracy of coarse scale classification using high scale information. *Photogrammetric Engineering and Remote Sensing* 64(2)**,** 127-132.

Lambin, E. F., · Geist, H. & Rindfuss, R.R. 2006. Introduction: Local processes with global impacts. Lambin, E. F. & Geist, H. J. (eds.) *Land-use and Land-cover Change: Local Processes and Global Impacts* 1-8. New York: Springer.

Li, J. & Heap, A.D., 2008. *A Review of Spatial Interpolation Methods for Environmental Scientists*. Geoscience Australia 2008/2003.

Lillesand, T., Kiefer, R. W. & Chipman, J. W. 2015. *Remote Sensing and Image Interpretation, 7th ed.* John Wiley & Sons.

Lin, C.Y., Lin, W.T. & Chou, W.C. 2002. Soil erosion prediction and sediment yield estimation: The Taiwan experience. *Soil and Tillage Research* 68(2)**,** 143-152.

Liu, X. 2005. Supervised classification and unsupervised classification. http://www.cfa.harvard .edu/~xliu/presentations/SRS1_project_report.PDF (accessed May 2015).

Malczewski, J. 2006. GIS-based multicriteria decision analysis: a survey of the literature. *International Journal of Geographical Information Science* 20(7)**,** 703-726.

Malczewski, J. & Rinner, C. 2015. *Multicriteria Decision Analysis in Geographic Information Science*. New York: Springer.

McCool, D. K., Foster, G. R., Mutchler, CK., & Meyer, LD. 1989. Revised slope length factor for the Universal Soil Loss Equation. *Transactions of the ASAE* 32(5), 1571-1576.

McCool, D.K., Foster, G. R., Weesies, G. A. 1997. Slope length and steepness factors (LS). Renard, K. G., Foster, G. R., Weesies, G. A., McCool, D.K & Yoder, D.C. (eds.) *Predicting Soil Erosion by Water: A Guide to Conservation Planning with the Revised Universal Soil Loss Equation (RUSLE)*, 101-142. Washington DC: U.S. Government Printing Office.

McDonagh, J., Bunning, S., McGarry, D., Liniger, H., Rioux, J., Nachtergaele, F., & Biancalani, R. 2009. *Field Manual for Local Level Land Degradation Assessment in Drylands LADA-L Part 1: Methodological Approach, Planning and Analysis*. Rome: FAO.

Microsoft Corporation and its data suppliers. 2016. Bing Maps Aerial. https://www.arcgis.com /home/item.html?id=ae8ed793f2fb4ab0be1b7638082e95b5 (accessed March 2016)

MoA. n.d. Shapefiles of Rivers. http://www.moa.gov.et (accessed Augest 2015).

Nachtergaele, F.O., Petri, M., Biancalani, R., Van Lynden, G. W., Van Lynden, G., van Velthuizen, H. & Bloise, M. 2011. *Global Land Degradation Information System (GLADIS)*: *An Information Database for Land Degradation Assessment at Global Level.* LADA Technical Report, 17. http://www.fao.org/nr/lada/index.php?option= com_docman&task=doc_download&gid=773&lang=en (accessed January 2016).

Nachtergaele, F.O., Velthuizen, H. Van, Verelst, L., Batjes, N.H., Dijkshoorn, J.A., Engelen, V.W.P. van, Fischer, G., Montanarella, L., Petri, M., Prieler, S., Teixeira, E., Wilberg, D., Shi, X. 2008. *Harmonized World Soil Database.* Version 1.0. http://www.fao.org/nr

/water/docs/Harm-World-Soil-DBv7cv.pdf (accessed November 2015).

Nagi, R. 2010. On map scale and raster resolution. https://blogs.esri.com/esri/arcgis/2010/12/12/12/on-map-scale-and-raster-resolution/ (accessed April 2016).

NASA. 2011. *Landsat7science data users handbook.* http://landsathandbook.gsfc.nasa.gov/data_properties/prog_sect6_3.html (accessed June 2016).

Nearing, M. 1997. A single, continuous function for slope steepness influence on soil loss. *Soil Science Society of America Journal 61*(3), 917-919.

Negash, M. 1989. The need for meteorological information to plan agroforestry on steep slopes in Ethiopia. Reifsnyder, W. E. & Darnhofer, T. O. (eds.) *Meteorology and Agroforestry: Proceedings of an International Workshop on Application of Meteorology to Agroforestry Systems Planning and Management.* Nairobi, 9 -13 February 1987, 181-189.

Nigussie, T. A., Fanta, A., Melesse, A. M. & Quraishi, S. 2014. Modeling rainfall erosivity from daily rainfall events, Upper Blue Nile basin, Ethiopia. Melesse, A.M., Abtew, W., Setegn, S. G. (eds.) *Nile River Basin*: *Ecohydrological Challenges, Climate Change and Hydropolitics* 307-335. New York: Springer.

NMA. n.d. *Rainfall*. http://www.ethiomet.gov.et (accessed September 2015).

Oldeman, L. 1994. The Global Extent of Soil Degradation.In *ISRIC Bi-Annual Report 1991-1992*, 19-36. Wageningen: International Soil Reference and Information Centre.

Oldeman, L., & van Lynden, G. 1996. *Revisiting the Glasod Methodology*. *Working Paper and Preprint, 96/03.* Wageningen: International Soil Reference and Information Centre.

Oldeman, L., Hakkeling, R., & Sombroek, W. 1991. World map of the status of human-induced soil degradation: an explanatory note, *second revised edition.* Wageningen: ISRIC and Nairobi: UNEP. http://www.isric.org/sites/default/files/datasets/Glasod.zip (accessed April 2016).

Oliveira, J.A., D. A., Dominguez, J. M. L., Nearing, M. A. & Oliveira, P. T. 2015. A GIS-based procedure for automatically calculating soil loss from the universal soil loss equation: GISus-M. *Applied Engineering in Agriculture* 31(6)**,** 907-917.

Osman, K. T. 2012. *Soils: Principles, Properties and Management*. New York: Springer

Osman, K. T. 2013. *Soil Degradation, Conservation and Remediation*. New York: Springer.

Prasuhn, V., Liniger, H., Gisler, S., Herweg, K., Candinas, A. & Clément, J.P. 2013 A high-resolution soil erosion risk map of Switzerland as strategic policy support system. *Land Use Policy* 32**,** 281-291. doi:10.1016/j.landusepol.2012.11.006

Qi, J., Chehbouni, A., Huete, A., Kerr, Y. & Sorooshian, S. 1994. A modified soil adjusted vegetation index. *Remote Sensing of Environment* 48(2)**,** 119-126.

Rabia, A.H. 2012a. GIS spatial modeling for land degradation assessment in Tigray, Ethiopia. *8th International Soil Science Congress on Land Degradation and Challenges in Sustainable Soil Management (Çeşme-Izmir, 15-17 May 2012),3,161-167.* Ege University.

Rabia, A.H. 2012b, Mapping soil erosion risk using RUSLE, GIS and Remote Sensing techniques, *The 4th International Congress of ECSSS, EUROSOIL on Soil Science for the Benefit of Mankind and Environment (Bari, 2-6 June 2012)*, 1082-1096.

Renard, K. G., McCool, D.K., Cooley, G.R., Foster, G. R., Istok, J.D., & Mutchler, C.K. 1997a. Rainfall-runoff erosivity factor (R). Renard, K. G., Foster, G. R., Weesies, G. A., McCool, D.K & Yoder, D.C. (eds.) *Predicting Soil Erosion by Water: A Guide to Conservation Planning with the Revised Universal Soil Loss Equation (RUSLE)*, 19-64. Washington DC: U.S. Government Printing Office.

Renard, K. G., Meyer, L.D., & Foster, G. R.,1997b. Introduction and history. Renard, K. G., Foster, G. R., Weesies, G. A., McCool, D.K & Yoder, D.C. (eds.) *Predicting Soil Erosion by Water: A Guide to Conservation Planning with the Revised Universal Soil Loss Equation (RUSLE)*, 1-18. Washington DC: U.S. Government Printing Office.

Renard, K.G., Yoder, D.C., Lightle, D. & Dabney, S. 2011. Universal soil loss equation and revised universal soil loss equation. Morgan R.P.C., & Nearing, M.A. (eds.) *Handbook of Erosion Modelling* 137-167. *Oxford: Blackwell Publishing Ltd*.

Robbins, C. W. 1984. Sodium adsorption ratio-exchangeable sodium percentage relationships in a high potassium saline-sodic soil. *Irrigation Science* 5(3)**,** 173-179.

Römkens, M.J.M., Young, R.A., Poesen, J.W.A., McCool, D.K., El-Swaify, S.A., & Bradford, J.M. 1997. Soil erodibility factor (K). Renard, K. G., Foster, G. R., Weesies, G. A., McCool, D.K & Yoder, D.C. (eds.) *Predicting Soil Erosion by Water: A Guide to Conservation Planning with the Revised Universal Soil Loss Equation (RUSLE)*, 65-100. Washington DC: U.S. Government Printing Office.

Saaty, T. L. 2008. Decision making with the analytic hierarchy process. *International Journal of Services Sciences* 1(1), 83-98.

Setegn, S. G., Srinivasan, R., Dargahi, B., Melesse, A. M., Loukas, A. G., Senay, G., & Yitayew, M. 2009. Spatial delineation of soil erosion vulnerability in the Lake Tana Basin, Ethiopia. *Hydrological Processes* 23(26), 3738-3750.

Shi, Z.H., Cai, C.F., Ding, S.W., Li, Z.X., Wang, T.W. & Sun, Z.C. 2002. Assessment of erosion risk with the RUSLE and GIS in the middle and lower reaches of Hanjiang River. *Proceedings of 12th ISCO Conference.* Beijing, 26 - 31 May 2002, 4, 73-78.

Shiferaw, B., & Holden, S. 1999. Soil erosion and smallholders' conservation decisions in the highlands of Ethiopia. *World development 27*(4), 739-752.

Singh, A. 1989. Review article digital change detection techniques using remotely-sensed data. *International Journal of Remote Sensing* 10(6)**,** 989-1003.

Smith, D. D. & Wischmeier, W. H. 1957. Factors affecting sheet and rill erosion. *Transactions, American Geophysical Union* 38(6), 889-896.

Snakin, V., Krechetov, P., Kuzovnikova, T., Alyabina, I., Gurov, A. & Stepichev, A. 1996. The system of assessment of soil degradation. *Soil Technology* 8(4), 331-343.

Song, X., Du, L., Kou, C., & Ma, Y. 2011. Assessment of soil erosion in water source area of the Danjiangkou reservoir using USLE and GIS. *Proceedings of the Second*

International Conference on Information Computing and Applications (Qinhuangdao, 28-31 October 2011), 7030, 57-64. Springer-Verlag Berlin Heidelberg.

Taddese, G. 2001. Land degradation: A challenge to Ethiopia. *Environmental management* 27**,** 815-824.

Teklu, T. 2014. Environment stress and increased vulnerability to impoverishment in rural Ethiopia: Case studies evidence. *International Journal of African Development 1*(2), 5.

Tesfa, A., & Mekuriaw, S. 2014. The Effect of Land Degradation on Farm Size Dynamics and Crop-Livestock Farming System in Ethiopia: A Review. *Open Journal of Soil Science 4*(1), 1-5

Tiani, A. M., Besa, M. C., Devisscher, T., Pavageau, C., Butterfield, R., Bharwani, S. & Bele, M. 2015. *Assessing Current Social Vulnerability to Climate Change: A Participatory Methodology*. Working Paper 169. Bogor: Center for International Forestry Research.

Tiruneh, G. & Ayalew, M. 2016. Soil loss estimation using geographic information system in enfraz watershed for soil conservation planning in highlands of Ethiopia. *International Journal of Agricultural Research Innovation and Technology* 5(2), 21-30.

Tully, K., Sullivan, C., Weil, R., & Sanchez, P. 2015. The state of soil degradation in Sub-Saharan Africa: baselines, trajectories, and solutions. *Sustainability 7*(6), 6523-6552.

UNFCCC. 2012. Slow onset events. http://unfccc.int/resource/docs/2012/tp/07.pdf (accessed April 2016).

U.S. Geological Survey. n.d. *Landsat Imageries and Shuttle Radar Topographic Mission (SRTM) Digital Elevation Model*. http://earthexplorer.usgs.gov (accessed September 2015).

U.S. Geological Survey.2015a. Landsat—Earth observation satellites: U.S. Geological Survey Fact Sheet 2015–3081. http://dx.doi.org/10.3133/fs20153081

U.S. Geological Survey.2015b. Landsat 8 (L8) data users handbook. Document Number LSDS-1574. Version 1.0. http://landsat.usgs.gov/documents/Landsat8DataUsersHandbook .pdf (accessed January 2016).

U.S. Geological Survey. 2016. *Frequently Asked Questions about the Landsat Missions*. http://landsat.usgs.gov/band_designations_landsat_satellites.php (accessed February 2016).

van der Knijff, J.M., Jones, R. J.A. & Montanarella, L. 1999. Soil Erosion Risk Assessment in Italy. European Soil Bureau, European Commission.

van der Knijff, J.M., Jones, R. J.A. & Montanarella, L. 2000. Soil Erosion Risk Assessment in Europe. European Soil Bureau, European Commission.

van Lynden, G. W.J. 2004. European and world soils: present situation and expected evolution. 1st *International Conference on Soil and Compost Eco-Biology (Leon, 15-17 September 2004)*, 55-63.

van Lynden, G. W.J. & Mantel, S. 2001. The role of GIS and remote sensing in land degradation assessment and conservation mapping: some user experiences and expectations. *International Journal of Applied Earth Observation and Geoinformation* 3**,** 61-68.

Viera, A. J. & Garrett, J. M. 2005. Understanding interobserver agreement: The kappa statistic. *Family Medicine* 37(5)**,** 360-363.

Waswa, B. S., Vlek, P. L., Tamene, L. & Okoth, P. F. 2012. Mapping land degradation patterns using NDVI as a Proxy: a case study of Kenya. *Resilience of Agricultural Systems Against Crises (Tropentag, September 19-21 2012)*, Göttingen-Kassel/Witzenhausen.

Williams, J., Jones, C. & Dyke, P. 1990. The EPIC model. Sharpley, A.N., and Williams, J.R.(eds.) *EPIC–Erosion/Productivity Impact Calculator: 1. Model Documentation*. Technical Bulletin No. 1768. U.S. Department of Agriculture.

Winchell, M.F., Jackson, S.H., Wadley, A.M., & Srinivasan, R. 2008. Extension and validation of a geographic information system-based method for calculating the revised universal soil loss equation length-slope factor for erosion risk assessments in large watersheds. *Journal of Soil and Water Conservation* 63(3), 105-111.

Wischmeier, W. H. & Smith, D. D. 1978. *Predicting Rainfall Erosion Losses: A Guide to Conservation Planning.* Agriculture Handbook No.537. Washington DC: U.S. Department of Agriculture.

World Bank. 2007. *The cost of land degradation in Ethiopia: A review of past studies*. Washington DC:World Bank. https://openknowledge.worldbank.org/handle/10986/7939 (accessed April, 2016)

Xu, L., Zhang, S., He, Z. & Guo, Y. 2009. The comparative study of three methods of remote sensing image change detection. *17th International Conference on Geoinformatics (Fairfax, VA,12-14 August 2009)*, 1-4. IEEE.

Yoder, D.C., Porter, J.P., Laflen, J.M., Simanton, J.R., Renard, K. G., McCool, D.K., & Foster, G. R. 1997. Cover-management factor (C). Renard, K. G., Foster, G. R., Weesies, G. A., McCool, D.K & Yoder, D.C. (eds.) *Predicting Soil Erosion by Water: A Guide to Conservation Planning with the Revised Universal Soil Loss Equation (RUSLE)*, 143-182. Washington DC: U.S. Government Printing Office.

Appendices

Appendix A: Meteorological stations and their mean annual rainfall

No	Station Name	X	Y	Elevation (m)	Mean annual rainfall (mm)
1	Amba Mariam	39.2	11.2	2990	901
2	Bati	40.0	11.2	1660	827
3	Combolcha	39.7	11.1	1857	1022
4	Degollo	39.3	10.4	2601	947
5	Guguftu	39.5	10.9	3431	1298
6	Kobbo	39.6	12.1	1470	681
7	Lalibela	39.0	12.0	2487	740
8	Mekane Selam	38.8	10.7	2605	881
9	Motta	37.9	11.1	2417	1173
10	Nefas Mewcha	38.5	11.7	3098	1024
11	Wegel tena	39.2	11.6	2952	720
12	Akesta	39.2	10.9	3086	843

Source: (NMA)

Appendix B: Percentage of clay in the soil

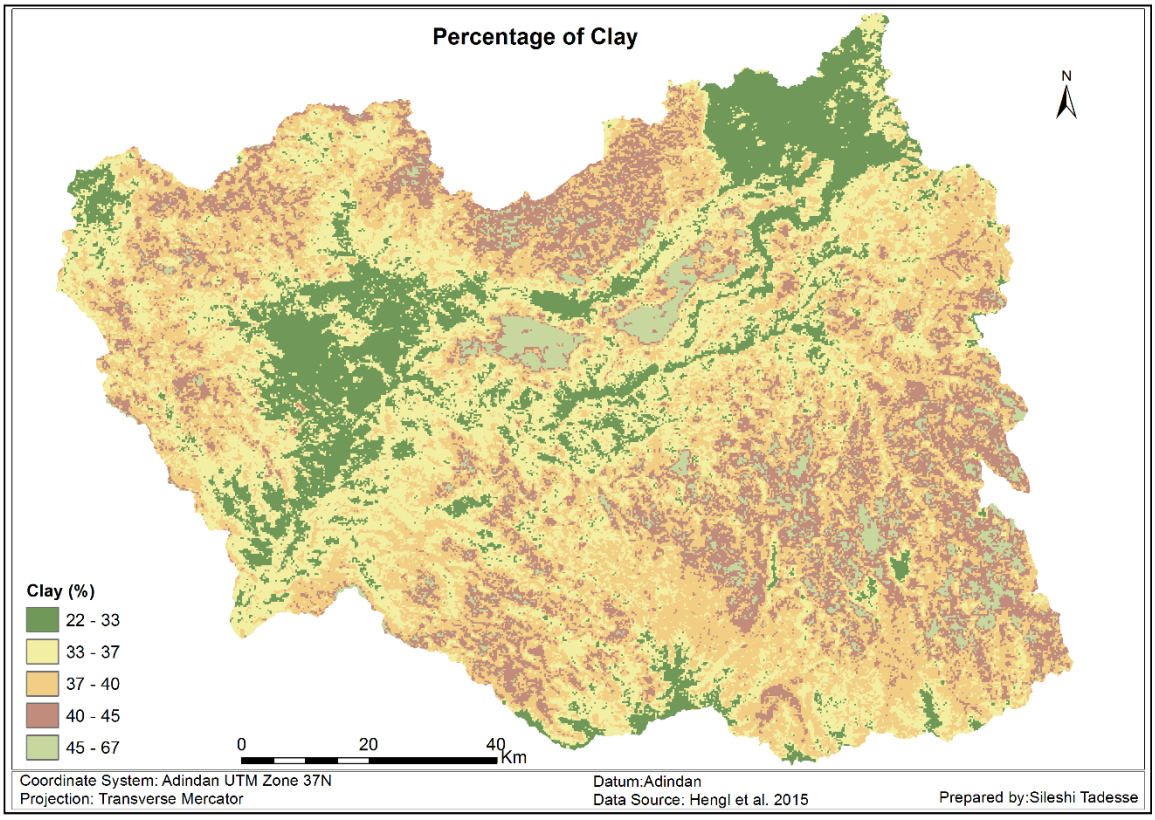

Appendix C: Percentage of silt in the soil

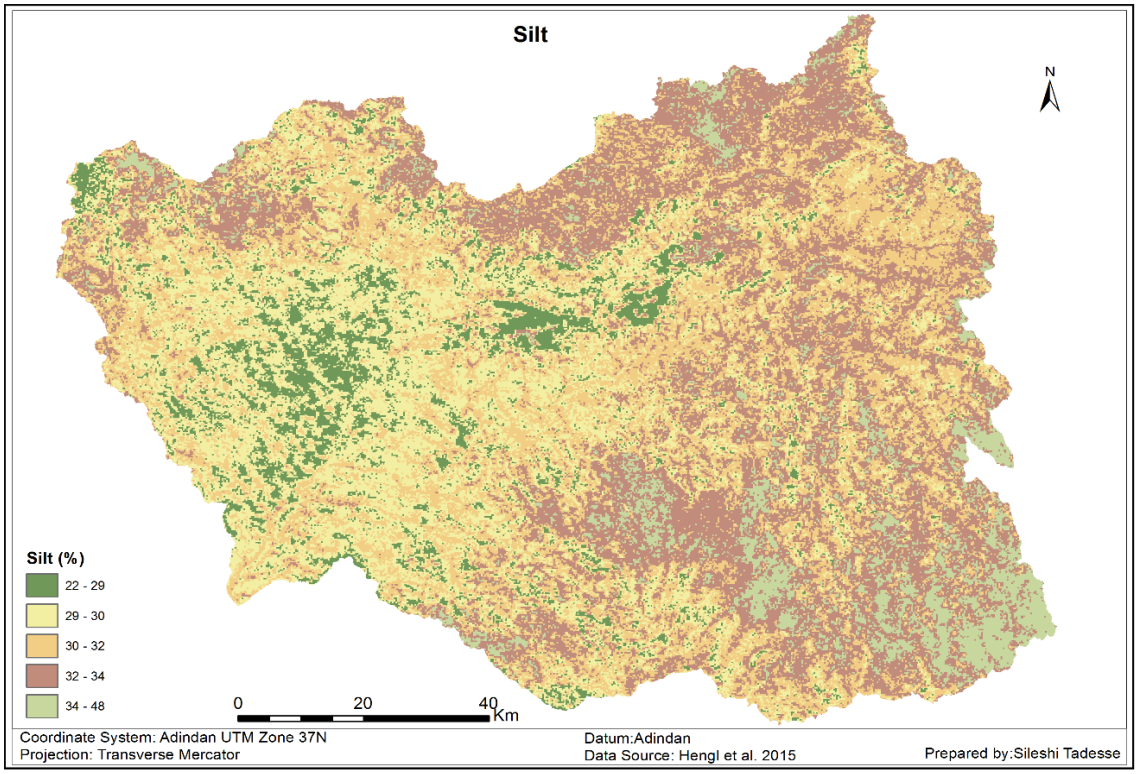

Appendix D: Percentage of sand in the soil

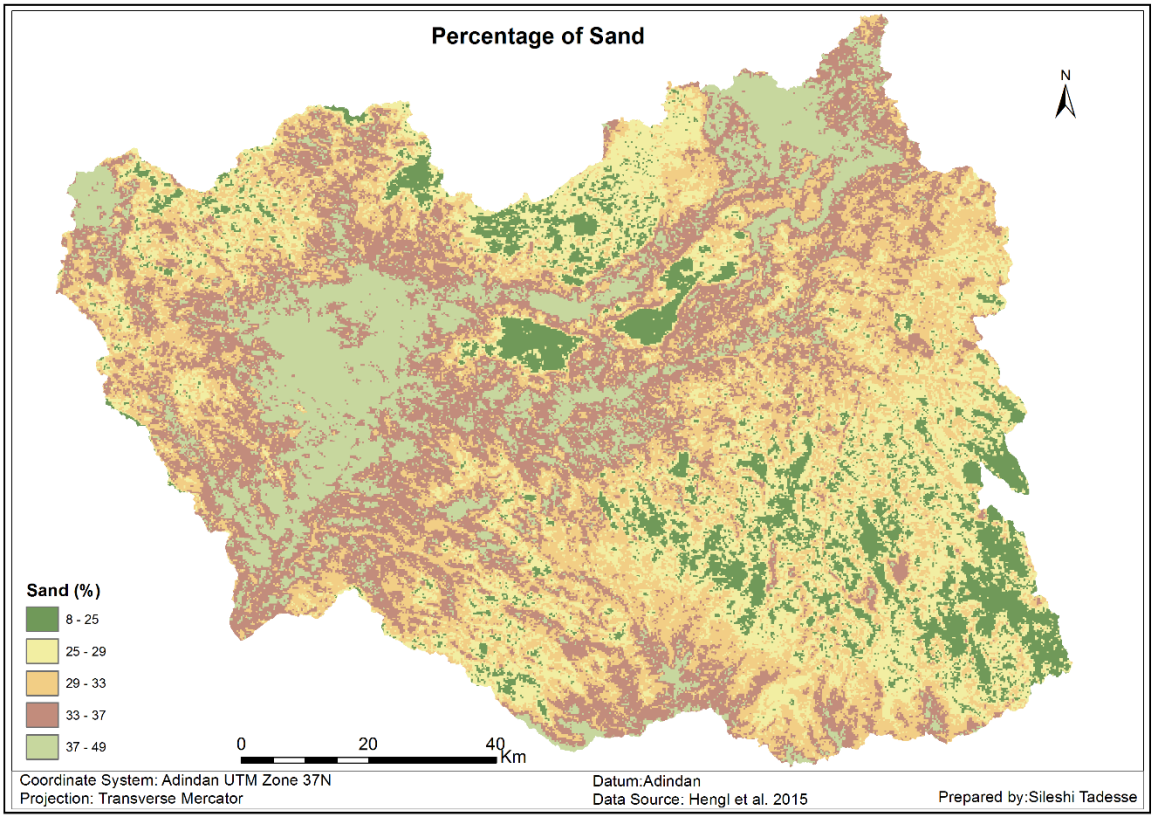

Appendix E: Soil organic carbon

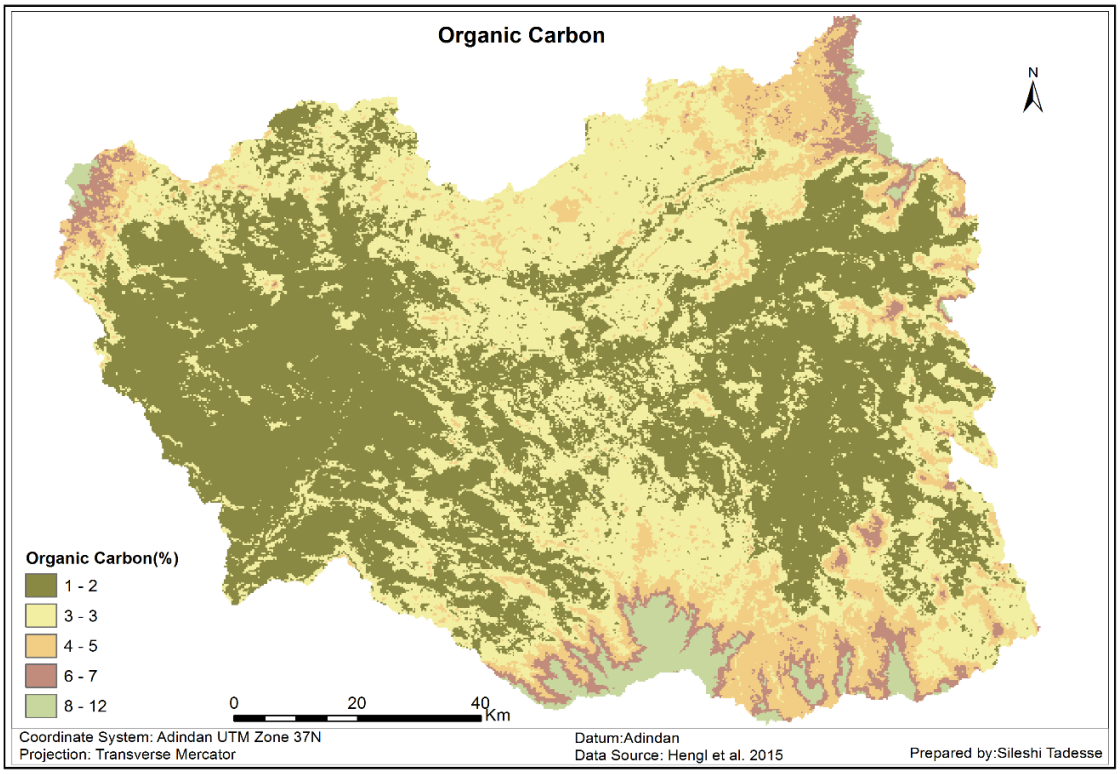

Appendix F: Slope map of Beshilo Basin

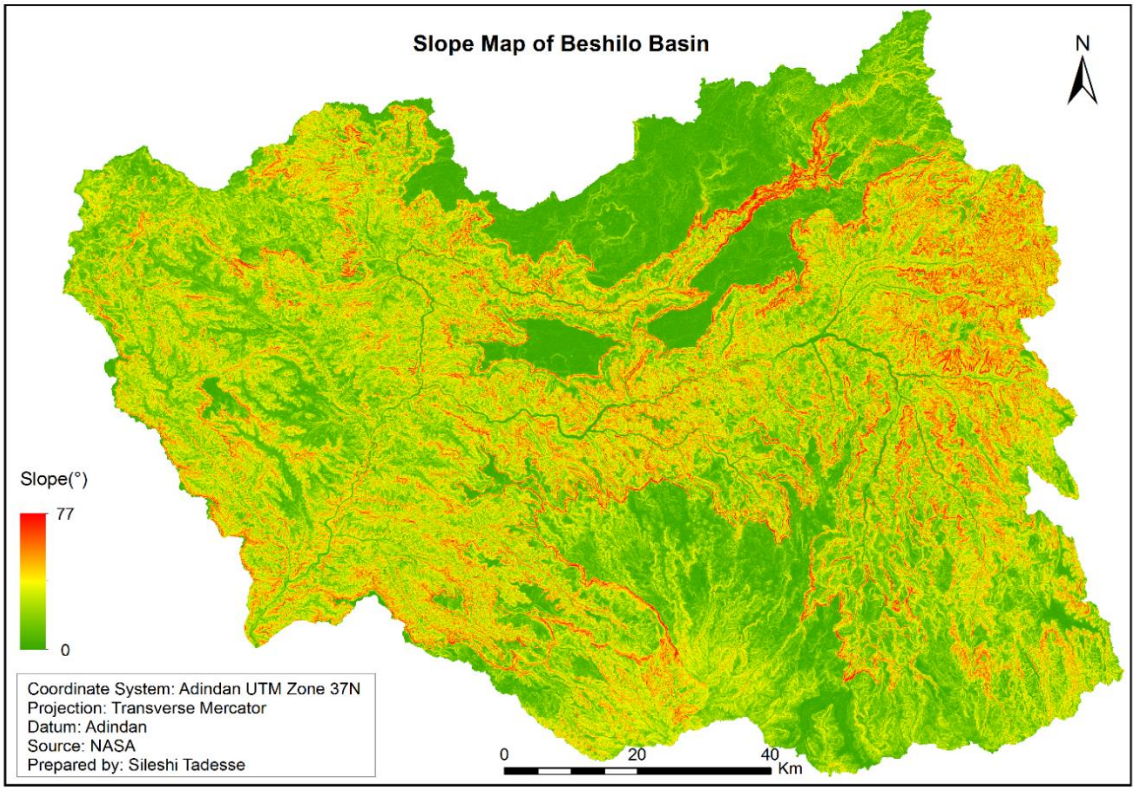

Appendix G: Slope length exponent

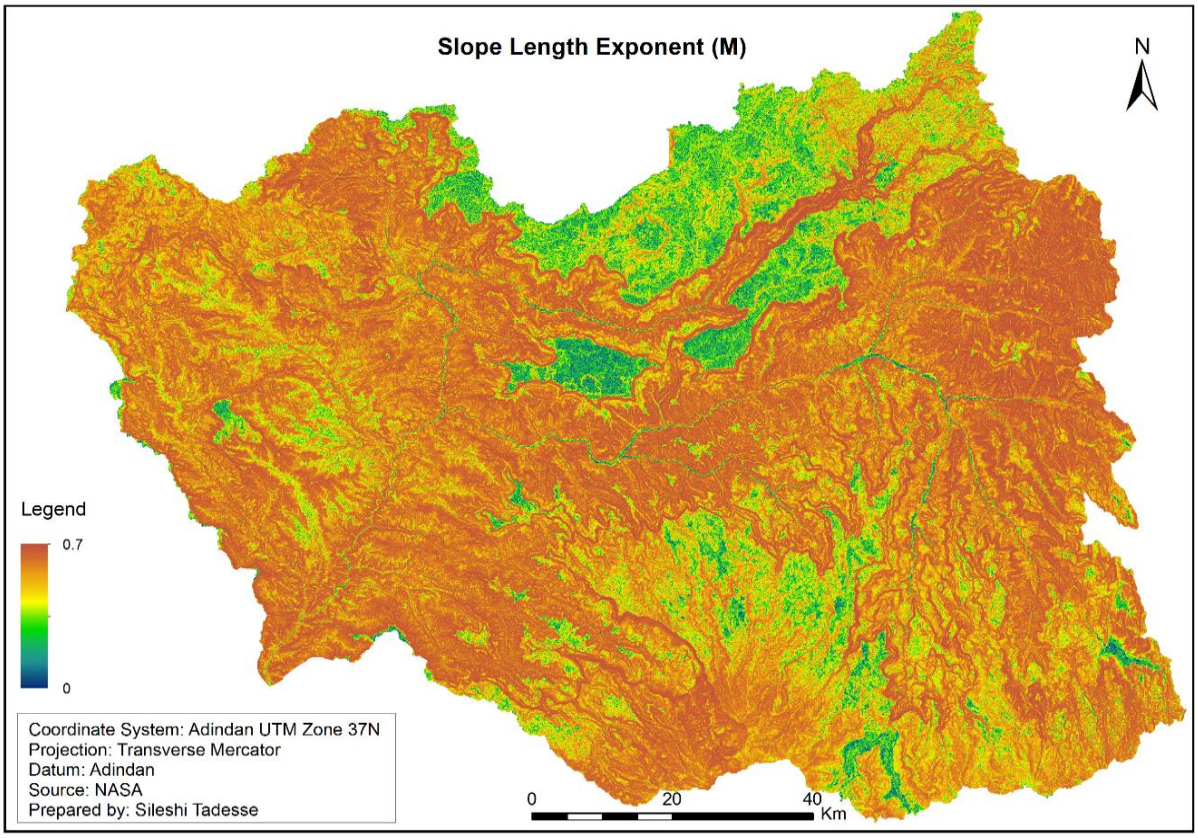

Appendix H: Slope length map of Beshilo basin

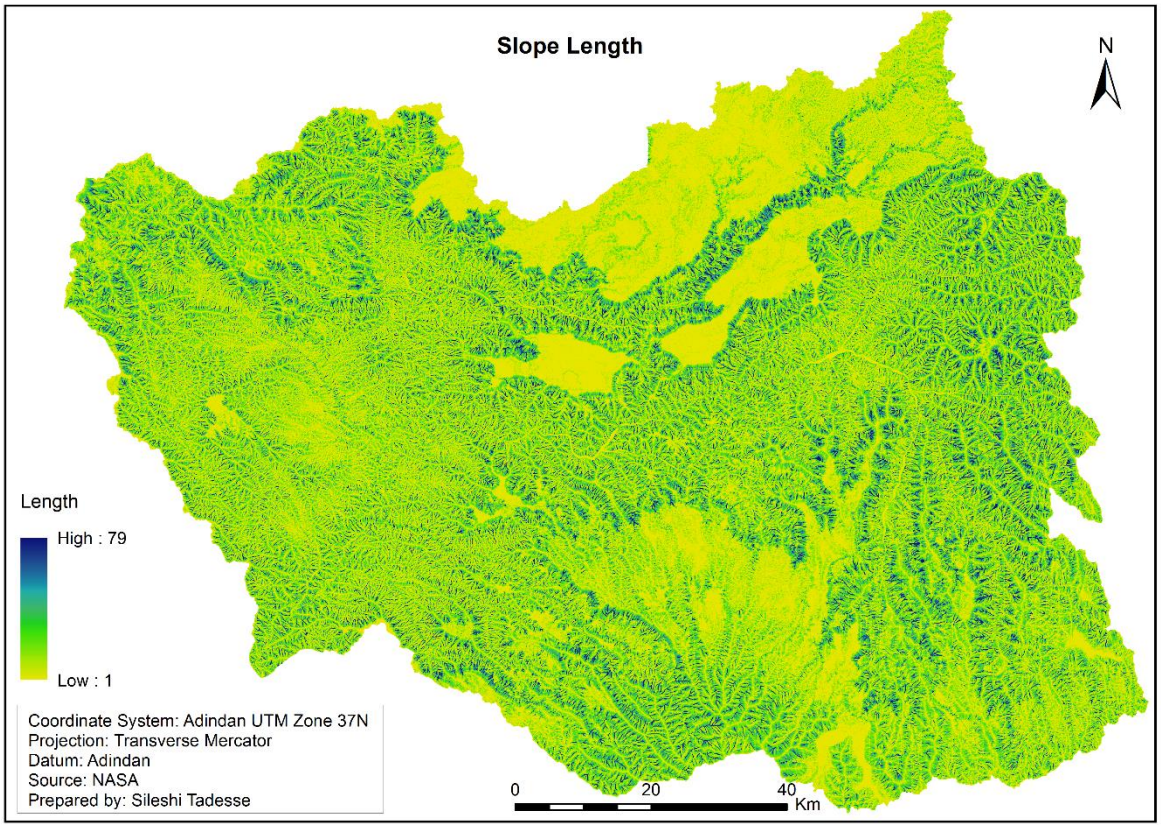

Appendix I: Slope steepness map of Beshilo basin

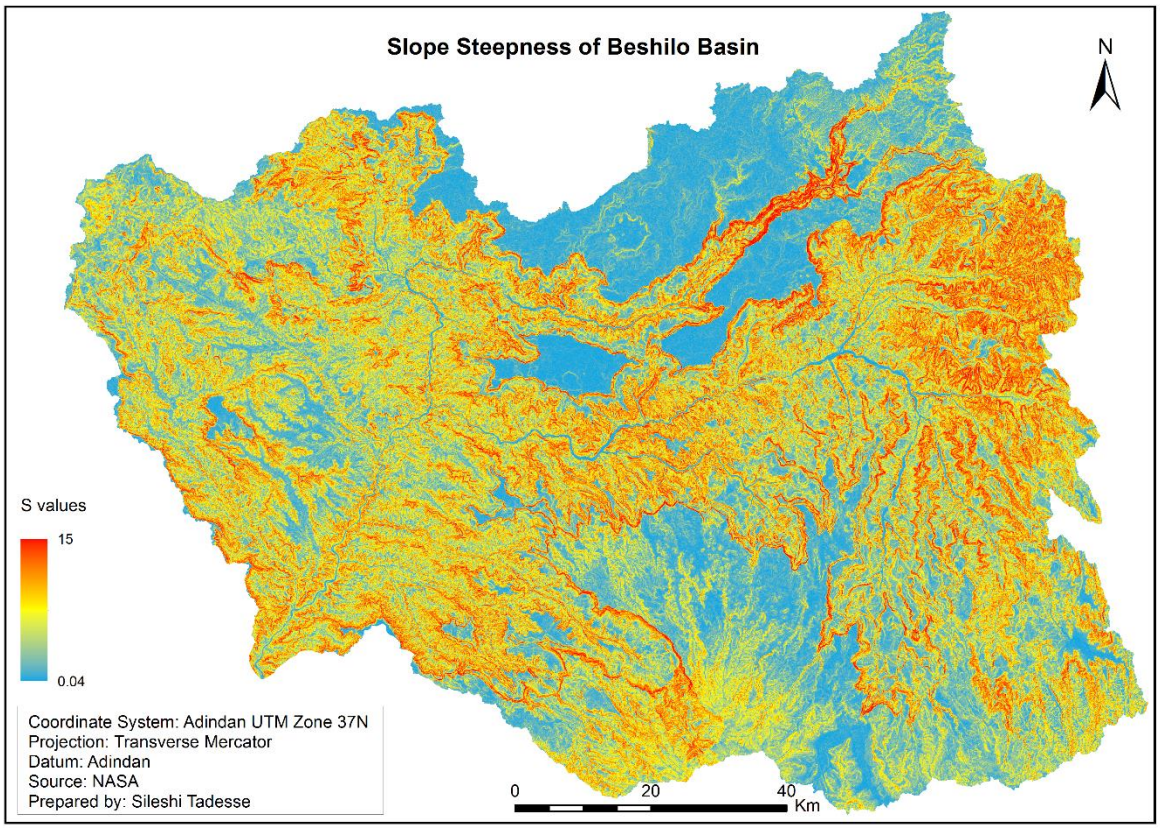

Appendix J: Relation between values of slope, slope length, steepness, LS factor and rill interrill ratio

Slope (%)	Slope length	Slope steepness	LS factor	Rill interrill ratio
4.8	1	0.4	0.4	0.3
6.9	1	0.7	0.7	0.4
7.1	6	0.8	5	0.5
8.3	1	0.8	0.8	0.4
8.3	1	0.8	0.8	0.5
8.8	2	0.9	1.7	0.5
9.5	1	1	1	0.5
14.7	3	1.9	5.7	0.6
14.9	3	2	5.9	0.6
18.2	3	2.1	6.2	0.6
22.1	9	3.1	27.8	0.6
22.2	2	2.4	4.9	0.6
23.1	4	2.6	10.6	0.6
23.5	4	3.4	13.6	0.6
24.3	3	5	15	0.6
25.4	1	4.2	4.2	0.6
27.1	8	5.4	43.5	0.6
27.9	4	4.5	17.9	0.6

31.6	4	4.7	19	0.6
32.2	2	2.8	5.6	0.6
33	6	5.5	33	0.6
34.9	1	5.7	5.7	0.6
35.9	4	6.6	26.5	0.7
36.3	3	5.8	17.4	0.7
37.3	4	6.1	24.4	0.7
39.5	3	6.1	18.2	0.7
39.7	5	6.6	32.8	0.7
43.2	2	8.6	17.2	0.7
45.4	16	7.7	123	0.7
46.3	5	8.7	43.4	0.7
47.3	2	8.7	17.4	0.7
48.7	6	8.2	49.4	0.7
49	2	8.5	16.9	0.7
49	3	9.3	27.9	0.7
52.6	2	9.3	18.5	0.7
55.5	10	10	100.4	0.7
56.3	3	10.2	30.5	0.7
56.6	6	11.2	67.1	0.7
58.3	3	10.3	30.8	0.7
58.5	2	10.4	20.8	0.7
59.5	4	10.1	40.5	0.7
61.7	3	10.6	31.8	0.7
61.7	7	10.8	75.7	0.7
66.7	5	11.7	58.5	0.7
68	3	11.5	34.5	0.7
69.1	2	11.6	23.1	0.7
82.4	3	12.7	38	0.7
96.4	2	13.4	26.8	0.7
109.4	3	13.9	41.6	0.7
114.6	4	14	56.2	0.7